CHALMERS
UNIVERSITY OF TECHNOLOGY

Liquid Hydrogen Fuel Distribution System Performance for Short Medium Range Civil Aircraft

Master's thesis in Applied Mechanics

Ali Azimi

DEPARTMENT OF APPLIED MECHANICS
Division of Fluid Mechanics
CHALMERS UNIVERSITY OF TECHNOLOGY
Gothenburg, Sweden 2022
www.chalmers.se

MASTER'S THESIS 2022

Liquid Hydrogen Fuel Distribution System Performance for Short Medium Range Civil Aircraft

Ali Azimi

Department of Applied Mechanics
Division of Fluid Mechanics
CHALMERS UNIVERSITY OF TECHNOLOGY
Gothenburg, Sweden 2022

Liquid Hydrogen Fuel Distribution System
Ali Azimi

Supervisor: Carlos Xisto, Chalmers Department of Applied Mechanics
Examiner: Carlos Xisto, Chalmers Department of Applied Mechanics

Master's Thesis 2022
Department of Applied Mechanics
Division of Fluid Mechanics
Chalmers University of Technology
SE-412 96 Gothenburg, Sweden
Telephone: +46 31-772 1000

Typeset in LaTeX
Printed by Chalmers Reproservice
Gothenburg, Sweden 2022

Liquid Hydrogen Fuel Distribution System
ALI AZIMI
Department of Applied Mechanics
Division of Fluid Mechanics
Chalmers University of Technology
SE-412 96 Gothenburg, Sweden

Abstract

Aviation is one of the most prominent parts of the transportation sector nowadays, and its share is growing globally, so it is necessary to reduce its emissions. The EU plan for net zero emissions by 2050 needs to be considered for civil aircraft as well. One of the most practical solutions for aviation emissions reduction is to use other options than fossil fuels, like liquid Hydrogen. This project is based on the Airbus model A321 as a twin-engine civil aircraft candidate. Liquid Hydrogen is in cryogenic condition ($22K, 1.6bar$), and it needs to be pumped during Maximum Take-Off (MTO) to a pressure of 40.6 bar in the combustion chamber. The pressure rise duty from the tank to the high-pressure pump must be done by two pumps in the fuel line a booster pump and a high-pressure pump. This study has two parts, the first concerns the fuel system design, and the second part comprises the design of the booster pump. We have designed the fuel system as a general study to see what components have to be through the fuel line from the tank to the high-pressure pump. These components include the pipeline to carry the liquid Hydrogen, valves for different roles in the system, and fitting for pipeline joints or direction changes. The booster pump is responsible for delivering the fuel from the tank to the fuel lines. According to Brewer's study [1], this booster pump can be of the centrifugal type with specific boundary conditions for design. The pump inlet/outlet boundary conditions are the direct results of the real gas modeling using CoolProp. CoolProps helps us to determine the properties of the LH2 at a given location in the fuel system stage to obtain preliminary values for the booster pump design. MTO is the booster pump design point for this research delivering a mass flow of 0.298 kg/s at a rotational speed of 12312 RPM. The CFD simulation is done using the ANSYS2021R1 package via the CFX solver. The values for preliminary design are used to generate the blade geometry, using Vista CPD and BladeGen. We have also considered off-design simulations for different points by changing mass flow/rotational speed to create a performance curve for the booster pump. This study includes the CFD design for the booster pump as the only component in which we assessed the preliminary design.

Keywords: Booster Pump, Cryogenic, Hydrogen, MTO

Acknowledgements

The thesis work was carried out at Chalmers Division of Fluid Dynamics. I extend my sincere gratitude to my supervisors, Carlos Xisto and Alexandre Capitao Patrao, for their extended support, guidance, and technical information that helped me in accomplishing the project.

Ali Azimi, August 2022

Contents

List of Figures

List of Tables

Nomenclature

Sets

ATF Aviation Turbine Fuel
BP Booster Pump
$ETOPS$ Extended-range Twin-engine Operational Performance Standards
HP High Pressure Pump
LH_2 Liquid Hydrogen
MC Mid Cruise
MCL Maximum Continuous Thrust
MTO Maximum Take-Off
$NPSH$ Net Positive Suction Head
PH_2 Hydrogen's Properties

Constants

α Flow Inlet Angle
β_2 Trailing Edge Angle
β_2' Slipped Blade Angle
ρ Density [kg/m^3]
σ Slip Factor
C_p Specific Heat Capacity [j/kgK]
e Roughness
g Gravitational Acceleration [m/s^2]
N Number of Stages
P_v Vapor Pressure [Pa]

Parameters

A_n Cross Sectional Area [m^2]
d Diameter [m]
d_{tip} Tip Diameter [m]
e Blade Thickness [m]
f Friction Factor
I Turbulence Intensity
K Head Loss Coefficient
L Length [m]
n_q Reference Rotational Speed
r Radius [m]
Re Reynolds Number
Re_d Pipe's Reynolds Number
u_{ref} Reference Velocity [m/s]
V Volume [m^3]

Z Number of Blades
Z_{ref} Reference Number of Blades
Variables
$\delta(x)$ Boundary Layer Thickness [m]
η Efficiency
η_h Hydraulic Efficiency
Ω Rotational Speed [1/s]
Ω_s Specific Speed
P Power Coefficient
$\dot{m}$ Mass Flow [kg/s]
$\dot{W}_c$ Compression Work per Second [W]
ϕ Flow Coefficient
ψ Stage Loading
τ Torque [kgm$^2/s^2$]
C Velocity in Turbomachine [m/s]
c_θ Tangential Velocity Component [m/s]
c_m Meridional Velocity Component [m/s]
c_r Radial Component Velocity [m/s]
D_s Specific Diameter
E Energy [j]
$E_{internal}$ Internal Energy [j]
E_{in} Inlet Energy [j]
$E_{kinetic}$ Kinetic Energy [j]
E_{out} Outlet Energy [j]
$E_{potential}$ Potential Energy [j]
E_{system} Total Energy of System [j]
E_{tot} Total Energy [j]
F_x Force in x Direction [N]
H Enthalpy [j]
H Head [m]
h Specific Enthalpy [j/kg]
h_f Pipe Friction Head Loss [m]
H_i Ideal Head [m]
h_m Valves Head Loss [m]
h_o Total Specific Enthalpy [j/kg]
h_s Specific Isentropic Enthalpy [j/kg]
$h_{o,rel}$ Total Relative Specific Enthalpy [j/kg]
h_{tot} Total Head Loss [m]
I Rothalpy [j/kg]
KE Kinetic Energy [j]
m Mass [kg]
n_q Specific Speed
P Pressure [Pa]
P_o Total Pressure [Pa]
PE Potential Energy [j]
Q Heat [j]

q	Specific Heat [j/kg]
S	Entropy [J/K]
s	Specific Entropy [j/kgK]
T	Temperature [T]
U	Velocity [m/s]
u	Velocity [m/s]
$U_{tip,max}$	Maximum Velocity at the Blade Tip [m/s]
UE	Internal Energy [j]
W	Relative Velocity in Turbomachine [m/s]
w	Work [j]
Z	Height [m]

1

Introduction

1.1 Background & Motivation

Airplanes are the most significant international transportation system for passengers all around the world. Airplanes started their role in the early decades of the 20th century, and gradually became widespread everywhere. Currently, the aviation sector is responsible for almost 4.5 billion passengers annually (data for 2019 [10]). Current aviation transportation is mainly based on kerosene consumption which is a fossil-based fuel. According to the statistics, there are 95 billion gallons by 2019 of jet fuel consumption [11] by the aviation section. The evolution of airplanes and their influences on human society is a topic that we will not cover in this research. At the beginning of the twenty-first century, humanity faced a new challenge that can lead to a danger for our civilization. Global warming is one of the main concerns to overcome in upcoming years, and the main reason behind that is greenhouse gases that are produced by human activities [12] since the industrialization era. Apart from some electric aircraft, the rest burn fossil fuel-based components. So it is essential to find an approach to reduce their share of emissions. Although aviation's share in yearly emissions is not huge in comparison to electricity production and the rest of transportation systems directly, its effect is higher due to non$-CO_2$ emission at altitude. Therefore, there are efforts to reduce emissions from the aviation sector. The EU has a plan to be carbon neutral by 2050 [13]. This ambition has become one of the newest topics in mechanical and aerospace engineering to help Europe's vision for emission reduction by 2050. There are several options to replace fossil-based fuels in the aviation sector. The usage of bio-fuels, electrical planes, ethanol/methanol-based, and liquid hydrogen-based airplanes are among the top candidates. The motivation behind the liquid hydrogen-based planes is that, first of all, ethanol and methanol also emit carbon dioxide, which makes them pollutant options like kerosene, also their chemical composition damages the internal part of the engine. Electrical airplanes need huge batteries and their range is short compared to the current planes. The third option (LH_2-based airplanes) is the most convenient choice until now since they have several advantages. Firstly, water is the main source of liquid Hydrogen and as a result of its combustion, vapor water will be the main emission released. Secondly, Hydrogen has a high energy content per unit of mass and its flammability range and combustion temperature are higher comparing the Hydrocarbons, which allows burning with leaner mixtures leading to less NOX emission [14].

These advantages make liquid Hydrogen one of the aptest options for future aviation fuel requirements. As this technology is new, there must be a design for the liquid Hydrogen fuel system to satisfy the requirement of the aviation sector.

1.2 Aim

In this research, we are going to design a setup including several components to pump the liquid Hydrogen fuel from the fuel tanks to the airplane engines. The liquid Hydrogen leaves the fuel tank in saturated liquid condition and it passes through the feeding pipes to reach the engine combustion chamber. This design is based on the Airbus A330 configuration as a twin engines civil airplane. The liquid Hydrogen in the saturated state is kept in two main fuel tanks at a low temperature. The tanks must keep the liquid Hydrogen at its saturated condition to avoid vaporization; thus it requires special insulation to minimize heat losses to the environment. The liquid Hydrogen should be pumped through the pipes to feed the engines.
First, we need to pump the liquid Hydrogen from the tank using the booster pump to overcome possible losses in the fuel system. This pressure drop happens because hydraulic components exist from the fuel tanks to the engine, including pipes and valves. The booster pump is responsible for just a portion of the pressurization process and the rest will be done by the engine-mounted high-pressure pumps before the engine's combustion chamber. Since we are injecting the fuel in the saturation condition, the Hydrogen is boiling, so cavitation is inevitable in the booster pump; however, we try to keep it away in the high-pressure pump. Liquid Hydrogen must leave the booster pump at an appropriate pressure to satisfy the main responsibility of this pump as we mentioned before. The liquid Hydrogen passes through the insulated pipe to reach the combustion chamber.
Secondly, we need to find suitable pipe dimensions, materials, and insulation systems to carry the fuel. Criteria for choosing the pipe properties are mainly reducing the hydraulic losses in the system and insulating the liquid Hydrogen from exchanging heat with the surrounding. The pipes should minimize the head and heat losses in the fuel system since they are the main responsible components for carrying the fuel. We have to find the appropriate values for pipes' inner diameter and roughness. Sine liquid Hydrogen is in the saturated state then we have to insulate the pipes to reduce the heat transfer as much as possible, to avoid boiling hydrogen in a vapor state. Finally, the design of the systems should meet some specific safety requirements which are regulated as federal regulations [15]. According to the regulations, there should be at least six booster pumps for a twin engines airplane, this safety factor makes sure that one booster pump starts working in case of main boost pump failure to inject fuel to the engines. Besides, the piping system should be placed just in the available space which is allowed, so it should not use fail-safe gap space at all.

1.3 Research Questions

The thesis aims at answering the following research questions:

1. What are the main hydraulic components involved in the fuel system?

2. What are the main geometrical and hydrodynamical properties of the piping systems and hydraulic components?
3. What are the geometrical features of the booster pump?
4. What is the best pressure ratio for the booster pump to operate efficiently?
5. What is the highest efficiency of the booster pump when it operates at the design point?
6. How can we operate the system with the highest achievable efficiency and minimum losses?
7. How can we minimize the cavitation effect on the booster pump?
8. Will the pump operates in the off-design situation too?

1.4 Specific Tasks

The main aim of the project is to pump the liquid Hydrogen from the fuel tanks to the combustion chamber, to fulfill that the liquid Hydrogen which is kept in cryogenic condition will be pressurized and sent out by a radial turbomachine. This radial turbomachine is a centrifugal booster pump that sucks fuel from the saturated state and sends it through the pipes to be burned in the combustion chamber. According to this, there are several tasks we have to do to complete the work.

1.4.1 Fuel System Design

- Liquid Hydrogen hydraulic flow calculation
  The first task is to find the fluid mechanics' parameter value for hydraulic flow calculations. We have to use the existing data for mass flow and liquid Hydrogen conditions in the tank to find the rest of the values using CoolProp's library and fluid mechanics relations.
- Fuel systems' hydraulic components design
  We have fluid conditions at both points (Fuel tanks and combustion chambers), then we have to consider delivering this fuel from the tanks to the combustion chambers through a system. The system must meet the safety regulations requirements and have the minimum complexity. It includes the valves and pipe choice, booster pumps' locations, and their numbers.
- Piping systems design and calculations
  To carry the fuel from the tanks to the hydraulic components, then to the engines. We have to use a suitable piping system that includes the pipe dimensions, material, and efficient insulation. Besides, we need to design the piping structure for the system that connects the booster pumps to the engines concerning the safety measures and flow requirements.

1.4.2 Booster Pump Design

- Determination of the thermodynamic states and pump initial conceptual data
  We need to have the main thermodynamics parameters to make the preliminary design for the booster pump. Therefore, thermodynamics states of the liquid Hydrogen should be determined before and after the booster pump.

Here, we need to make some assumptions for pressure ratio and total-to-total efficiency to create an iterative procedure based on which, the optimum point in design will be obtained. Also, we use dimensionless numbers to find the respective values for rotational speed and impeller diameter. The code is written in Python and relies on CoolProp for real gas calculations.

- Meanline design of the booster pump
  The meanline design of the booster pump uses the generated values by Python code to create a preliminary design of the centrifugal pump. Python code generates the non-dimension parameters to input them in the Vista CPD toolbox. Meanline design data is transferred to the blade parameterization software so that a blade geometry could be generated and later on simulated in CFD.
- CFD simulation of the booster pump
  This step is the key point of the design to find out parts prone to cavitation, and show the flow parameters contours to check whether the design meets our requirements or not.
- Design Modifications
  This stage is necessary to modify the created design for efficiency improvement and to get rid of the backflow and swirls. Besides, we can alter the design to improve power consumption and the pump's duty of liquid pressurization. Moreover, we need to consider the off-design condition as well and perform essential modifications to make sure the pump works properly with the lower mass flow or different rotational speed.

1.5 Scope and Boundaries

There are some boundaries in this project that we have to think about initially to design the system within this scope. The approach of the fuel system design and then the booster pump preliminary design is based on several criteria to ensure that the pump meets safety and design requirements.
This project is designing the fuel system and its CFD simulation for the booster pump. The work includes a system design for the components that carry the fuel from tanks to the engines. This approach discusses what hydraulic parts are required to pressurize the liquid Hydrogen which is kept in cryogenic conditions at T=22 K and P=1.6 bar and deliver it to the combustion chamber. This liquid Hydrogen needs to be transferred from tanks with minimum heat exchange with surroundings to have the least possible portion of vapor in the pumped fuel. Therefore, the first part of the project is the system design to figure out what hydraulic items should be assigned. This design considers pumps' configuration in the airplane to ensure meeting the project's requirement for safety and mass flow distribution. We will discuss piping configuration as well to create the design of hydraulic components like required valves, elbows, and tees; however, We will not go into a detailed design for hydraulic components (except booster pump) and tanks since this is not in the project's scope. The booster pump is the only part that we proceed with its detailed CFD simulation. The booster pump design is based on meanline code and then preliminary design calculation to have initial values for hydraulic calculations and blade geometry initialization. We will not go through volute geometry. The

preliminary geometry will be used to make the mesh in Turbogrid and be defined as a problem in the CFX solver.
Not only the pump design is mainly for the design point which is the MTO (Maximum Take-Off), but also it should be able to work for off-design points as well like MCL (Maximum Continuous Thrust), MC (Mid Cruise), and Idle. However, this depends on the available time for the study to go through a detailed CFD study for all off-design scenarios.
We will not consider any experimental test or real model manufacturing. Moreover, the high-pressure pump and combustion chamber's heat exchanger CFD design will not be covered in this study. We will only use their boundary values for calculation and our engineering judgments.

1.6 Limitations and Delimitations

We can not change the fuel in this system, and its initial conditions from the storage tanks are already fixed. The liquid fuel's density should not vary much since we are treating the problem as an incompressible task, so we do not want a large vapor portion in the pipes after the first stage of pumping. The limitation for fuel's characteristics also contains its initial conditions as we already mentioned, since the Hydrogen requires a very low temperature to be in liquid form so the LH_2 fuel initial temperature is a limitation that we cannot ignore. On the other hand, the tank pressure is 1.6 bar for the design point and given data, which is fixed. The mass flow needs to be considered constant for each design scenario (our design point is MTO), thus we are limited to changing mass flow distribution and its values.
The fuel system that we are going through to design is based on the Airbus A321 configuration. This platform makes some limitations for our study since this will affect the piping configuration, number, and configuration of the booster pumps and other hydraulic components. The dimensions, gap space, and safety requirements for a twin engines civil aircraft are the main parameters that limit choices for our design. Therefore, pipe length and fuel distribution in the airplane need to be fitted with the wished platform.
The combustion chamber needs fuel at 40.6 bar, this pressure is required for the combustion chamber to work efficiently, so this needs to be taken care of to not deviate from the required pressure after the high-pressure pump outlet. The high-pressure pump outlet is connected to the combustion chamber, it is the last pressurization stage for our system. This pressure for the combustion chamber is another limitation we must consider as a fixed value.
The proposed turbomachine for this study is a centrifugal pump, this choice is based on several main reasons, centrifugal pumps have a wide operating range, better lubrication, and better stall characteristics compared to the other candidates like inducer, vane, and piston. In addition, we have chosen a pump since the working fluid is the liquid Hydrogen, which is not compressible like gaseous fluids. Turbomachine type is another fixed part of the study that we cannot change. [1]
Liquid Hydrogen fuel system components are part of the project that we are free to choose, as far as they meet the safety requirements and design tasks. This means that we can select the number of hydraulic valves and their types based on the flow

characteristics and mechanical prerequisites. Besides, the pipe's diameter and its network arrangement are our wishes. Fuel systems components' location, their load, and flows do not have limitations (except for safety and duty requirements).
The booster pump is the main part of the project, and we will go through a detailed design as we mentioned before. The pump's flow characteristics and its geometry is a matter of choice and efficiency not a limitation in the research. Moreover, the guessed values for the total efficiency of the pump, booster pump pressure ratio, and high-pressure pump pressure ratio are part of the iterative process and are subject to changes.

1.7 Thesis Outline

In this study, we have designed the fuel system for a twin engines airplane (Airbus A321), which is based on liquid Hydrogen fuel to fulfill the EU net zero emission plan by 2050. We have designed a system configuration and CFD design for the booster pump.
For technical background, it is explained the applicable knowledge in this study. The overall definition of the relevant hydraulic components such as valves and fittings, fluid mechanics governing equations, and centrifugal pump geometrical relations are the main content.
To design the fuel system and booster pump, the methodology chapter begins with using CoolProp as the primary tool to determine the flow's characteristics in each stage, then this meanline code's results are used for pump preliminary design estimations. The initial design is given to the Vista CPD to generate the meanline data for blade parametrization, Turbogrid is used for meshing, and CFX is used for CFD computations, all tools are part of the ANSYS Workbench 2021R1 suite. The project's first part is the system design of the components' arrangement, according to which we will find piping characteristics and hydraulic parts to give the fuel from the fuel tanks to the engines. The second part of the study discusses detailed CFD simulation for the booster pump to find optimum values for its working design point and its performance in off-design conditions too.
The CFD results for the design point of the centrifugal pump (both cases A and B) are shown in the result and discussion chapter. Besides, the off-design CFD contours for both cases and their performance curves are the later subjects for the fourth section of the report. Respective discussion for each contour or performance curve accompanies each figure for better understanding.
Conclusion and future works title is the last part of this study to indicate the gist of the project and clues for upcoming research on the liquid hydrogen fuel system topic.

2

Technical Background

2.1 Fuel System

A321 is a twin-engine civil airplane from the Airbus A320 family. A321 first time entered the service in 1994 as a narrow-body civil airliner jet. This aircraft is one of the most successful commercial airplanes that has been ever made. A321 is capable to carry 180 to 220 passengers with a range between 5900 km to 7400 km for different variants. A321 family has several variants that have minor differences in terms of fuel consumption, interior design, and range. The general dimensions and characteristics of the A321neo model are illustrated in Table 2.1 [9] :

Characteristic		Characteristic	
pax max seating	244	cabin length	34.44 m
typical seating	180-220	fuselage width	3.95 m
max pallet number underfloor	10	max cabin width	3.7 m
water volume	$59m^3$	height	11.76 m
overall length	44.51 m	range	7400 km
max take-off weight	97 ton	max fuel capacity	329400 liters

Table 2.1: A321neo Characterstics [9]

The fuel for the A320 family is jet fuel or aviation turbine fuel (ATF) which is composed mainly of Kerosene-type jet fuel. This fossil fuel contains between 8 to 16 carbons per molecule [16].

The fuel system in A321 for Kerosene fuel-based airplane consists of different hydraulic components to pressurize, carry and regulate the fuel in the system. These components are between the fuel tanks and engines to pump the fuel according to the flight stages.

The airplane has three different flight stages and one motionless stage idle. Three flight stages are considered MTO (Maximum Take-Off), MCL (Maximum Climb), and MC (Mid-Cruise). Idle is the step in that an airplane is stopped and has the minimum fuel mass flow and required power. In contrast, MTO requires the maximum mass flow and power for the vehicle to take-off. Moreover, the airplane needs the highest pressure ratio during the MTO stage after the high-pressure pump. In two other phases, MCL and MC, need less mass flow and lower pressure ratio accordingly.

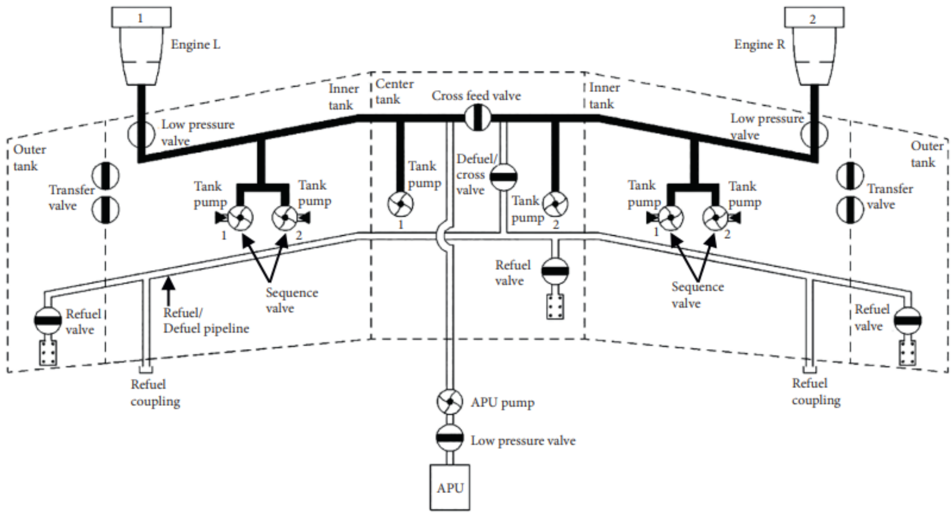

Figure 2.1: Configuration of the fuel system of A320 aircraft [2]

2.1.1 Piping System and Fuel Tanks

There are two unlike non-integral tanks in the structure. The smaller one is located on top of the front part and the larger tank, which consists of two identical portions is on the rear part, as you can see in Figure **??**. These tanks keep liquid Hydrogen in cryogenic conditions to give the fuel through the system into the engines' combustion chambers. These tanks are fixed on top of the aircraft body with a firm structure [17]. The piping system is an insulated network that has to be implemented inside the body structure. Pipes are connected to the booster pumps' outlets and they end in the combustion chamber. Tees and elbows are part of the network that we explain more in the hydraulic components section. The piping network for the A320 Kerosene based is shown in Figure 2.1.

2.1.2 Hydraulic Components

The fuel system has several different parts as we explained before. Tanks, piping systems, and booster pumps are the main units, in addition, the hydraulic components also exist. These components are valves, elbows, and tees in the system. Liquid Hydrogen fuel is kept in cryogenic condition (22 K, 1.6 bar), but it is required to be almost 40.6 bar for the MTO stage (or other conditions like MCL or MC), so we have to pressurize the fuel and send it to the combustion chamber. This process is based on two pressurization steps: (first booster pumps and second high-pressure pumps). However, pressurization seems to be enough to meet the chamber's requirements, fuel line has to have other hydraulic components as well, to regulate, release or prevent return flow in the system. Besides, the piping system inside the body structure has to be fitted with the airplane's internal space, so using tees for cross sections and elbows for the angled line is inevitable.

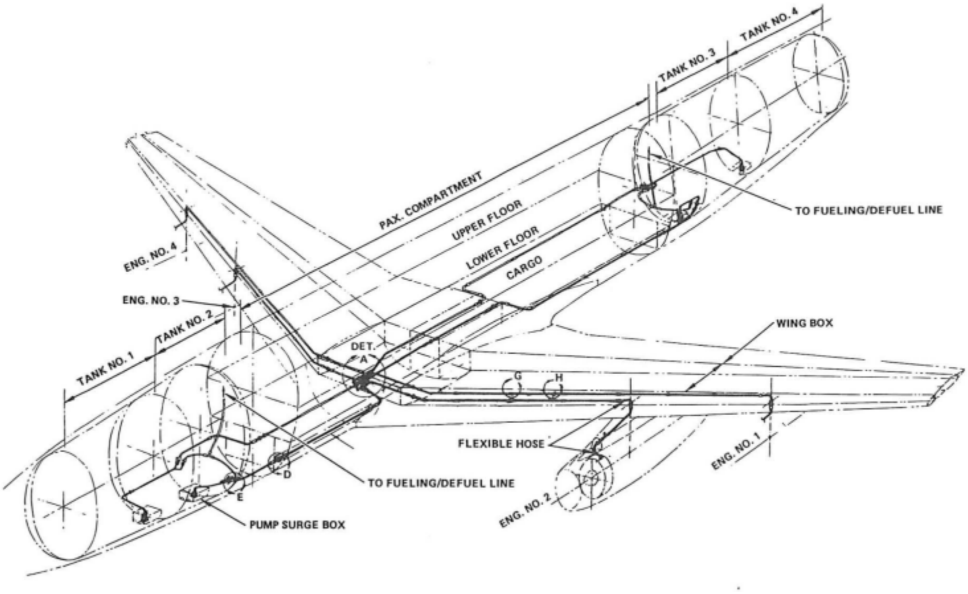

Figure 2.2: Engine Fuel Deliver System [1]

2.1.2.1 Non-Return Valve

This valve is a kind of well-known valve even by its name. They just allow flow in one direction to move through the pipelines, where pressure is likely to cause reverse flow in the system. However, pressure drop through a non-return valve is huge and needs to be taken into account in calculations for system pressure drop. There are different types of non-return valves like swing or clapper that we will not go into detail about [18].

2.1.2.2 Relief Valve

This valve is a safety component to release excess pressure. In case of excess pressure (when the pressure in the system is more than the design value), this valve will protect the fuel arrangement from fracture or explosion. The relief valve's importance is more when pump failure happens in the system. This causes a pressure gradient in the system that needed to be handled by a relief valve. The relief valve is the last device to prevent the problem in the system (as a result of over-pressurization), so it is expected to be very reliable; therefore, its design should be as simple as possible [19].

2.1.2.3 Regulator Valve

The pressure regulator valves are a type of valve for flow pressure and mass flow control within the system. Regulator valves are essential to optimize the performance of a system. The simplest regulators have an aperture, which opens or closes to control the flow rate. In a hydraulic circuit, many different types of the regulator can be utilized, from the simplest like orifice to the complex types. Although a regulator is a cheap option to provide good performance for a hydraulic system, it causes a pressure drop when the valve is partially closed (or open). This can affect the performance negatively too. The size of the control valve depends on the fluid density, and minimum and maximum flow rate [20].

2.1.2.4 Shut-Off Valve

The shut-Off valves are used to stop or continue the flow immediately in the system. This can be because of the external liquid or air leakage into the piping system. These valves are the best solutions for the system services when it is not necessary to stop the whole system. The valve's size depends on the pressure, temperature, and environment, where it is working [21]. The shut-off valve also is considered a piece of safety equipment, since it will operate in case of a failure or leakage as we mentioned [22].

2.1.2.5 Fuel Cross-Feed Valve

The cross-feed valve directs the fuel to both engines from any of the available fuel tanks. This valve helps the system's fuel consumption to be balanced (gravity center) since we have three portions of fuel tanks and two engines [23]. Besides, their role is important during booster pumps' failure to disturb the fuel from the remaining tanks to both engines [1].

2.1.2.6 Elbow Fitting

The L shape fitting is to be used for angled lines. This will change the flow's direction to the desired one. They can have different angles like 45, 60, and 90, see Figure 2.3. Their insulation and material should be compatible with the rest of the piping network. Moreover, the pressure drop through the elbow should be calculated and considered in the calculations [3].

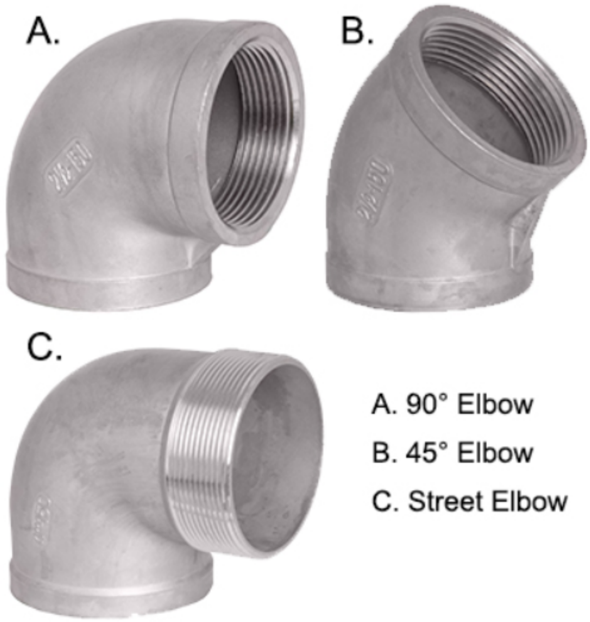

Figure 2.3: Elbow Fittings [3]

2.1.2.7 Tee Fitting

The pipe tee is a fitting with three connections illustrated in Figure 2.4. This one has two outlets in the same line in opposite directions and one inlet perpendicular to the outlets' line. This fitting is used for the cases like booster pump's outlet connection and cross-feed valve implementation. Because of high-pressure drop-through tees, it is very important to count them in pressure drop consideration [4].

Figure 2.4: Tee Fitting [4]

2.1.2.8 Fuel Pumps

The LH2 system is considered to pressurize the fuel from the cryogenic conditions to the desired pressure in the combustion chamber (according to the flight stage). This process happens through two stages, the first stage is done by a booster pump and the second one is done before the engine by the high-pressure pump. The booster pump's role is to overcome the pressure drop throughout the system. Pressurization by booster pump is not part of the main compression to fulfill the engine's demand, but the high-pressure pump is obligated to deliver compressed liquid Hydrogen respective to the chamber's requirement.

2.1.3 Safety Regulations

The airplane fuel system should be designed carefully and precisely since it deals with many people's lives, particularly civil aircraft that we are talking about. These safety measures are based on previous designs and current regulations that globally are considered by aircraft manufacturers. We will not explain safety measures in detail, but just list them as stated in the sources:

1. Be designed and arranged to provide independence between multiple fuel storage and supply systems so that failure of any one component in one system will not result in loss of fuel storage or supply of another system [15]
2. Provide the fuel necessary to ensure each powerplant and auxiliary power unit functions properly in all likely operating conditions [15]
3. Provide the flight crew with a means to determine the total useable fuel available and provide an uninterrupted supply of that fuel when the system is correctly operated, accounting for likely fuel fluctuations [15]
4. Provide a means to safely remove or isolate the fuel stored in the system from the airplane [24]
5. Be designed to retain fuel under all likely operating conditions and minimize hazards to the occupants during any survivable emergency landing [24]
6. For two-engine airplanes to be certificated for ETOPS (Extended-range Twin-engine Operational Performance Standards) beyond 180 minutes, one fuel boost pump in each main tank and at least one crossfeed valve, or other means for transferring fuel, must be powered by an independent electrical power source other than the rest of the power sources. This requirement does not apply if the normal fuel boost pressure, crossfeed valve actuation, or fuel transfer capability is not provided by electrical power [15].
7. Each main pump must be used that is necessary for each operating condition and attitude for which compliance with this section is shown and the appropriate emergency pump must be substituted for each main pump so used. [15]
8. Main pumps: For each main pump, provision must be made to allow the bypass of each positive displacement fuel pump other than a fuel injection pump (a pump that supplies the proper flow and pressure for fuel injection when the injection is not accomplished in a carburetor) approved as part of the engine [15].

   note: Each fuel pump is required for proper engine operation.
9. Emergency pumps: There must be emergency pumps or another main pump to feed each engine immediately after the failure of any main pump (other than a fuel injection pump approved as part of the engine) [15].

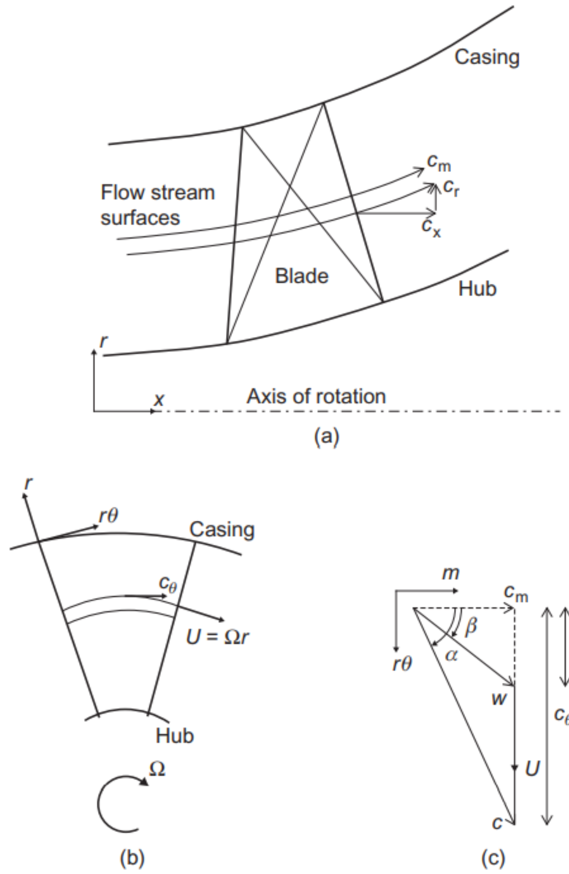

Figure 2.5: The coordinate system and flow velocities within a turbomachine. (a) Meridional or side view, (b) view along the axis, and (c) view looking down onto a stream surface [5]

2.2 Fluid Mechanics in Turbomachinery

2.2.1 Frame of Reference

The coordinate system is the work frame for fluid dynamics, according to which we can determine the fluid's element motion, then analyze it. The coordinate framework can be categorized as $2D$ or $3D$. The three-dimensional workspace can be cylindrical, spherical, or Cartesian. Each coordinate system has three different parameters to locate the fluid's element.

Turbomachines consist of rotating and stationary blades around an axis, which reflects their cylindrical shape. That is why cylindrical coordinate is the bests choice for studying turbomachinery [5].

The cylindrical system aligned with the axis of rotation creates the base for this analysis in turbomachinery. The three parameters to describe fluid motion are axial x, radial r, and tangential θ.

The flow in a turbomachine has components of variables along all three axes, which vary in all directions. Nevertheless, for simplification of the analysis, it is normally considered that the flow does not vary in the tangential direction.

The study of the fluid elements within the rotating blades of a turbomachine is performed in a frame of reference that is stationary relative to the blades. In this system, the flow moves steadily, while in the non-relative frame of reference it is unsteady. This will ease mathematical calculations, so relative quantities application in turbomachinery are inevitable [5].

2.2.2 Thermodynamics

2.2.2.1 Energy

Energy is a quantitive related to a body or physical system that can be transferred from one form to the other between bodies or systems. A fluid element can contain energy in the forms of internal energy inherent in its internal structure, kinetic energy in its motion, and potential energy associated with external forces acting on the fluid's mass [7]. Note equation 2.1:

$$E_{tot} = E_{internal} + E_{kinetic} + E_{potential} = UE + KE + PE \text{ [7]} \tag{2.1}$$

Internal energy is inherent energy for the inner structure of the fluid element as we mentioned. This property is extensive since it depends on the mass. In thermodynamics, the specific internal energy is based on a specific mass and it is kj per each kg of that phase [7].

2.2.2.2 Enthalpy

The heat transfer in a constant-pressure, quasi-equilibrium process is equal to the change in enthalpy, which includes both the change in internal energy and the work for this particular process. Enthalpy is a very useful property for both thermodynamics and fluid mechanics applications. This quantitive is applicable to calculate work or heat transfer in a system defined by equation 2.2 and the specific enthalpy by equation 2.3 [25]:

$$H = U + PV \tag{2.2}$$

Or per unit of mass:

$$h = u + pv \tag{2.3}$$

Another sub-definition of enthalpy is total enthalpy in equation 2.4, which is the enthalpy that fluid would have in the case of stagnation through an adiabatic process.

$$h_o = h + \frac{u^2}{2} \tag{2.4}$$

2.2.2.3 Entropy

Entropy is a property that refers to the disorder in the system. Entropy is a measure of system thermal energy that is unable to contribute to useful work. It is an extensive property like internal energy and enthalpy, so it can be indicated as per unit of mass. Like enthalpy, the statistical values for entropy in each condition can be found through tables for different fluids [25]. For a reversible process (no loss), it can be indicated by equation 2.5:

$$S_2 - S_1 = \int_1^2 (\frac{\delta Q}{T})_{rev} \tag{2.5}$$

2.2.2.4 Rothalpy

Rothalpy is a constant parameter along the streamlines through a turbomachine. It reflects rotational stagnation enthalpy, and it is an important fluid mechanic property to study turbomachinery [5]. Rothalpy is written by equation 2.6 or in static enthalpy format equation 2.7:

$$I = h_o - Uc_\theta \tag{2.6}$$

$$I = h + \frac{1}{2}c^2 - Uc_\theta \tag{2.7}$$

Defining relative stagnation enthalpy can simplify the above relations to equation 2.8:

$$I = h_{o,rel} - \frac{1}{2}U^2 \tag{2.8}$$

2.2.2.5 Laws of Thermodynamics

1. First Law of Thermodynamics
   The first law of thermodynamics may seem to be a familiar expression, that energy cannot be created or destroyed, it just transfers from one system to the other. The first law is a consequence of the energy equation, to show that the net change of energy in the system is incoming energy to the system minus outgoing energy [26]. For a system, equations 2.9 and 2.10 are direct results of the first law.

$$E_{in} - E_{out} = \Delta E_{System} \tag{2.9}$$

$$\Delta E_{System} = Q - W \tag{2.10}$$

2. Second Law of Thermodynamics
   It can be stated in different ways, but one of the most common expressions for the second law is: it is not possible in a system that all heat to be converted to the work [26].
   Assume a heat engine where heat is supplied and work extracted. More units of heat need to be supplied to the engine than the units of work we can recover from it. This is due to irreversibilities within the engine, such as i.e. friction. These irreversibilities make it impossible to reverse the process. These irreversibilities are indicated by entropy [26].

2.2.3 Governing Equations of the Fluid Mechanics

2.2.3.1 Continuity Equation

Continuity is the conservation mass law for a control volume. It states that there is no mass creation or destruction in a system. If you consider a fluid element with a volume of dv, then inlet mass flow to the control volume is equal to the outlet mass flow [5]. Equation 2.11 is the mass flow through a cross-section area with a diameter of d:

$$d\dot{m} = \frac{dm}{dt} = \rho c dA_n \tag{2.11}$$

Then it gives another relation for continuity by equation 2.12:

$$\dot{m} = \rho_1 c_1 A_{n1} = \rho_2 c_2 A_{n2} = \rho c A_n \tag{2.12}$$

2.2.3.2 Momentum Equation

One of the most basic and practical principles in mechanics is Newton's second law of motion. The momentum equation relates the sum of the external forces acting on a fluid element to its acceleration, or to the rate of change of momentum in the direction of the consequent external force (equations 2.13 and 2.14). In the investigation of turbomachines, many applications of the momentum equation can be found, e.g., the force exerted upon a blade in a compressor or turbine cascade caused by the deflection or acceleration of fluid passing the blades [5].

$$\Sigma F_x = \frac{d}{dt}(m c_x) \tag{2.13}$$

$$\Sigma F_x = \dot{m}(c_{x_2} - c_{x_1}) \tag{2.14}$$

2.2.3.3 Bernoulli Equation

For the adiabatic flow, with no work we have equation 2.15 [5]:

$$(h_2 - h_1) + \frac{1}{2}(c_2^2 - c_2^2) + g(z_2 - z_1) = 0 \tag{2.15}$$

If the system is an infinitesimal small control volume, the following equation 2.16 is derived [5]:

$$dh + cdc + gdz = 0 \tag{2.16}$$

By integration, we will have the Bernoulli equation for incompressible flow (if we assume constant density) by equation 2.17 [5]:

$$\frac{1}{\rho}(P_{o_2} - P_{o_1}) + g(z_2 - z_1) = 0 \tag{2.17}$$

2.2.3.4 Euler Rigid Body Dynamic Equation

For a rotary machine running at rotational velocity (Ω), the rate at which the rotor does work on the fluid can be found with equation 2.18 [5]:

$$\dot{W}_c = \tau\Omega = \dot{m}(U_2 C_{\theta_2} - U_1 C_{\theta_1}) \tag{2.18}$$

Therefore, the work done on the fluid per unit of mass or specific work is in equation 2.19 [5]:

$$\Delta W_c = \frac{\dot{W}_c}{\dot{m}} = \frac{\tau\Omega}{\dot{m}} = U_2 C_{\theta_2} - U_1 C_{\theta_1} > 0 \tag{2.19}$$

This equation is referred to as Euler's pump or compressor equation.

2.3 Hydraulic Head Loss in Pipes

To calculate hydraulic losses in a system we have to consider the losses for pipes, valves, and other hydraulic components like shaped pipes and connections. The hydraulic losses calculation is based on the flow regime whether it is turbulent or laminar. Flow regime determination is based on the Reynolds number range as we mentioned before.
The friction factor is a very important factor to consider in the head loss in the system. A friction factor is a dimensionless number that can be calculated based on the range of the Reynolds number. In the case of laminar flow, the friction factor is calculated by equation 2.20 ($Re < 2000$) [7]:

$$f = \frac{64}{Re} \tag{2.20}$$

And for turbulent flow ($Re > 2000$) the equation 2.21 shows friction factor value [7]:

$$\frac{1}{f^{1/2}} = -1.8log[\frac{6.9}{Re_d} + (\frac{e/d}{3.7})^{1.11}] \tag{2.21}$$

The friction factor is a necessary factor to calculate head loss through a tube or piping system. The equation 2.22 is a general equation to investigate head loss through a pipe with a diameter of d and length of L, in which the flow is moving with a mean velocity of u [7]:

$$h_f = f\frac{L}{d}\frac{u^2}{2g} \tag{2.22}$$

Apart from pipe friction which is an inner loss and happens through straight pipes (even without any direction changes). The head loss through a valve or elbow can be calculated by the K factors. This coefficient is a number that we use when we calculate head loss through hydraulic components except for straight pipelines [7]. The head loss through a hydraulic component is given by equation 2.23:

$$h_m = \Sigma K\frac{u^2}{2g} \tag{2.23}$$

We have tabulated K values from White 2009 [7] in Table 2.2. Then the total loss in the system is :

$$h_{tot} = \frac{u^2}{2g}(\frac{fL}{d} + \Sigma K) \tag{2.24}$$

Type	$d = 0.5'$	$d = 1'$	$d = 2'$
Globe valve	14	8.2	6.9
Gate valve	0.3	0.24	0.16
Swing check valve	5.1	2.9	2.1
90^o Elbow	2.0	1.5	0.95
Tee	2.4	1.8	1.4

Table 2.2: K values from White 2009 [7]

2.4 Heat Loss in a Vacuum Insulated Pipe

To calculate heat loss through an insulated piping system, we need to use specific correlations according to the [6]. This model is based on vacuum-insulated pipes for LNG in cryogenic conditions (which is similar to the LH_2 state) and evaluates convection and conduction simultaneously. Referring to Figure 2.6, the equation 2.25 shows heat loss through a vacuum-insulated tube (no conduction in vacuum):

$$q = \frac{T_4 - T_3}{\frac{1}{hA}} = \frac{T_4 - T_3}{\frac{1}{hA} + \frac{lnr_3/r_2}{2\pi kL}} \tag{2.25}$$

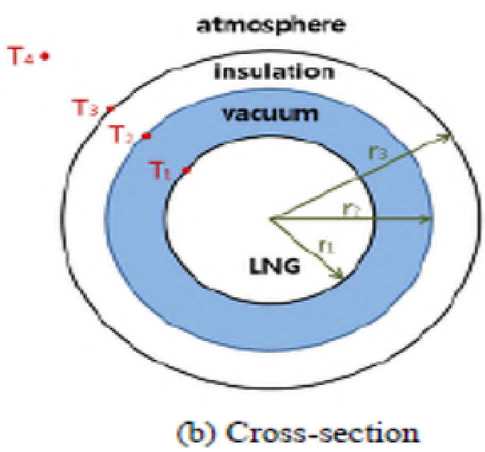

Figure 2.6: Vacuum-Insulated Pipe Cross-Section [6]

2.5 Pump Technical Background

We categorize turbomachines in every machine in which power is transferred either to or from, a continuously flowing fluid by the dynamic motion of one or more rotating blade rows. The word turbo or turbine is of Latin roots and indicates that which spins or whirls around [5]. Basically, a rotating blade row, a rotor, or an impeller modifies the stagnation enthalpy of the fluid moving through it by doing or receiving work, depending upon the outcome needed of the machine. These enthalpy changes are linked with the pressure changes happening at the same time in the fluid. Two main classifications of turbomachine are specified: first, those that absorb energy to expand the fluid pressure or head (compressors and pumps); second, those that deliver power by expanding fluid to a lower pressure or head (turbines) [5].

2.5.1 Fluid Mechanics in Centrifugal Pump

2.5.1.1 Velocity Diagram

The velocity diagram is the fundamental step for flow motion examination in a turbomachine. This focuses on flow motion from the inlet stage of the pump (or compressor) to the outlet section. The diagram helps the designer to understand how the velocity vector changes through the pump's inner structure. The velocity diagrams normally consist of three main components: 1) Absolute velocity (C) 2) Blade velocity (U) 3) Relative velocity (W) (absolute velocity relative to the blade velocity) illustrated in Figure 2.7

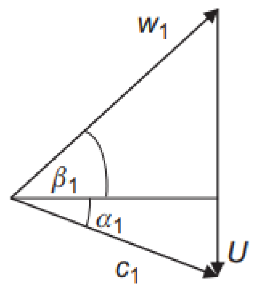

Figure 2.7: Velocity triangles for an axial compressor inlet [5]

$$W + U = C \tag{2.26}$$

2.5.1.2 Non-Dimensional Numbers

The performance of a turbomachine can be expressed in terms of the control variables, geometric variables, and fluid properties. Take as a sample a hydraulic pump. It is suitable to consider the net energy transfer, gH; the efficiency; η; and the delivered power P as dependent variables and to report the three equations 2.27, 2.28 and 2.29 [5]:

$$gH = f(Q, \Omega, D, \rho, \mu, e, \frac{l_1}{D}, \frac{l_2}{D}, ...) \tag{2.27}$$

$$\eta = f(Q, \Omega, D, \rho, \mu, e, \frac{l_1}{D}, \frac{l_2}{D}, ...) \tag{2.28}$$

$$P = f(Q, \Omega, D, \rho, \mu, e, \frac{l_1}{D}, \frac{l_2}{D}, ...) \tag{2.29}$$

There is a possibility to define dimensionless numbers to ease our study of turbomachines, thanks to the π theorem. Hence, the three above groups can be reduced to the following equations 2.30, 2.31 and 2.32 [5]:

$$\psi = \frac{gH}{(\Omega D^2)} = f(\frac{Q}{\Omega D^3}, \frac{\rho \Omega D^2}{\mu}, \frac{e}{D}) \tag{2.30}$$

$$\eta = f(\frac{Q}{\Omega D^3}, \frac{\rho \Omega D^2}{\mu}, \frac{e}{D}) \tag{2.31}$$

$$\hat{P} = f(\frac{Q}{\Omega D^3}, \frac{\rho \Omega D^2}{\mu}, \frac{e}{D}) \tag{2.32}$$

The created non-dimensional variable $Q/(\Omega D^3)$ is a volumetric flow coefficient. For turbomachines working with the compressible flow, an alternative that is normally used is the flow coefficient $\phi = c_m/U$, where U is the mean blade speed and c_m is the average meridional velocity [5].
The non-dimensional group $\rho \Omega D^2/\mu$ is a form of Reynolds number, denoted Re. Reynolds number describes the ratio between the inertial forces and the viscous forces within a flow. Low viscosity fluid moving at a high rate, the Reynolds is high; contrariwise, for slow-motion fluid with high viscosity, the Reynolds number is low. The empirical effect of $Re > 2 \times 10^5$ on the performance of turbomachines can be ignored. This is valid because, at high Re, the viscous boundary layers on the blades of a turbomachine are typically turbulent and very flimsy. They, thus, have a negligible consequence on the global flow field [5].
The consequences of surface finish are reflected by the non-dimensional group, e/D, called the roughness ratio or relative roughness. At a high Reynolds number (Re), more significant surface roughness tends to increase skin friction losses and decrease efficiency. The results at lower Reynolds numbers are more complicated as the boundary layers might be laminar or experiencing a shift to turbulence [5].
Two nondimensional parameters named the specific speed, Ω_s, and specific diameter, D_s, are often used to determine the selection of the most proper machine. The specific speed is derived from the non-dimensional groups defined in equations 2.30, 2.31, and 2.32 in such a way that the characteristic diameter D of the turbomachine is omitted. The value of Ω_s offers the designer a directory to the sort of machine that will deliver the expected requirement of high efficiency at the design requirement (Figure 2.8). Likewise, the specific diameter (D_s) is obtained from these groups by Ω elimination [5]:

$$\Omega_s = \frac{\Phi^{1/2}}{\psi^{3/4}} = \frac{\Omega Q^{1/2}}{(gH)^{3/4}} \tag{2.33}$$

$$D_s = \frac{\psi_1^{1/4}}{\Phi_1^{1/2}} = D\frac{(gH)^{3/4}}{Q^{1/2}} \tag{2.34}$$

Also according to the Gulich 2008 [27], we can write equations 2.35, 2.36 and 2.37

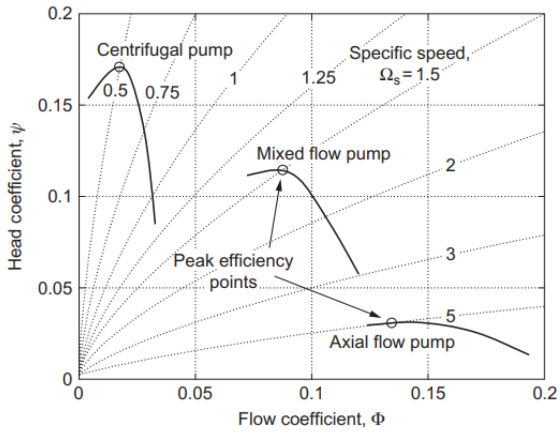

Figure 2.8: Contours of specific speed showing characteristics of various pump types [5]

to design for optimum efficiency of a radial pump:

$$\Omega_s = \frac{n_q/52.9}{2} \tag{2.35}$$

$$\Omega_s = \frac{\Omega\sqrt{Q}}{(gH)^{0.75}} \tag{2.36}$$

$$\psi_{opt} = \frac{2gH}{(\Omega r_2)^2} \tag{2.37}$$

In these relations, r_2 is the impeller exit radius, and H is the head rise per stage of the pump. Besides, n_q is the specific speed according to the Gulich [27].
Besides, the flow coefficient according to the ANSYS TurboGrid user guide [8] is as below equation 2.38 :

$$\phi = \frac{Q}{0.5\Omega D_2^3} \tag{2.38}$$

The word, pump, refers to machines that boost the pressure of a flowing liquid. [5] A centrifugal compressor or pump consists necessarily of a rotating impeller followed by a diffuser. Figure 2.9 illustrates the different elements of a centrifugal compressor. Fluid is drawn in through the inlet casing into the eye of the impeller. The role of the impeller is to expand the power level of the fluid by spinning it outward, thereby raising the angular momentum of the fluid. Both the static pressure and the velocity are increased within the impeller. The objective of the diffuser is to transform the kinetic energy of the fluid flowing from the impeller into pressure energy. This procedure can be done by unrestricted diffusion in the annular area surrounding the impeller. Outside the diffuser is a scroll or volute whose function is to gather the discharge from the diffuser and supply it to the outlet pipe. For low-speed pump applications where complexity and high cost should be avoided even in case of lower efficiency, the volute follows instantly after the impeller. The hub is the curved surface of the revolution of the impeller *ab*; the shroud is the curved surface *cd* making the outer boundary to the flow of fluid. At the entrance to the impeller,

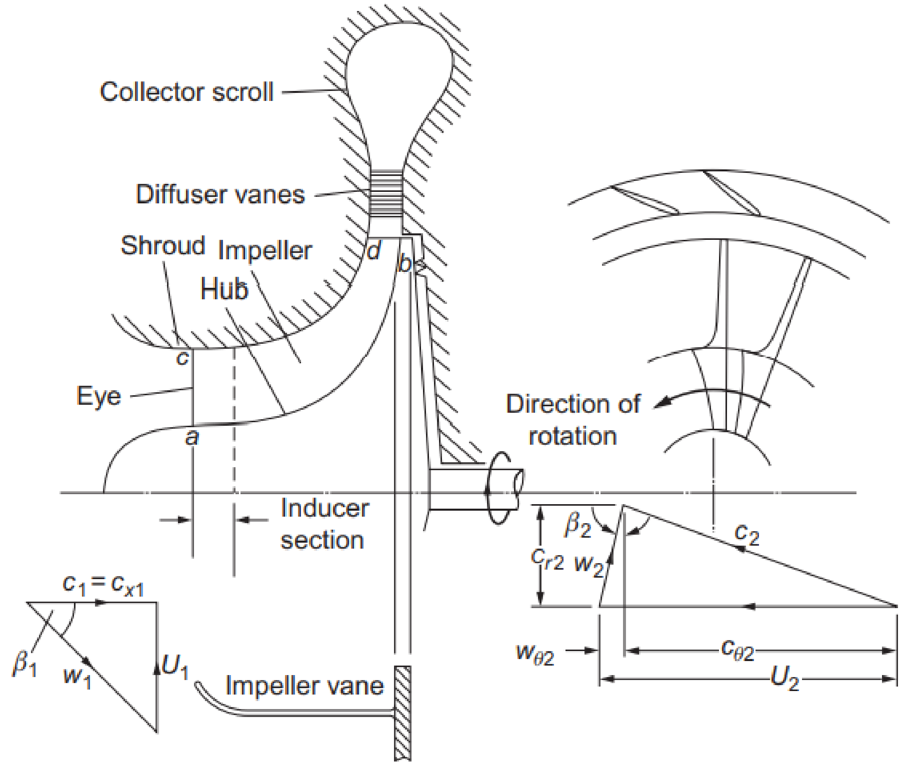

Figure 2.9: Centrifugal compressor stage and velocity diagrams at impeller entry and exit [5]

the relative flow has a velocity w_1 at angle β_1 to the axis of rotation. This relative flow is diverted into the axial direction by the inducer part or spinning guide vanes. The inducer begins at the eye and normally finishes in the part where the flow is beginning to turn into the radial direction [5].

2.5.1.3 Head Increased of a Centrifugal Pump

The real produced head H, calculated as the head difference for the inlet and the outlet of the pump, and is the manometric head, which is less than the ideal head H_i represented in equation 2.39 by the share of the internal losses. The hydraulic efficiency of the pump is as below [5]:

$$\eta_h = \frac{H}{H_i} = \frac{gH}{U_2 c_\theta} \tag{2.39}$$

Then we can make it directly connected to the impeller vane outlet angle by equations 2.41 and 2.40:

$$H = \eta_h U_2^2 (1 - \phi_2 tan\beta_2)/g \tag{2.40}$$

$$H = \eta_h \sigma U_2^2 \frac{(1 - \phi_2 tan\beta_2^{'})}{g} \tag{2.41}$$

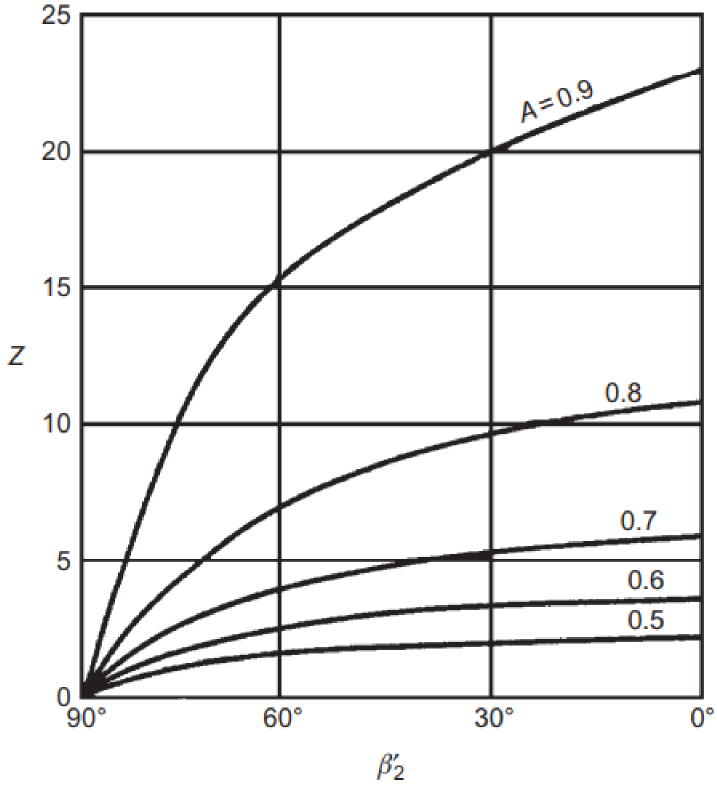

Figure 2.10: Head Correction Factor for Centrifugal Impellers [5]

Centrifugal pump impellers have between 5 and 12 vanes leaned back to the direction of trajectory, with a vane tip angle β_2' of between 50° and 70°. An understanding of blade number, β_2' and ϕ_2 (normally small and on the order of 0.1), commonly allows σ to be determined (Figure 2.10). The effect of slip, it should be considered, drives the relative flow angle β_2 to be larger than the vane tip angle β_2' [5].

2.5.1.4 Thermodynamic Analysis of a Centrifugal Pump

The flow via a centrifugal pump stage is a complex 3D movement and a full examination shows many problems. We can get approximate explanations by flow model simplification, e.g., by using the so-called 1D technique that considers that the fluid is uniform over specific flow cross sections. These cross sections are taken before and after the impeller as well as at the inlet and exit of the entire turbomachine. Where inlet vanes are used to give prerotation to the fluid joining the impeller, the 1D approach is not valid anymore and an extension of the analysis is then needed [5].

$3D$ motion has three components of velocity, c_r, c_θ, and c_x, in the radial, tangential, and axial directions which gives $c = c_r^2 + c_x^2 + c_\theta^2$. From previous equation2.6, rothalpy can be written by the new relation 2.42 [5]:

$$I = h + \frac{1}{2}(c_r^2 + c_x^2 + c_\theta^2 - 2Uc_\theta) \tag{2.42}$$

From the velocity triangle, $U - c_\theta = w_\theta$, and $w^2 = c_r^2 + w_\theta^2 + c_x^2$ it become:

$$I = h + \frac{1}{2}(w^2 - U^2) \tag{2.43}$$

$$I = h_{o,rel} - \frac{1}{2}U^2 \tag{2.44}$$

Across the impeller $I_1 = I_2$, so it gives equation 2.45:

$$h_2 - h_1 = \frac{1}{2}(U_2^2 - U_1^2) + \frac{1}{2}(w_1^2 - w_2^2) \tag{2.45}$$

The equation 2.45, shows why the static enthalpy rise in a centrifugal pump is large compared with a single-stage axial type. On the right-hand side of the relation 2.45, the second term, $(1/2)(w_1^2 - w_2^2)$, is the contribution from the diffusion of relative velocity, also obtained for axial pumps. The first term,$(1/2)(U_2^2 - U_1^2)$, is the contribution from the centrifugal action driven by the difference in radius. The connection between the enthalpies at state points 1 and 2 can be traced in Figure 2.11 [5].

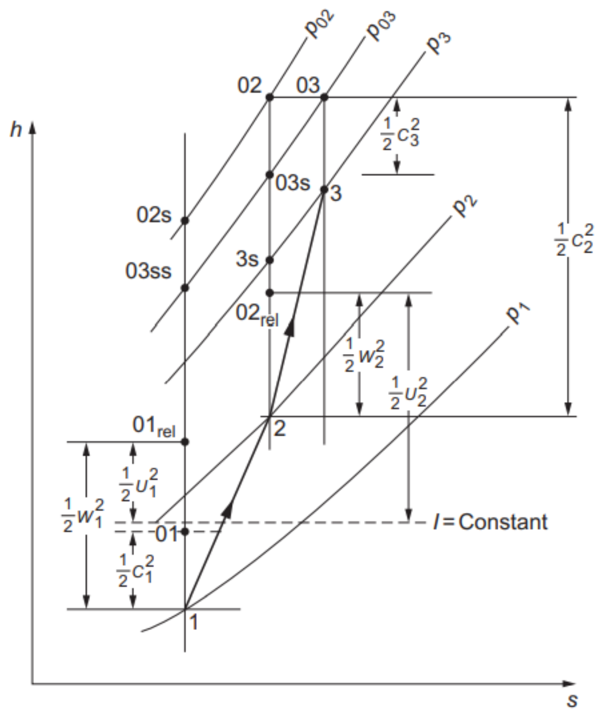

Figure 2.11: Moiler Diagram for the Pump Stage [5]

According to Figure 2.11, and in the inlet velocity diagram, the absolute flow has no whirl element or angular momentum and $c_{\theta 1} = 0$ In centrifugal compressors and pumps, this is normal where the flow is free to join axially. The specific work done on the fluid is written as [5]:

$$\Delta W = h_{o2} - h_{o1} = gH_i \tag{2.46}$$

For hydraulic turbomachines (like pumps), where H_i (the "ideal" head) is the total head rise through the pump without all internal losses. In high-pressure ratio pumps, it may be necessary to impart prerotation to the flow entering the impeller as a means of a high relative inlet velocity reduction. The outcomes of high relative velocity at the impeller inlet are experienced as Mach number effects in compressors and cavitation effects in pumps. The normal procedure of installing prerotation demands the installation of a row of inlet guide vanes upstream of the impeller, the location depending upon the type of inlet [5].

2.5.1.5 Blade Geometry

Blade geometry is a crucial part of the design for any turbomachine; however, the main parameters are designed based on previous works, we have tried to bring up just the most important equations. It should be noted that for some input values (particularly for the Vista toolbox in ANSYS), we have mentioned the references and the motivations in the methodology section because it is not necessary to go through the detailed geometry analysis papers and repeat them here.
Gulich 2008 [27] has suggested the approximation for the blade thickness is calculated by equation 2.47:

$$e = 0.015 d_2 [\frac{Z_{ref}}{Z}]^{0.4}[1 + 0.25[\frac{U_2}{U_{ref}}]^2][1 + 0.5[\frac{n_q}{n_{q,ref}}]^2] \tag{2.47}$$

e is the blade thickness
Z is the number of blades
Z_{ref} is seven according to table 14.3 Gulich 2008 [27]
U_2 is the blade velocity at the outlet
$U_{2,ref}$ is 100 [m/s] according to table 14.3 Gulich 2008 [27]
$n_{q,ref}$ is 100 according to table 14.3 Gulich 2008 [27]
n_q is a specific speed coefficient
Moreover, to determine the maximum tip velocity for high viscosity it can be written from table 7.2 Gulich 2008 [27] by equation 2.48:

$$U_{tip,max} = 45 - 0.42(n_q/n_{q,ref}) \tag{2.48}$$

2.5.2 Pump Performance

2.5.2.1 Efficiencies in Pump

According to the second law of thermodynamics, we have a portion of energy that will not be converted to functional work in a system. This portion of the energy is considered a loss in the system, which refers to the conversion of the energy to heating the surroundings, or friction loss during the motion. The generated heat in an adiabatic system is due to the potential work conversion. As mentioned before, this heat generation happens because of irreversibility in the system. If the process is isentropic, then there are no irreversibilities; however, for an actual process (which we have in reality), frictions and heat losses exist as irreversibilities to make the process irreversible. For the performance evaluation of a system or a machine, we

can use the concept of a reversible process to determine how efficient a machine is. The performance of a pump or compressor can be defined as the ratio of the reversible (isentropic) work that system could fulfill in absence of irreversibilities to the actual work (or energy conversion to practical work).
The power intake to the pump (or compressor) is consistently smaller than the power provided at the coupling because of exterior energy losses in the bearings, glands, etc. Thus, the general efficiency of the compressor or pump is calculated by equation 2.49 [5]:

$$\eta = \frac{W_{ideal}}{W_{actual}} = \frac{h_{2s} - h_1}{h_2 - h_1} \tag{2.49}$$

Therefore; the hydraulic efficiency for a pump is defined by equation 2.50 [5]:

$$\eta_h = \frac{W_{min}}{W_c} = \frac{g[H_2 - H_1]}{\Delta W_c} \tag{2.50}$$

2.5.2.2 Off-Design

Off-design is considered a situation for turbomachines, in which the mass flow or rotational speed is different than the design point. Design of a turbomachine from scratch requires design point consideration while it has to satisfy the off-design too. This will happen for turbomachines when the mass flow or rotational speed differs from what the designer intended to set the values for the machines. The off-design situation is not an abnormal phenomenon, but it is part of turbomachines' normal working cycle when the pump or compressor deviates from the design point. Since the pump will operate for different mass flows and rotational speeds (according to their working condition for different situations), this applies to the fuel pumps working in the airplane too. Fuel pumps in the airplane have different mass flows according to the flight's stage which is maximum for MTO and minimum for Idle conditions. During take-off, the airplane requires a high mass flow of fuel to power engines strongly for stall avoidance, and for idle the aircraft is stopped to be loaded or unloaded. If mass flow drops then the absolute velocity is decreased, based on the continuity equation. Since off-design conditions might make the pump prone to cavitation so it is highly recommended to carry out off-design analysis and post-processing to figure it out.

2.5.2.3 Cavitation

Cavitation is a phenomenon, according to which, the tiny bubbles in the flow start to break up near turbomachine's blades and cause erosion. The reason behind the cavitation is that the static pressure drops below the vapor pressure in the working fluid for the current temperature. When the pressure increases again then the bubbles start collision. This collision, however tiny for a single bubble collision, causes stress on the blades. This stress will affect the blades (also some other parts like the shaft and hub) in terms of erosion; therefore, after a while, the pump cannot work properly and it will be broken.
As we explained cavitation is a harmful phenomenon that must be avoided or at least its consequences become weakened by some considerations. Besides, this can

rise efficiency too. First, we have to define the net positive suction head (NPSH), which is a head parameter as below equation 2.51 [5]:

$$H_s = (P_o - P_v)/\rho g \tag{2.51}$$

Where P_o is the absolute stagnation pressure of the liquid and P_v is its absolute vapor pressure [5].
As the liquid goes through the impeller, there are shifts in pressure levels. In the surroundings of the impeller blades' leading edges on the suction surfaces, there will be fast growth in velocity and an affiliated decline in pressure. If the absolute pressure of the liquid falls below the vapor pressure then cavitation will happen. The fluid then pushes into the impeller and the active motion of the blades forces the pressure to increase. This pressure gradient makes the cavitation bubbles collapse and the consequent implosion of the bubbles and shock waves leads to a gradual erosion of the blades. Cavitation can also occur near the impeller exit of radial flow and mixed flow impellers where the velocities have larger values. The blade tip of the axial-flow pump is the most vulnerable part for cavitation [5]. The cavitation criteria for vapor pressure related to the blade cavitation coefficient can be found by equation 2.52:

$$P = P_v = P_1 - \sigma_b(\frac{1}{2}\rho w_1^2) \tag{2.52}$$

Where σ_b is the blade cavitation coefficient corresponding to the cavitation point [5].

3

Methodology

3.1 Fuel System Design

3.1.1 Pumps' Arrangement

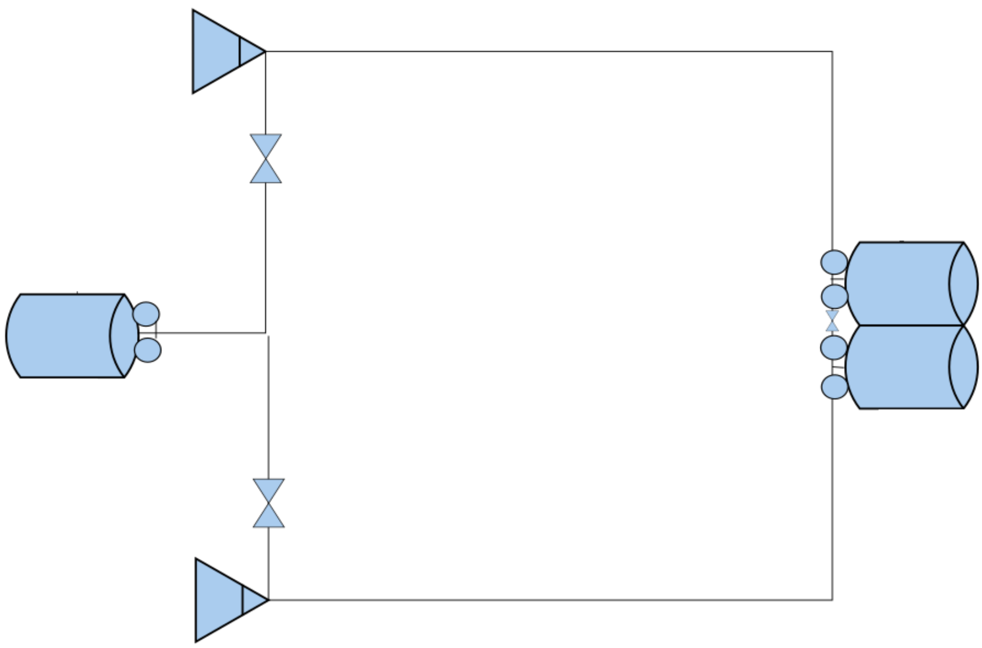

Figure 3.1: Booster Pumps Arrangement (After the joint, the detailed line is not included), The blue circles symbolize booster pumps

The pumps' arrangement refers to how should the pumps be implemented within the fuel system in connection to the tanks and piping system with respect to the regulations [15] as we mentioned before.
The booster pump is the first pump in the fuel line after the tank. The pump is responsible to pressurize the fuel from the tanks and deliver them into the engines' combustion chambers. The booster pump is a crucial component in the fuel system since it has to deliver the fuel to the engines and in case of a problem or crash, the aircraft will be in a dangerous situation. However, the booster pump is not responsible for the high pressurization of the liquid Hydrogen, it should be noted that its responsibility is very important.

According to the regulations, there should be at least one emergency booster pump for each tank to fulfill safety requirements for the airplane. The rationale behind that is for the emergency pump to come to power in case of the main booster pump failure. Since fuel injection to the airplane's engines is a continuous process otherwise the engines cannot work anymore! The airplane has two tanks, the smaller tank is located at the front top of the airplane and the larger one is on top of the aircraft's back. These tanks carry liquid Hydrogen as the system fuel. The tank's design and configuration are not part of this project's scope as we noted previously. The larger tank consists of two identical portions, which means that we have to consider them as two separate tanks to implement booster pumps in accordance.
Therefore, we have three portions of tanks to deliver the fuel for the engines, then in total, we will have six booster pumps shown in Figure 3.1. Four booster pumps are in the same line for the larger tank and two other pumps are on the other side of the cross-feed valves for the smaller one. This arrangement helps the airplane to keep its gravity center while flying to consume fuel equally from the two portions of the larger tank.

3.1.2 Valves

Valves are the hydraulic components, which help the system to deliver the fuel according to the system requirements. The fuel after the booster pump and before the high-pressure pump needs to be handled properly with respect to the safety requirement. We have to implement the appropriate type of valves in this line (from the booster pump to the high-pressure one) for the system. The valves' arrangement for the system is illustrated in Figure 3.2 and Figure 3.5.

3.1.2.1 Corss-Feed Valve

Probably the most important type of valve configuration must be considered for cross-feed valves. Their role is to disturb the flow equally in case of engine failure or booster pump failure. Cross-feed valves balance the fuel distribution between two engines and three tanks if an emergency situation happens. In case of engine failure, in addition to the shut-off valves, the cross-feed valves make sure to disconnect the fuel line from the right engine or the left pipelines completely. Besides, if two booster pumps (the main one and the emergency one) stop working, then the cross-feed valves help the other engine receive the fuel from the other side tank as well until an emergency landing.
There are three cross-feed valves in this design that are shown in Figure 3.1. The first valve is between two portions of the backward tank. This valve can be the most important cross-feed valve to feed the other side engine with the opposite side tank in case of booster pumps fail. The other two valves are between the small tank booster pump and the motor. The valve is open to help the small tank by the main booster pump for both engines feeding. This valve will be closed in an emergency to not support damaged engines for fire prevention. If the main booster pump of the small tanks fails, then the emergency substitute will come to power, and the connected cross-feed valve will operate now. In case of a small tank out of the fuel

cycle, then both cross-feed valves for the front part will be used to disturb the fuel equally from rear portions to both engines.

3.1.2.2 Non-return Valve

Each line of the fuel has to supply the fuel just in one direction. The reason is that we do not want the reverse flow in the pipes to damage the booster pumps and other components. The non-return valves are not necessary for the connection between parallel pumps in front of a single tank or the coupled back portions since in case of an emergency the flow must be able to pass through the parallel pumps to reach the combustion chamber through the cross-feed valves (which we explain later). Besides, this piping portion between two booster pumps for a single tank is small and it does not require reverse flow prevention. (Figure 3.2)

3.1.2.3 Relief Valve

Pipelines or the whole fuel system be likely over-pressured in some cases. Relief valves are one of the handiest solutions to treat such incidences through a configuration. These valves will operate to avoid internal or external damage to the aircraft structure since over-pressurized pipelines can lead to explosions or pipe leakage. The relief valves are implemented per line for each engine. In the case of a twin engines aircraft, this requires two relief valves to make sure the fuel supply will meet the safety regulations. We do not use a relief valve per line of fuel from the booster pump, since the probability of over-pressurization is more likely after the line's joint. In addition, one relief valve can release the pressure through the system and it is not necessary to add more; however, we need two because the cross-feed valve can close half of the system in case of one engine failure, then the other side should be able to operate by itself. (Figure 3.2)

3.1.2.4 Regulator Valve

The mass flow through each line (connected lines to the booster pumps) needs to be specified according to the flight stage. This is very important since we have to support an exact value of mass flow (not more, not less) to have the optimum efficiency for each step. The regulator valves are responsible for controlling mass flow to be compatible with the flight requirements. Each line from the booster pump includes one regulator valve. Every single line from the identical back portions of the large tank needs one regulator valve and the lines from the front tank and two lines, one valve per line (the reason behind having two lines for the smaller tank will be explained later in this chapter). (Figure 3.2)

3.1.2.5 Shut-Off Valve

To stop the flow in emergencies (to prevent explosion), the shut-off valve is used. They are applicable in case of cleaning or repairment as well, to stop the fluid from flowing out. There are four shut-off valves in the system. Two valves are implemented from the small tank lines and the other two valves are in the lines from the large tanks' portions. We do not use shut-off valves after the joint because it is necessary to stop the flow from the back tanks and the front ones separately. This will make it easier to handle the flow individually in case of engine failure or tank problems. (Figure 3.2)

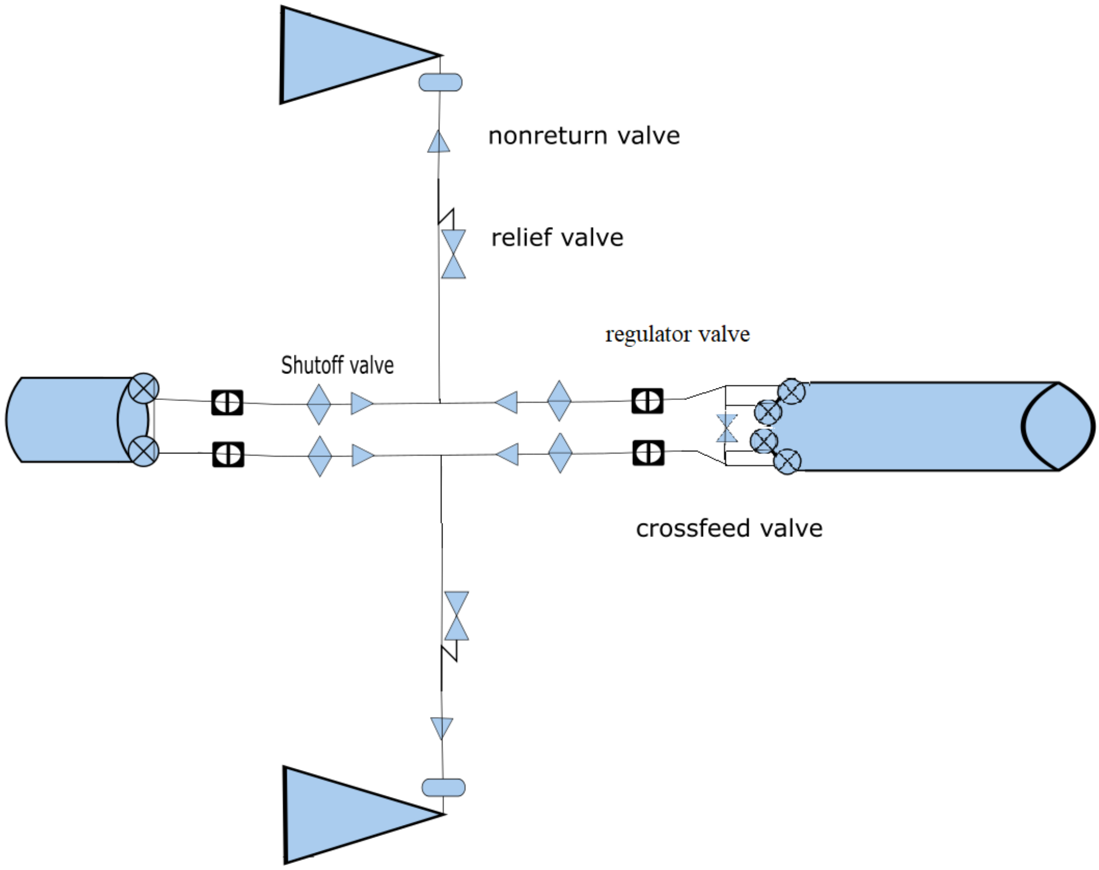

Figure 3.2: Valve's Arrangement

3.1.3 Piping Arrangement

All the hydraulic components are connected through the pipelines from the booster pumps to the combustion chambers. The piping arrangement is implemented based on the available space for the pipes to go through and the minimum possible pressure drop for the system.
As we mentioned before, it should be avoided to implement pipelines through the safe gap (Figure 3.5) in the airplane structure. The pipelines will be embedded in the lower part of the body (below the safe gap), then vertically go down to reach the wings space, where it delivers the fuel to the combustion chambers shown in Figure 3.3. Booster pumps are connected to the pipeline via tees in the rear tanks, either the main pump or emergency; however, the front tank is connected through the two separate pipes to avoid pressure drops. In the case of one-line connection for the front pumps, we have to add a reverse tee for them. It causes big pressure drops and even reverses flow in case of the front booster pump fails, and the other comes into the cycle, so we have implemented two separate lines for them. When

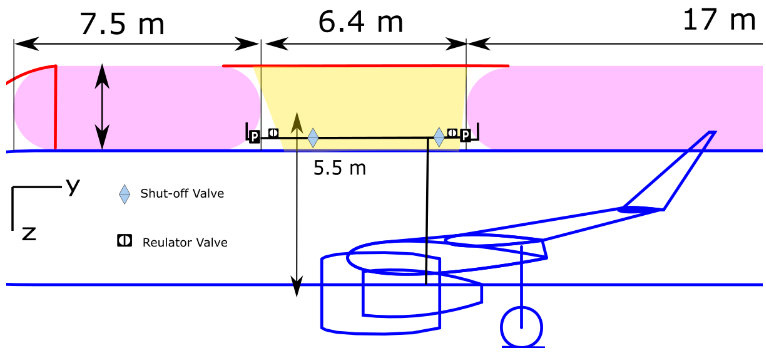

Figure 3.3: Vertical pipeline implementation, yz view

we have vertical or other angled direction changes, elbows are used to change the flow path. We have considered three tees for the system, the first for the booster pump connection, the second for the joint, and the third for the combustion chamber connection. Besides, there are three 90^o elbows in the system, the first is for the B point, the next is in C, and the last one is in point D which are illustrated in Figure 3.4.

The pipeline length for the longest line makes the base calculation for the design. That includes the path from the booster pump to the combustion chamber. The pipe length after the high-pressure pump is also included in this estimation. According to the point references in Figure 3.4 and the dimensions shown in Figure 3.5, we can write total length by equation 3.1:

$$L_{tot} = L_{AB} + L_{BC} + L_{CD} + L_{DE} = (\frac{3.95 - 2.6}{2}) + 3.2 + 5.6 + (5.5 - \frac{2.6}{2}) = 13.67[m] \tag{3.1}$$

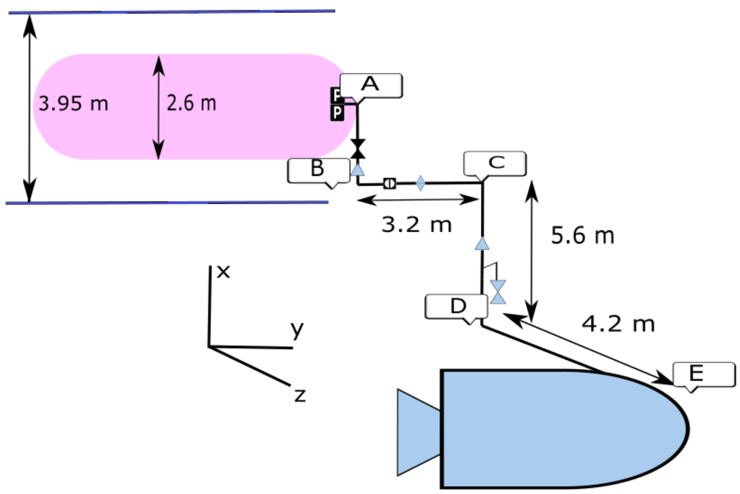

Figure 3.4: Pipeline length from the front tank to the left engine

The length of the pipeline with a safety factor of 50% (1.5 times the total length)is

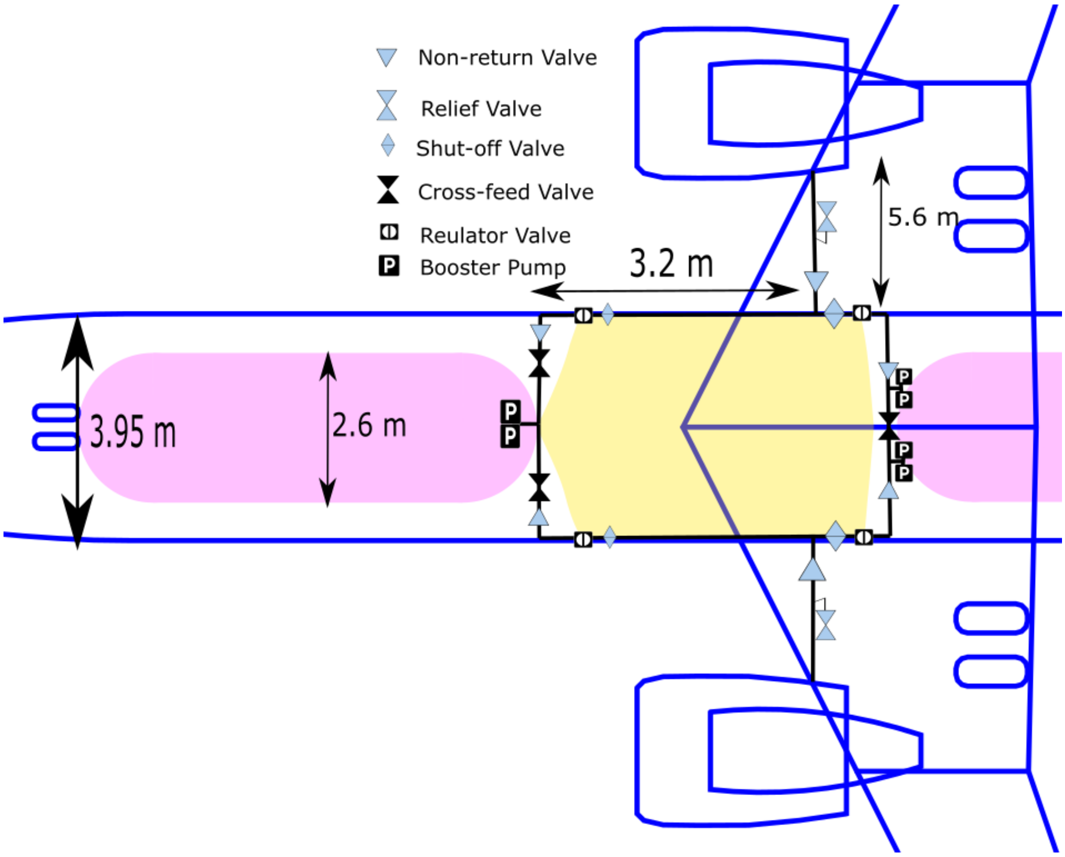

Figure 3.5: A321 Piping Configuration (xy view, the body's width is enlarged to reflect the components

used for calculations accordingly. The pipe diameter will be discussed later in this chapter.

3.2 Basic Calculations

3.2.1 Flow Regime

The first step in arrangement design is to choose the optimum diameter for the pipeline. The diameter is chosen based on the Reynolds number value. We will proceed to determine the flow regime based on the Reynolds number (equation 3.2) as a function of the unknown value for the pipe diameter (d) since we need it as the characteristic length for the Re number calculation. We have used the CoolProps package in Python to call the properties for LH_2 accordingly.

$$Re = \frac{\rho u d}{\mu} \tag{3.2}$$

The flow velocity in the pipe can be calculated through the relation 3.3, where d is unknown:

$$u = \frac{\dot{m}}{\rho \frac{\pi d^2}{4}} \tag{3.3}$$

The pipe should be stainless steel because of the stainless steel 300 series, which is a suitable choice for cryogenic fluid. It can carry the liquid as cold as $20[K]$ (which is compatible with LH_2 at $22[K]$). We will look for the respective pipe in Mohinder 2000 [28]. The pipe diameter is chosen between $1.5'$ to $2.5'$ to have minimum pressure drops. The diameter vs pressure drops reflects an optimum value for the design [1]. As specified by [28] tables for the pipes and tubes, we have chosen the $2'(5.08[cm])$ diameter pipe of stainless steel 300 series for the system as the main line.
Then we can calculate flow velocity and Re number ($\dot{m} = 0.298[kg/s]$, $\rho = 68.866[kg/m^3]$, and $\mu = 1.1535 \times 10^{-5}[\frac{Ns}{m^2}]$):

$$u = \frac{\dot{m}}{\rho\frac{\pi d^2}{4}} = 2.146[m/s] \tag{3.4}$$

And:

$$Re = \frac{\rho u d}{\mu} = 647590.8 \tag{3.5}$$

The Re number is higher than 2000, so our flow regime is considered as turbulent. We will further proceed to calculate head loss and heat loss through the system.

3.2.2 Head Loss

Head loss is a crucial element for predicting what pressure ratio we have to use through the booster pump. This pressure rise for the booster pump is to overcome losses through the system to carry the fuel for the high-pressure pump inlet. Total head loss is due to the two main factors in the system, the first is the hydraulic components, and the second is the piping network. The head loss is measured as a length property with a meter unit (m).
To calculate the head loss, first, we need to evaluate the friction factor for the piping system. The friction factor depends on the flow regime, to find the proper relation for calculation. This is done through python code by defining an $if/else$ condition phrase according to the Re number. In case of a laminar flow ($Re < 2000$) the equation 2.20 gives the f value:

$$f = \frac{64}{Re} \tag{3.6}$$

For the turbulent flow ($Re > 2000$), equation 2.21 shows the friction factor:

$$\frac{1}{f^{1/2}} = -1.8log[\frac{6.9}{Re_d} + (\frac{e/d}{3.7})^{1.11}] = 0.03786 \tag{3.7}$$

The roughness (e) is 0.0005 according to the Fractory [29] for the stainless steel 300 series.
By having the friction factor value, then we will proceed to calculate the head loss through the piping system by equation 2.22.

$$h_f = f\frac{L}{d}\frac{u^2}{2g} = 3.84[m] \tag{3.8}$$

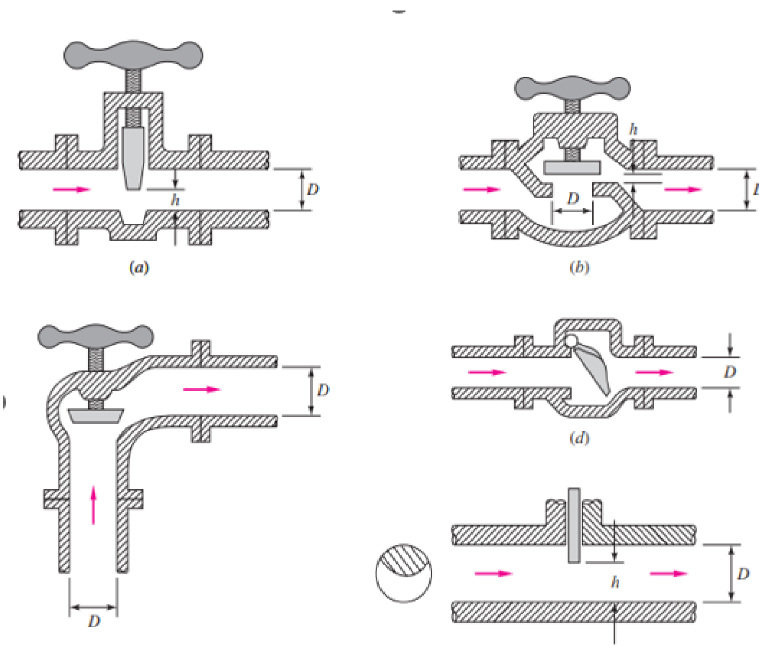

Figure 3.6: (a) gate valve; (b) globe valve; (c) angle valve;(d) swing-check valve; (e) disk type gate valve [7]

Hydraulic components' head loss depends on both valves and fittings. The K value for these calculations needed to be found based on the White 2009 [7], Langton 2009 [30], and Table 2.2. We have considered the longest line as the base calculation for hydraulic components from the rear tank's booster pump to the combustion chamber:

$$K_{Tees(tot)} = 3\Sigma K_{Tee} = 3 \times 0.277 = 0.831 \tag{3.9}$$

$$K_{Elbows(tot)} = 3\Sigma K_{Elbow} = 3 \times 0.6 = 1.8 \tag{3.10}$$

We can assume that the valves shown in Figure 3.6 have similar configurations to the respective valves that are used in the design, then we can determine K values accordingly.
Shut-off valves operate like gate valves with a $K = 0.11$ for flanged type with $d = 2'$,
Regulator valves operate like globe valves with a $K = 5.9$ for a flanged type with $d = 2'$ and,
Non-return valves operate like swing check valves with a $K = 2.0$ for a flanged type with $d = 2'$ (This K needs to be doubled because we have two non-return valves).
We do not consider head loss through the relief and crossfeed valves, since they do not operate normally in the system. In the case of the relief one, it has a separate line for relief, so it would not cause pressure drops. The Crossfeed valve's pressure drop is ignorable because their performance is on/off, so they will be completely open or closed in the system.

$$K_{Valves(tot)} = \Sigma((2 \times 2+)5.9 + 0.11) = 10.01 \tag{3.11}$$

Now we can sum up K values for all hydraulic components:

$$K_m = \Sigma 12.641 \tag{3.12}$$

So the head loss is:

$$h_m = \Sigma K \frac{u^2}{2g} = 3.34[m] \tag{3.13}$$

Therefore, the total head loss in the systems is:

$$h_{tot} = 3.34 + 3.84 = 7.18[m] \tag{3.14}$$

This head loss seems to be a small value, especially when we consider the respective pressure drop:

$$P_{Loss} = \rho_{LH2} g h_{tot} = 68.866 \times 9.81 \times 7.18 = 4850.63Pa = 4.85[kPa] \tag{3.15}$$

This value for pressure drop is small, so it will not be a determinative factor for the pressure rise through the booster pump. We discuss this in the pump's preliminary design section.

3.2.3 Heat Loss

It is necessary to consider heat loss through the system because the liquid Hydrogen is in cryogenic condition, and it is a must to avoid its vaporization as much as possible.
The pipeline insulation is considered similar to the vacuum-insulated pipes for liquid natural gas because both are kept in cryogenic conditions. The insulation material is polyethylene for vacuum-insulated design based on the [6]. Vacuum-jacket types of pipes are the best choice for the system and referring to the [31].
According to the [32], the k leakage factor for the vacuum-jacket pipe is 0.72 $[BTU/hrft]$ ($= 0.498[W/m]$) for a $2'$ pipe diameter.

$$\dot{Q}_{Leakage} = \ k_{Leakage} \times L = 0.498 \times 20.5 = 10.218[W] \tag{3.16}$$

The heat capacity for the liquid hydrogen is $C_P = 10781.609[J/kgK]$ (based on the CoolProp value), therefore; the temperature rise for the MTO stage (highest mass flow rate) is:

$$\Delta T = \frac{\dot{Q}_{Leakage}}{C_P \dot{m}} = \frac{10.218}{0.298 \times 10781.609} = 0.00318[K] \tag{3.17}$$

This value is small, and we can ignore it.

3.3 Booster Pump Preliminary Design

3.3.1 Pressure Ratio and Head Rise

To find out the suitable outlet pressure for the booster pump, we have to guess the pressure ratio through the pump. This pressure increase from the inlet pressure of 1.6 *bar* to a value that satisfies system criteria. The booster pump pressure ratio needs to minimize the booster pump's cavitation and prevent cavitation for the high-pressure pump downstream. To avoid cavitation in the high-pressure pump,

we will go through an iterative process. First, we will guess an outlet pressure for the booster pump, this outlet pressure is assumed to be the same as the high-pressure pump inlet. Then the high-pressure pump pressure ratio is known, as we had already a high-pressure pump's outlet. Then we check the cavitation criteria for a high-pressure pump. The flowchart for iteration is illustrated in Figure 3.7.
The first guess (1.8 *bar*), and the second guess (2.5 *bar*) did not work because of the cavitation criteria for the high-pressure pump. Then we proceeded with a pressure ratio of 2.3 (results in $P_2 = 3.68 bar$), accounting the pressure loss ($P_{Loss} = 4850Pa$ and P_3 is the high pressure pump inlet):

$$P_3 = P_2 - P_{Loss} = 368000 - 4850 = 363150[kPa] \tag{3.18}$$

CoolProp gives us the saturation pressure for the high-pressure pump inlet as $P_v = 168993.5[Pa]$.

$$NPSH = \frac{363150 - 168993.5}{68.596 \times 9.81} = 288.5[m] \tag{3.19}$$

Considering the total head losses in the system due to the pipeline friction and valve pressure drop, we deem this to be an acceptable value for the pressure ratio, although we do not have sufficient information about the $NPSHr$ (required head) by the high-pressure pump.
The head rise through the booster pump is the main parameter to input in Vista to generate the design. The head rise is a key factor for pump design as we mentioned before. We can calculate the head rise as below:

$$H_{rise} = \frac{P_2 - P_1}{\rho g} = \frac{368000 - 160000}{9.81 \times 68.687} = 308.6[m] \tag{3.20}$$

This head rise must be done by the booster pump as a single component. Since the liquid Hydrogen is a low viscosity fluid, we will design the booster pump as a multi-stages pump to generate the whole head rise. Moreover, the multistage pump will cover a more extensive pressure range for the case, which has a positive aspect for our case performance.
We want to disturb the head rise per stage efficiently. Multistage centrifugal pumps deliver better efficiency due to more sealed impeller clearances and shorter impeller diameters. Design requires a head rise of almost $100[m]$ per stage to be able to operate with low mass flow and high rotational speed. We have chosen three stages for the case. This can be written as:

$$H_{perstage} = \frac{H_{Rise}}{N_{stages}} = \frac{308.6}{3} = 102.8[m] \tag{3.21}$$

3.3.2 Non-Dimensional Numbers in Booster Pump

Dimensionless numbers are parameters that can help us to determine design factors for the pump to achieve maximum efficiency. We have used the Gulich 2008 [27] values to choose the appropriate non-dimension numbers for the perfect design.
Referring to table 2.3 of Gulich 2008 [27] for the radial pump with the maximum head rise of $400[m]$, we can consider $n_q = 50$ and $\psi = 0.45$ for the optimum design point.

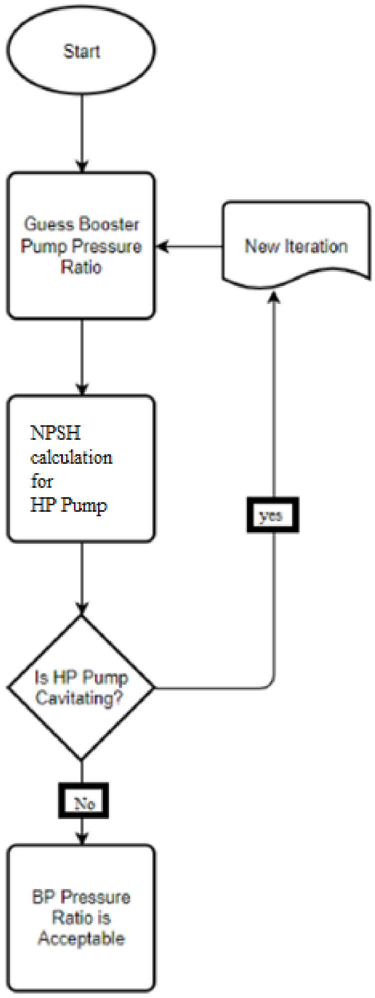

Figure 3.7: Iterative Process

It gives us the optimum Ω_s according to the equation 2.35:

$$\Omega_s = \frac{n_q/52.9}{2} = 0.472 \tag{3.22}$$

By having Ω_s, we can write the respective function in CoolProp to obtain Ω and r_2 (impeller outlet radius) based on two equations 2.36 and 2.37:

$$\Omega_s = \frac{\Omega\sqrt{Q}}{(gH)^{0.75}} = \frac{\Omega \times \sqrt{0.00433}}{(9.81 \times 102.8)^{0.75}} = 0.472 \tag{3.23}$$

$$\psi = \frac{2gH}{(\Omega r_2)^2} = \frac{2 \times 9.81 \times 102.8}{(\Omega r_2)^2} = 0.45 \tag{3.24}$$

It should be noted that H here is the head rise per stage as we already calculated. Q as the volumetric flow rate is:

$$Q = \frac{\dot{m}}{\rho} = \frac{0.298}{68.687} = 0.00433[m^3/s] = 15.578[m^3/hr] \tag{3.25}$$

By solving equations 3.23 and 3.24 then we have :

$$\Omega = 1283.6[rad/s] = 12312[RPM] \tag{3.26}$$

And,

$$r_2 = 0.0368[m] \tag{3.27}$$

Finally, we can write the flow coefficient based on equation 2.38 [8]:

$$\phi = \frac{Q}{0.5\Omega D_2^3} = \frac{0.00433}{0.5 \times 1283.6 \times (2 \times 0.0368)^3} = 0.0169 \tag{3.28}$$

3.3.3 Efficiency of the Booster Pump

To obtain the thermodynamics values after the booster pump, we need to have an extra property in addition to the outlet pressure (as we have based on the iterative process). Although we can assume the density constant, it has a very slight change that is necessary for CoolProp calculations. State 1 is the booster pump inlet from the tank and state 2 is the booster pump outlet.
In agreement with fundamental thermodynamic relations for enthalpy/efficiency we can write equation 3.29:

$$h_2 = \frac{h_{2s} - h_1}{\eta_{BP}} + h_1 = \frac{20492.26 - 17475.88}{75\%} + 17475.88 = 21497.72[kJ/kg] \tag{3.29}$$

h_2 is the real enthalpy for state 2 and the h_{2s} is its isentropic enthalpy, which is obtained from the CoolProp by having two properties, P_2 and $s_2 = s_1$.
η_{BP} is the booster pump efficiency that is unknown at this stage; thus, we have guessed the value of 75%. This efficiency must be reasonable according to the Vista efficiency prediction (48%) and final CFD results, so it is also an iterative process with the first guess of 50%, and the second, guess of 60%.
Now, we have enthalpy in state 2 plus the pressure outlet to determine other properties.

3.4 Booster Pump CFD Design

3.4.1 Geometry

Blade and Impeller geometry are key factors for turbomachines (particularly pumps) in design. Blade affects the flow motion, pump efficiency, cavitation and performance. Booster pump design requires blade consideration as well, we have chosen several design parameters based on literature suggestions.

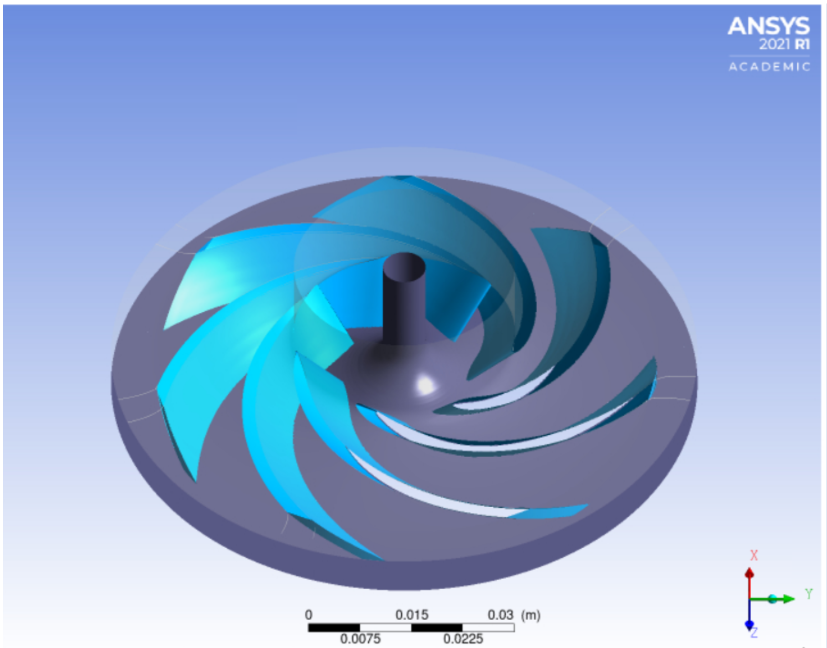

Figure 3.8: Pump Geometry

3.4.1.1 Operating Conditions

Flow inlet angle is considered to be $\alpha_1 = 90^o$ according to the ANSYS user guide [8] as by default, Gulich 2008 recommendations [27] and Li 2020 [33]. This approach's flow angle is without pre-rotation.
We set the meridional velocity ratio as 1.1 by default.

3.4.1.2 Hub Diameter

The hub diameter section consists of two subsections, shaft minimum diameter factor, and hub diameter to the shaft diameter ratio. These settings are the same as by default respectively 1.1 and 1.5.

3.4.1.3 Leading Edge Blade Angles

That by-default selection is also the case for the leading edge blade angles of the hub and mean-line as 19^o by cotangent method calculations [8].

For the shroud tab, we have to specify either the incidence angle or shroud blade angle in case of the user-defined choice. The default value for incidence is zero ($i = 0^o$) based on the ANSYS user guide for TurboGrid. We will determine the shroud blade angle by referring to the previous studies on centrifugal pump performance like Design and Optimization of a Centrifugal Pump by Alawahedi2021 [34], and The Influence of Blade Angle on the Performance of Plastic Centrifugal Pump by Li 2020 [33]. The optimum range is between 19^o to 23^o, and we have chosen the average value of 21^o to input for Vista.

3.4.1.4 Tip Diameter

For this tab, we already have the head coefficient factor as 0.45 based on the equation 2.38 to use in Vista.

3.4.1.5 Trailing Edge Blade Angles

The blade angle in the trailing edge is the most significant angle to specify for the pump design because its role in flow separation is determinative. This angle specification is shown is Figure 3.9. This angle is chosen according to the The Li 2020 [33], and Gundale 2013 [35] in a range of 16^o to 25^o. According to Gulich 2008 [27], this value should be chosen not calculated. Therefore, the value of 22.5^o is selected for Vista. This value can be modified later in BladeGen with respect to the possible flow separation issues.
The rake angle is the second sub-value to be selected in this tab. The value of is zero by default. Previous studies have shown that small positive values for the rake angle can improve the performance of the radial turbomachines Ariga 1998 [36]. Thus, we have decided to proceed with the rake angle of 2^o.

3.4.1.6 Number of Vanes and Vane Thickness

The number of the vanes is typically 5 to 9 Yadav 2016 [37], but for the majority of cases, 6 or 7 vanes are a practical selection according to Korkmaz 2017 [38]. Besides, the trailing edge blade angle is 22.5^o representing an optimum choice for 6 or 7 vanes according to Figure 3.10. It should be noted that the number of the vanes can be added later in case of flow separation that requires more blades to have additional control on the flow. Consequently, the seven number of vanes is considered in this stage.
Finally, we need to find the thickness (e) to tip diameter (d_{tip}) ratio. First, we have to find the blade thickness based on the previous equation 2.47, and table 14.3 from Gulich 2008 [27]. The reference values for $U_{ref} = 100[m/s]$, $Z_{ref} = 7$, and $n_{q,ref} = 100$.
This empirical equation is valid up to the ten blades, and according to the CoolProp's result for $d_2 = 2r_2 = 73.6[mm]$, then:

$$U_2 = r_2\Omega = 47.23[m/s] \tag{3.30}$$

$$e = 0.015d_2[\frac{Z_{ref}}{Z}]^{0.4}[1 + 0.25[\frac{U_2}{U_{ref}}]^2][1 + 0.5[\frac{n_q}{n_{q,ref}}]^2] \tag{3.31}$$

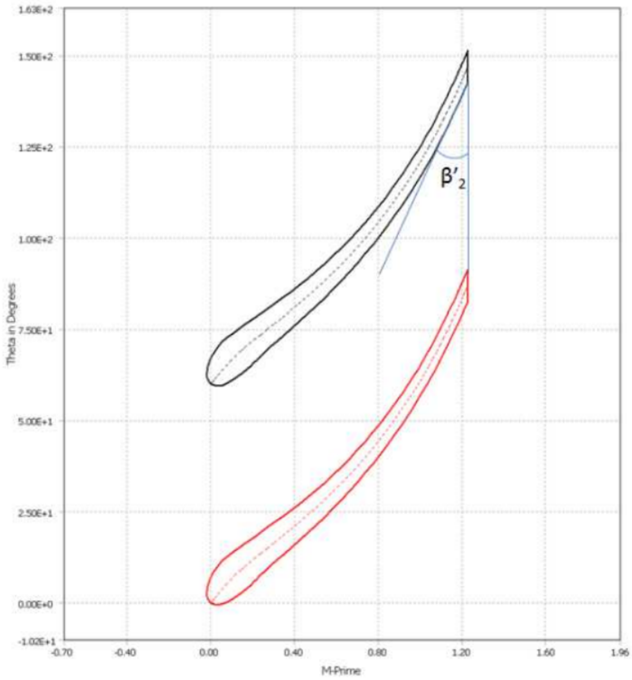

Figure 3.9: Trailing edge blade angle [8]

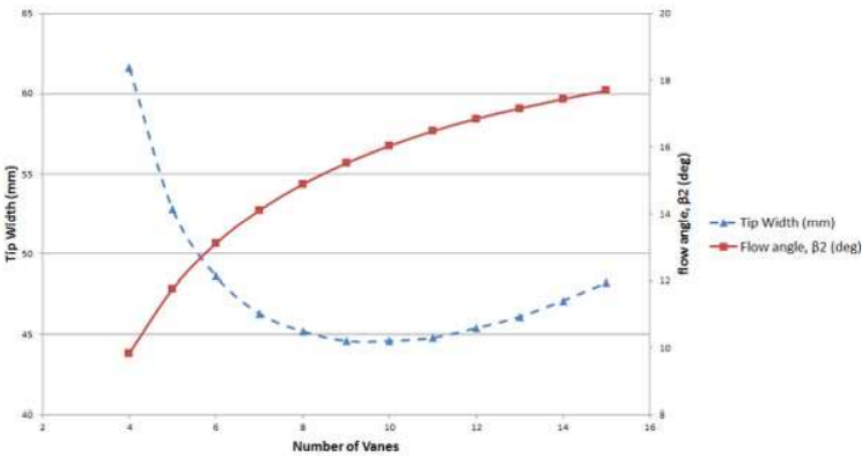

Figure 3.10: Influence of the Number of Vanes on Impeller Tip Width and Relative Flow Angle at the Trailing Edge [8]

And,

$$e = 0.015 \times 0.0736[\frac{7}{7}]^{0.4}[1 + 0.25[\frac{47.23}{100}]^2][1 + 0.5[\frac{50}{100}]^2] = 0.00131[m] \quad (3.32)$$

Now, we have to determine a valid number for tip diameter. This can be done according to the equation 2.48, and table 7.2 from Gulich 2008 [27]to find optimum values for tip velocity followed by tip diameter. The maximum value for more than 3 blades with $n_{q,ref} = 1$ is :

$$U_{tip,max} = 45 - 0.42(n_q/n_{q,ref}) = 45 - 0.42 \times 50 = 24[m/s] \quad (3.33)$$

It results in $d_{tip,max} = 37.2[mm]$. The minimum value for tip velocity is $U_{tip,min} = 12[m/s]$ as stated in Gulich [27], to gives the value for tip diameter($d_{tip,min}$) of 18.6 [mm]. The average value is 27.6 [mm], which is for high viscosity/density fluid according to the reference. Therefore, a coefficient of 2.0 is considered to make that applicable for low viscosity/density fluid. An approximation of 50 [mm] for tip diameter is valid, then blade thickness to tip diameter ratio is:

$$e/d_{tip} = 1.31/50 \simeq 0.026 \quad (3.34)$$

The hub inlet draft angle is the same as the default value of 30^o.
Since we have flow separation with the current geometry, we have modified the design in BladeGen to generate a new blade configuration less susceptible to flow separation. That is done via blade thickness and blade trailing edge angle adaptations.

3.4.2 Mesh

To generate the design, we have to mesh the centrifugal pump as a primary step toward CFD analysis. The meshing has been done through TurboGrid. Ansys TurboGrid automates the generation of high-quality hexahedral meshes required for blade passages in revolving machinery. TurboGrid reduces mesh dependencies when analyzing distinctions in performance predictions among designs.

3.4.2.1 Global Size Factor

In mesh size, we have used the global size factor method with a size factor of 2.5. This is due to the fact that increasing the size factor will make the mesh resolution better (from the default value of 1.0). However, if we choose boundary layer refinement the overall mesh size will change, but the size factor is constant. It should be noted that the change in overall mesh size is not linear.

3.4.2.2 Boundary Layer Refinement

The boundary layer area is characterized by the set of topology blocks along the sides of the blade. Boundary layer refinement control needs to be set for the mesh too. The Method selections can be proportional to mesh size or first element offset. We have chosen the second option as the method for boundary layer refinement.

Parameters offset size should be specified in that case. First, we have to calculate the impeller Reynolds number:

$$Re = \frac{D^2_{impeller}\Omega\rho}{\mu} = \frac{(0.0736)^2 \times 1283.6 \times 68.687}{1.1535 \times 10^{-5}} = 4.1403 \times 10^7 \tag{3.35}$$

After the Reynolds number calculation, we have to use empirical equations to find the first element size height from the wall. We have tried two approaches to find the optimum value for prism layer thickness. The first approach is based on the equation 3.36 from the Boundary Layer Theory by Schlichting [39] for turbulent flow:

$$\delta(x) = \frac{0.37x}{Re^{(1/5)}} = \frac{0.37 \times 0.0736}{(4.1403 \times 10^7)^{(1/5)}} = 8.159 \times 10^{-4}[m] = 800[\mu m] \tag{3.36}$$

The second approach is according to the Volupe online platform [40] as y+ calculator to find the first cell height. To input appropriate values for the solver, we need to find stream velocity. We have used the average value for inlet velocity (2.146[m/s]) and the local velocity for the fluid adjacent to the blade tip ($U = U_{2,tip} = 47.23[m/s]$), equal to 24.6 [m/s]. Characteristics length is equal to the impeller diameter, and dynamic viscosity and density are the same as previous values. It results in the first cell height value of 0.22 [μm] in offset input.
Initially, the first approach is used, but it will make the mesh very coarse and leads to error in mesh for trailing edges. The second approach value makes the total number of elements very large, so it makes the simulation costly. Therefore, we will proceed with the higher number for the prism layer height as 1[μm].

3.4.2.3 Expansion Rate

The box for constant first element offset is checked to be able to specify the expansion rate. Since we do not have a cut-off in the leading edge/trailing edge, the default value of 1.0 is not touched.
Target maximum expansion rate is available also when the constant first element offset is checked. This option allows determining the maximum expansion rate for the TurboGrid to prevent it from exceeding by several methods like boundary layer refinement. The maximum expansion rate is chosen to be 1.3 to reduce the mesh overall volume. The mesh data is represented in Tables 3.1 and 3.2. Also, the trailing edge meshing in Figure 3.11, leading-edge meshing in Figure 3.12 near the wall, and overall meshing in Figure 3.13 are illustrated.

Node	Number
all domains	3447547
passages	3302210
inlet	145337

Table 3.1: Mesh generator node counts

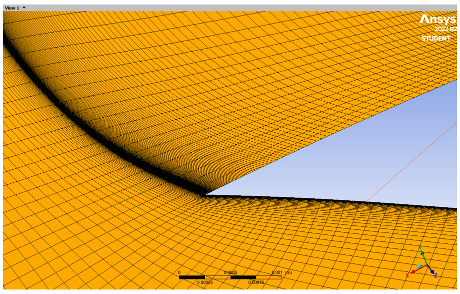

Figure 3.11: View 2 Trailing Edge Boundary Layer Mesh

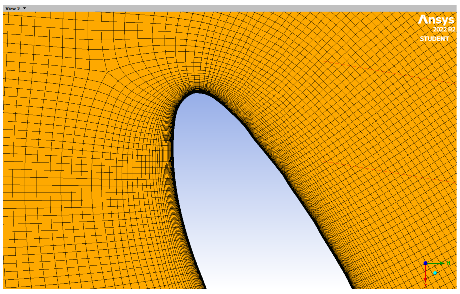

Figure 3.12: View 2 Leading Edge Boundary Layer Mesh

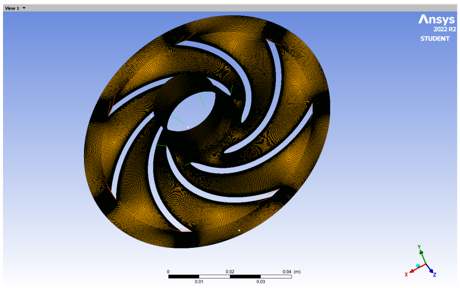

Figure 3.13: View 1 TruboGrid Mesh

Elements	Number
all domains	3326540
passages	3191020
inlet	135520

Table 3.2: Mesh generator element counts

3.4.3 Solver Settings

After transferring data from the TurboGrid to the CFX, it requires to make the settings compatible with the booster pump design case. This solver can create the appropriate approach for CFD analysis of turbomachines. The Turbo Mode is selected for configuring the pump's different parts and components for specifying boundary layers and other input values.

3.4.3.1 Material

The function fluid in this study is liquid hydrogen. The Hydrogen properties are listed in the PH_2 file with respect to their thermodynamic states; therefore, it is necessary to define it as new material to transfer the data. The thermodynamic state for the LH_2 is considered to be liquid since we are dealing with liquid hydrogen in a saturation state.

3.4.3.2 Basic Settings

Domain type is chosen fluid domain since we have a liquid phase, then LH_2 is added to the basic settings tab.
Morphology is continuous fluid for our case when we try to study fluid mechanics' behavior excluding cavitation in this stage.
The reference pressure is set to $0bar$ to ease our calculation and discussion of the results.
Domain motion is considered rotating (with 12312 RPM) because the domain revolves with a specified rotational speed relevant to the global Z axis.
The gravity effect is not influential for the case, so the buoyancy model is set to non-buoyant.
Since our geometry does not vary, so we do not use the mesh deformation option.

3.4.3.3 Fluid Model

For heat transfer, the thermal energy option is for low-speed fluid, which is not preferable for sub-cooled liquid like cryogenic hydrogen. The third option isothermal does not consider heat transfer through the pump. Thus, the heat transfer is selected as total energy, which includes high-speed energy effects.
To have accurate boundary layer simulations, the shear stress transport model is chosen for the turbulence model by automatic wall function. Moreover, the adverse pressure gradient in the pump requires highly accurate predictions of the onset and the amount of flow separation.
Combustion and radiation boxes are unchecked because the fluid does not react in the pump.

3.4.3.4 Boundary Conditions

The inlet boundary condition for INBlock INFLOW is chosen as total pressure of 1.6 bar with a total temperature of 22.0211 K. The flow regime is subsonic, and the flow has just one cylindrical component for axial direction.
The outlet boundary condition for Passage OUTFLOW is chosen as a mass flow rate of 0.298 [kg/s] (for all total sectors), The flow regime is subsonic here as well.

3.4.3.5 Initialization

The frame type is stationary relative to the machine. Initialization for static pressure comparative to reference pressure is $1.6bar$ and temperature $22K$. The initial values are selected due to the liquid hydrogen initial condition in the tank to accelerate the simulation and calculation.
The turbulence model needs to be specified as well. For fully developed flow [41], we can find the turbulence intensity by equation 3.37:

$$I = 0.016Re^{(\frac{-1}{8})} = 0.016 \times 4.1403 \times 10^{7} = 0.01786 \tag{3.37}$$

Therefore, the low-intensity (1%)turbulence model is chosen.

3.4.3.6 Solver Control

The high-resolution choice utilizes high-resolution advection and a high-resolution transient scheme for the solver, both for the advection scheme and turbulence numeric.
The maximum number of iterations is 400 because, after that based on the later simulation, there will be oscillating residual for the rest of the simulation.
For fluid timescale control, the auto timescale option is chosen. Also, for the length scale option, the conservative is selected.
The residual target is considered 10^{-6}.

3.4.4 Off-Design

To simulate the off-design performance of the booster pump it is necessary to check the CFD simulations for those situations too. To create the off-design cases, mass flow and rotational speed are subject to change. It can take a range from 30% to 110% relative to design point mass flow and rotational speed. However, for some lower rotational speeds, the mass flow is required to be compatible to run the case smoothly; otherwise, if the pump cannot carry the duty then the simulation will crash.

4

Results and Discussion

The results of the CFD simulation of the booster pump and the final fuel system configuration are presented in this chapter. In addition to the design point contours and charts, we have added the off-design cases too. Design "A" is the early design with the first blade geometry, and design "B" is the modified design based on the new blade geometry.

4.1 Fuel System Arrangement

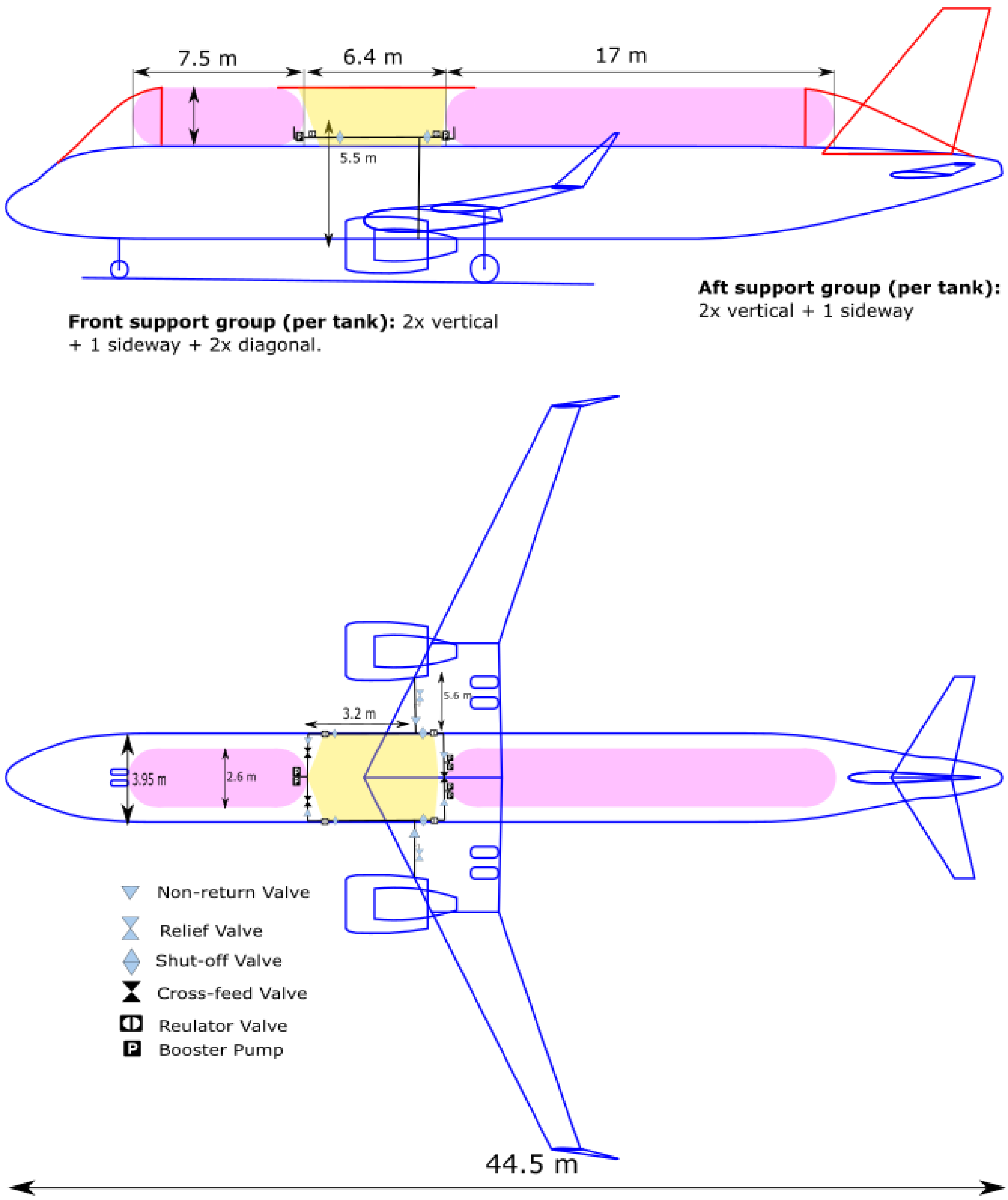

Figure 4.1: LH_2 fuel system configuration for Airbus A321

Figure 4.1 shows the final proposed fuel system for the Airbus A-321 with mentioned hydraulic components.

4.2 Design "A" for Booster Pump Performance at Design Point

Parameter	Value	Unit
mass flow	0.298	kg/s
volumetric flow	0.00434	m^3/s
rotational speed	12312	RPM
head	147.41	m
shaft power	449.86	W
total efficiency	95.75	%
static efficiency	69.58	%
pressure ratio	1.46	-

Table 4.1: Booster Pump General Characteristics for Design "A" at Design Point

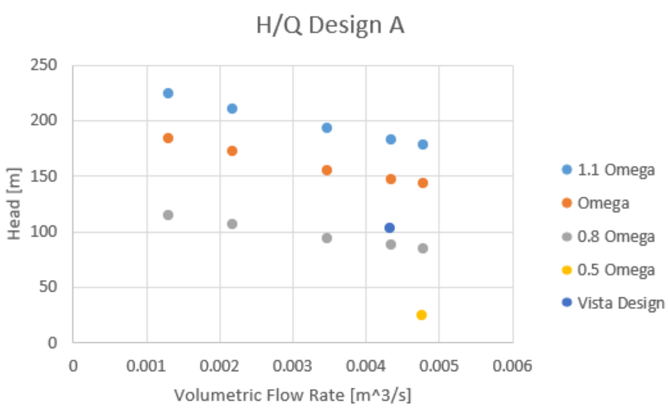

Figure 4.2: Pump "A" characteristic curve (Head Rise Per Stage/Volumetric Flow Rate)

Figure 4.2 shows the design "A" performance. Increasing rotational speed increases the head rise per stage by the pump for off-design cases, but volumetric flow rate growth will decrease the head rise per stage by the pump.

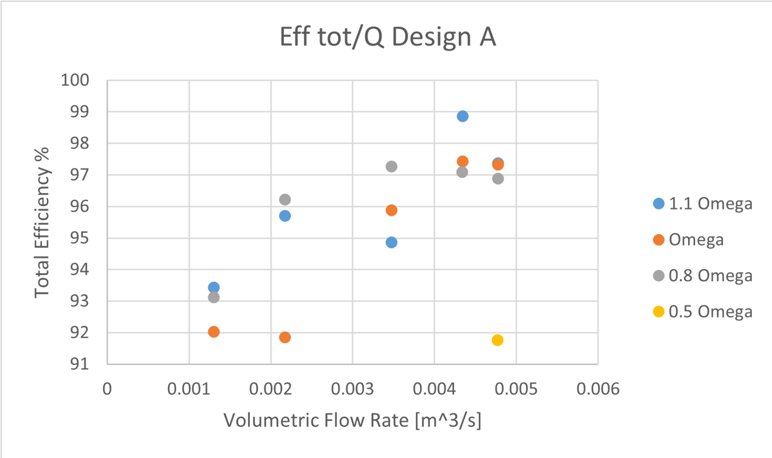

Figure 4.3: Pump "A" characteristic curve (Total Efficiency/Volumetric Flow Rate)

Figure 4.3 shows the design "A" performance. The volumetric flow rate increase will rise the efficiency in general except for the off-design point with the rotational speed equal to half of the design point. In general, higher rotational speed has increased the efficiency; however, for rotational speed at design points, where we have a low volumetric flow rate, the efficiency drops. In general, we have high efficiency for the pump, which can be due to several reasons. For example, in this study, the cavitation model is not considered in the simulation, which can affect the efficiency drastically, particularly because the liquid hydrogen is in saturation condition. Additionally, the calculated shaft power which is used to obtain the efficiency by the solver is not the real shaft power. Because it has not considered disk friction on the front and back cavities of the impeller, leakage flow power loss through the front and rear seals, and bearing windage power losses.

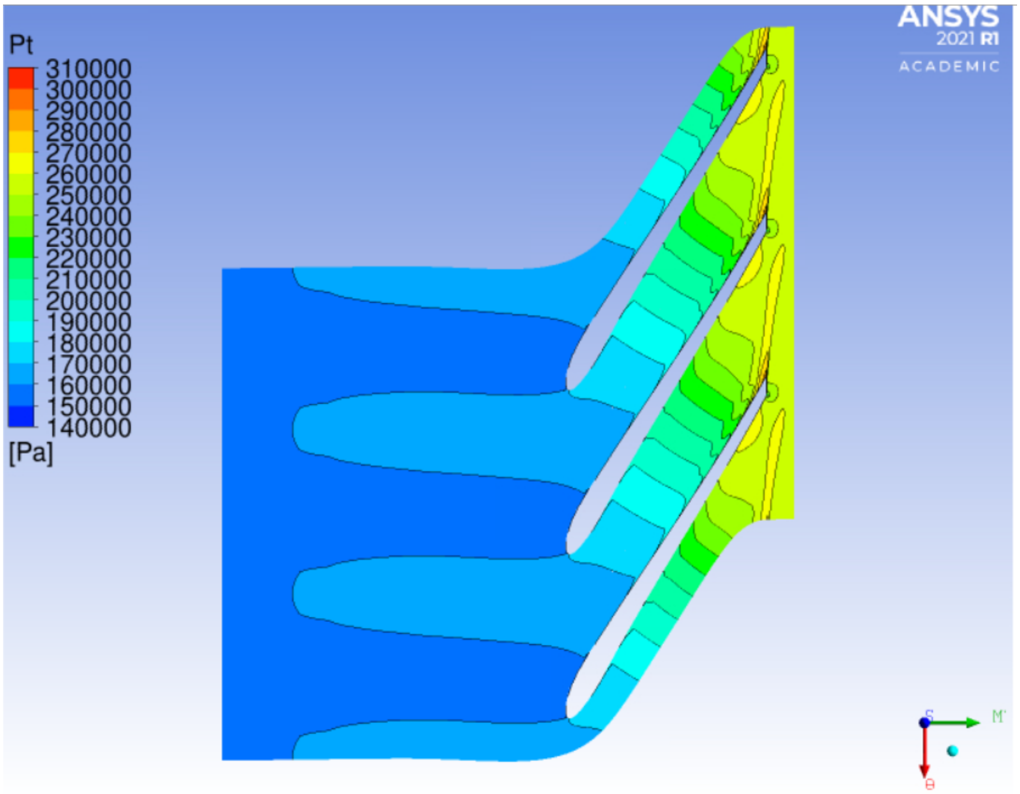

Figure 4.4: Total pressure contour, blade to blade view

Figure 4.4 shows the total pressure for the blade-to-blade view of case A. The pressure gradient gradually increases from the $1.4 bar$ to around $2.4 bar$. The highest pressure ($3.1 bar$) happens near the blade trailing edge, and these pressure gradients make the blades susceptible to mechanical stresses.

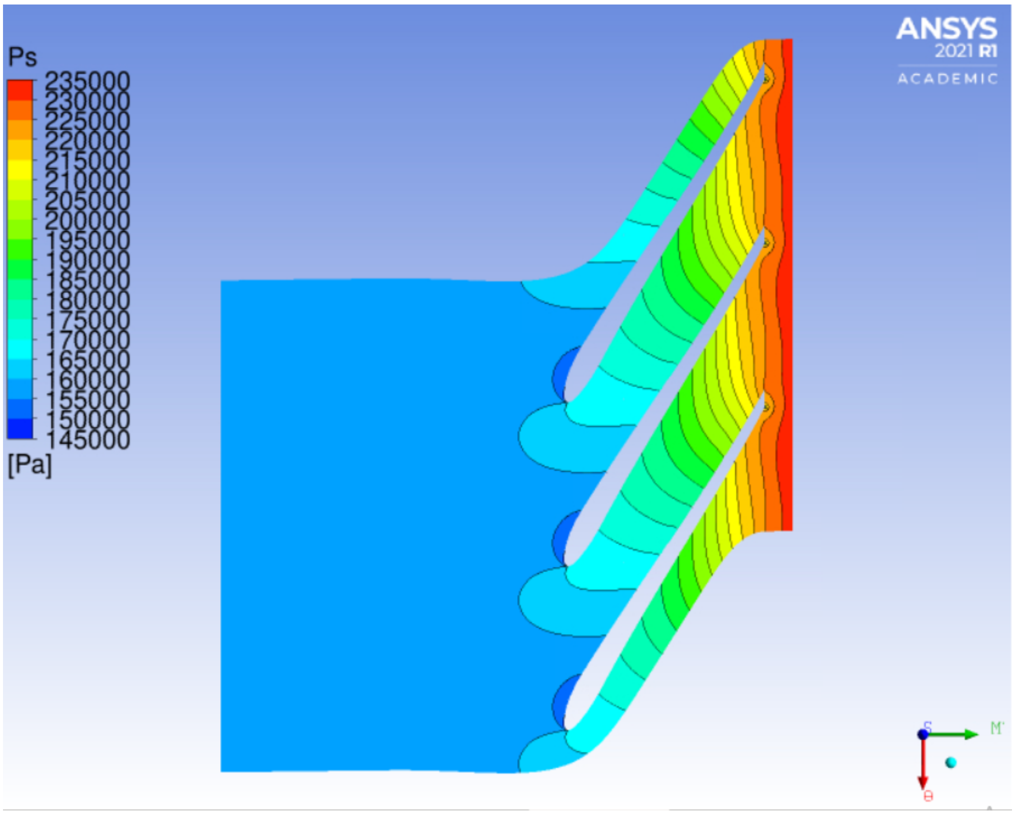

Figure 4.5: Static pressure contour, blade to blade view

Figure 4.5 shows the static pressure for the blade-to-blade view of case "A". The pressure gradient gradually increases from the 1.45bar to around 2.35bar near the blade trailing edge. The highest pressure (2.35bar) happens near the positive meridional direction. The pressure gradient for the static pressure distribution is moderate, and there is not much strong gradient of pressure near the blade's root.

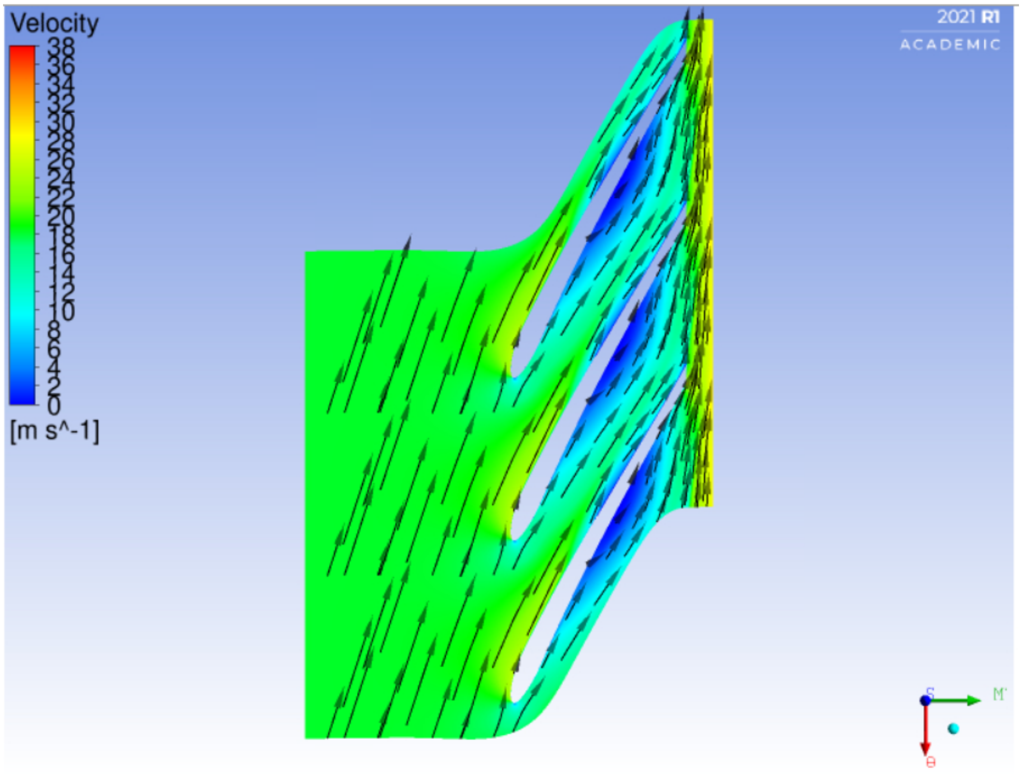

Figure 4.6: Velocity contour, blade to blade view

Figure 4.6 shows the velocity distribution for the blade-to-blade view of case "A". Lowest velocity value occurs under the blade chamber (high-pressure zone). The velocity vectors show separation here, where there are no inclined vectors to the blades. The semi-circulation flow exists near the low-pressure site, which indicates unwanted flow separation.

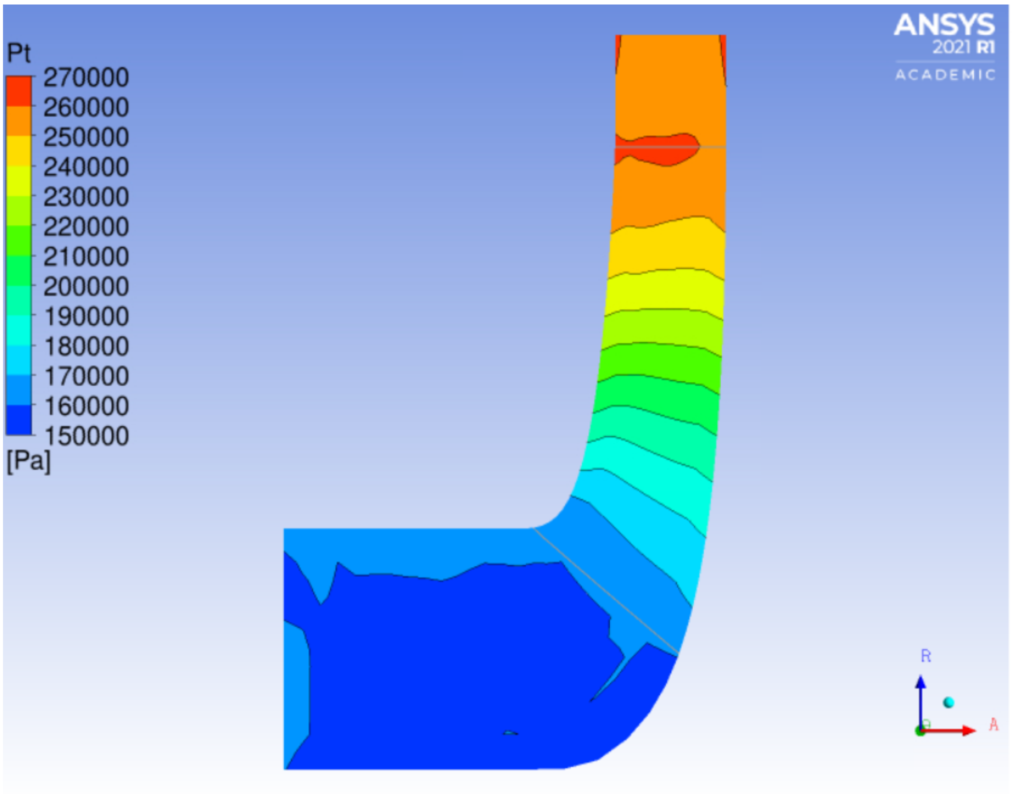

Figure 4.7: Mass averaged total pressure contour, meridional surface view
Figure 4.7 shows the total pressure distribution across the meridional cross-section. The total pressure inlet starts from $1.5bar$ in the eye to $2.6bar$ in the volute region. This pressure increases from the eye gradually to the volute. There is a high-pressure spot of $2.7bar$ near the volute exit; however, it is not located in the far radial direction.

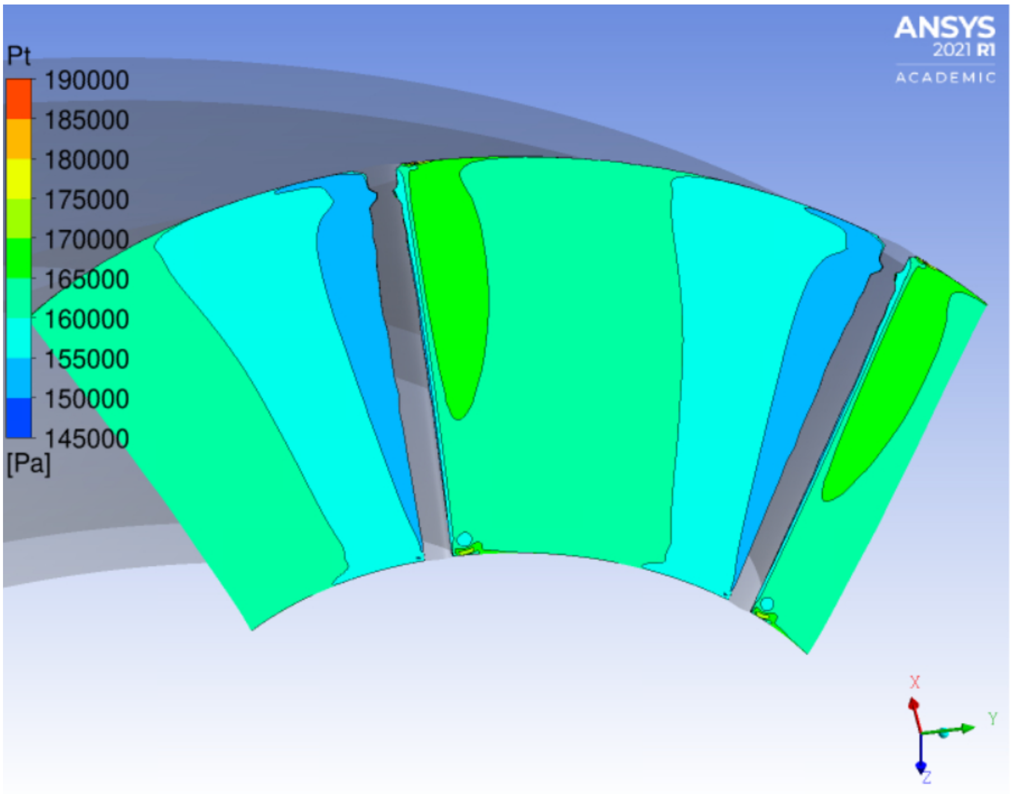

Figure 4.8: Total pressure contour, blade LE

Figure 4.8 shows the total pressure distribution across the blades leading edge cross-section. There are three pressure regions around the blade. The pressure of $1.62 bar$ composes the further left side of the blade and right side near the hub surface. Then there is a lower pressure zone (lower than $1.6 bar$) on the left side, which is followed by a lower pressure region of $1.52 bar$ to make the blade suction side. The leading edge near the shroud surface experiences a higher pressure value of $1.7 bar$ since it is the pressure side.

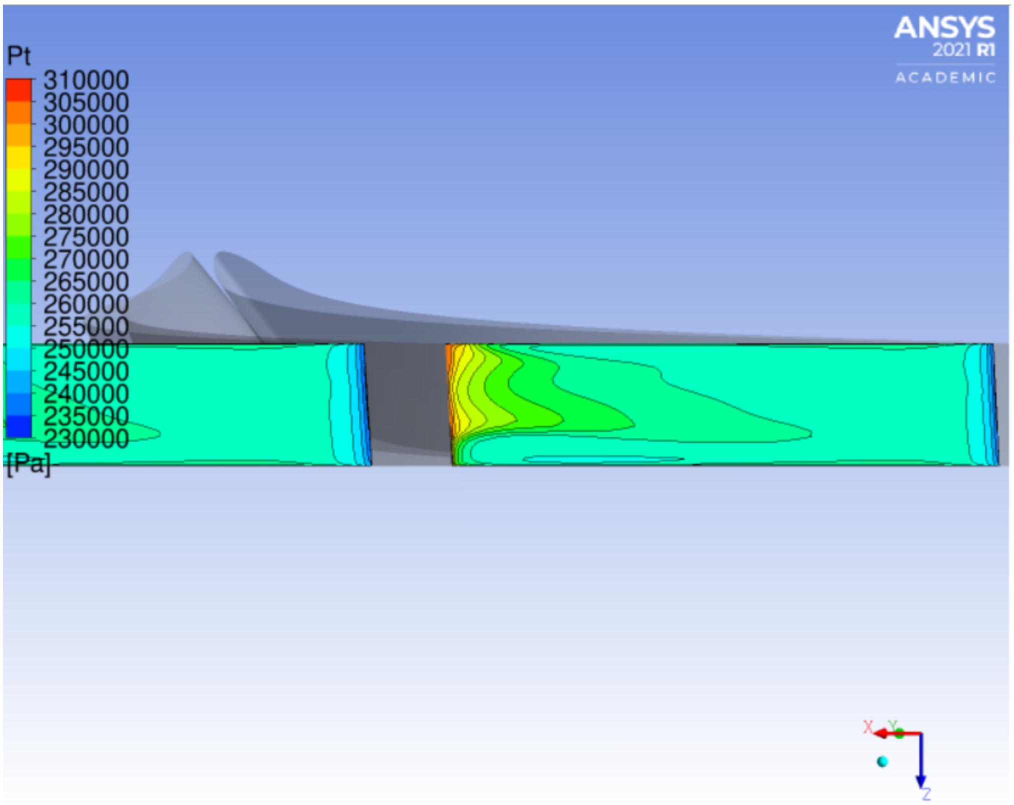

Figure 4.9: Total pressure contour, blade TE

Figure 4.9 shows the total pressure distribution across the blades trailing edge cross-section. There is a lower pressure gradient on the suction side which is very thin because of the sectional view, and a higher pressure gradient on the pressure side to an extent of $3.1 bar$ that is happening locally. The pressure outlet of $2.6 bar$ is almost visible in the whole outlet section. There is not much difference between the hub surface pressure and shroud surface pressure in this contour.

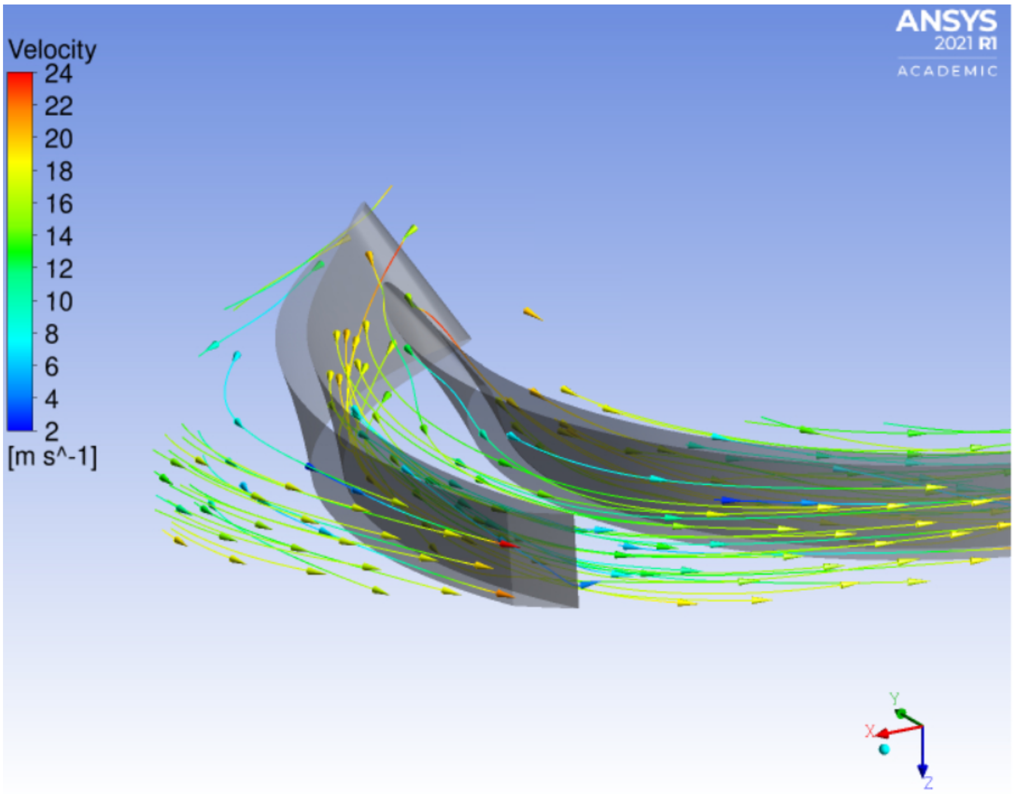

Figure 4.10: Velocity vectors TE view

Figure 4.10 shows the velocity vectors in the trailing edge sectional view. The velocity vectors in design "A" are not inclined perfectly to the blades; therefore, it causes flow separation. Flow separation is not a welcomed phenomenon because it reduces efficiency while deteriorating the cavitation.

4.3 Design "B" for Booster Pump Performance at Design Point

Parameter	Value	Unit
mass flow	0.298	kg/s
volumetric flow	0.00434	m^3/s
rotational speed	12312	RPM
head	147.46	m
shaft power	442.33	W
total efficiency	97.42	%
static efficiency	72.35	%
pressure ratio	1.46	-

Table 4.2: Booster Pump General Characteristics for Design "B" at Design Point

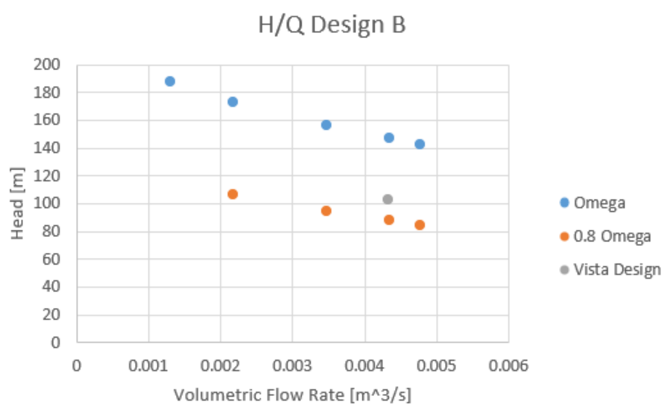

Figure 4.11: Pump "*B*" characteristic curve (Head Rise per Stage/Volumetric Flow Rate)

Figure 4.11 shows the design "*B*" performance. Increasing rotational speed increases the head rise per stage by the pump for off-design cases, but volumetric flow rate growth will decrease the head rise per stage by the pump.

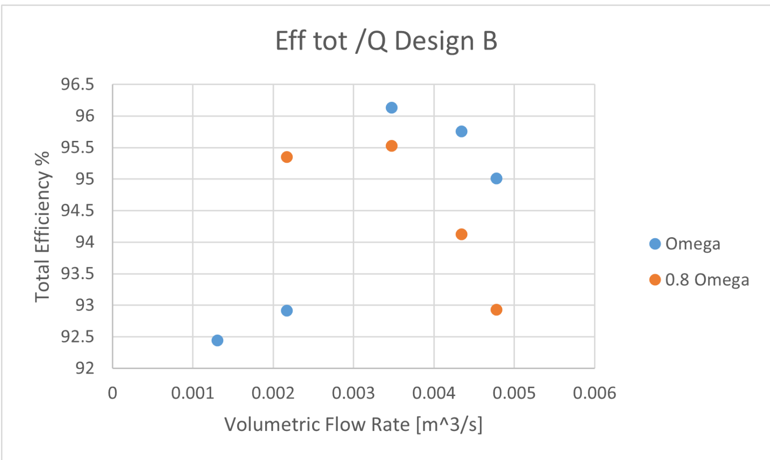

Figure 4.12: Pump "*B*" characteristic curve (Total Efficiency/Volumetric Flow Rate)

Figure 4.12 shows the design "*B*" performance. The volumetric flow rate increase or decrease will affect the efficiency unpleasantly. The best condition for pump "B" is the design point, where the pump shows higher efficiency. This design has thicker vanes which make the flow more inclined to the blades. More inclined flow, give more control over the flow to the blades which leads to less separation. In general, we have high efficiency for the pump, which can be due to several reasons. For example, in this study, the cavitation model is not considered in the simulation, which can affect the efficiency drastically, particularly because the liquid hydrogen is in saturation condition. Additionally, the calculated shaft power which is used to obtain the efficiency by the solver is not the real shaft power. Because it has not considered disk friction on the front and back cavities of the impeller, leakage flow power loss through the front and rear seals, and bearing windage power losses.

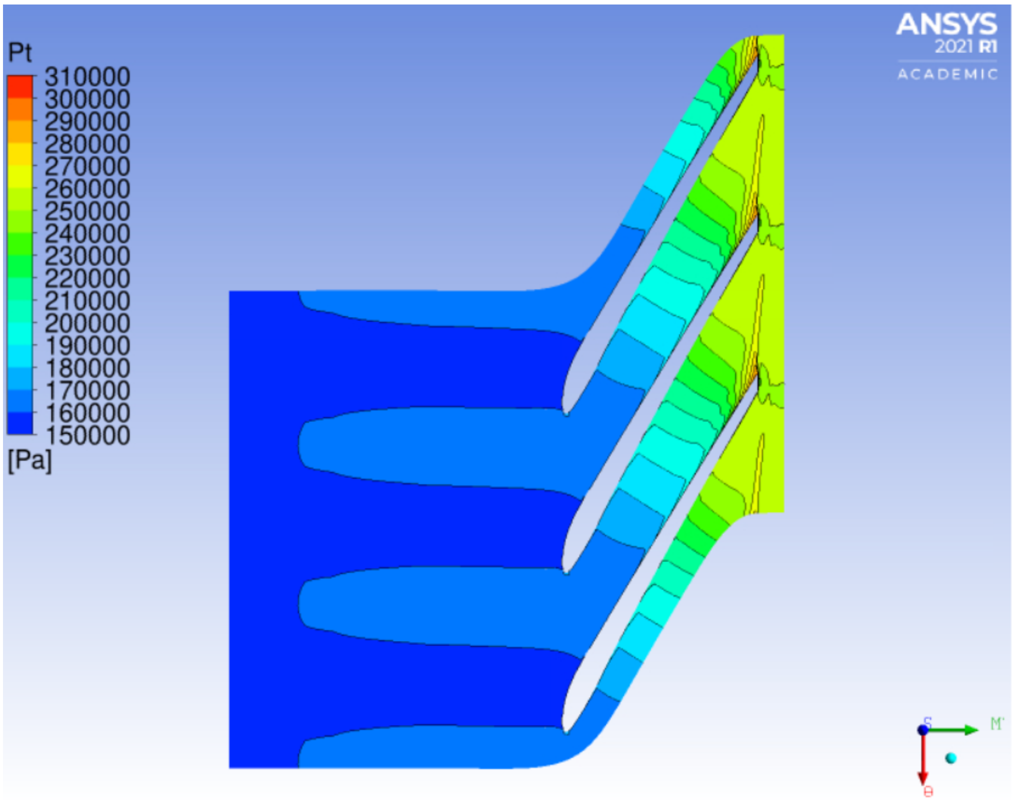

Figure 4.13: Total pressure contour, blade to blade view

Figure 4.13 shows the total pressure for the blade-to-blade view of case B. The pressure gradient gradually increases from the $1.5bar$ to around $2.7bar$ near the blade trailing edge with the highest value of $3.1bar$.

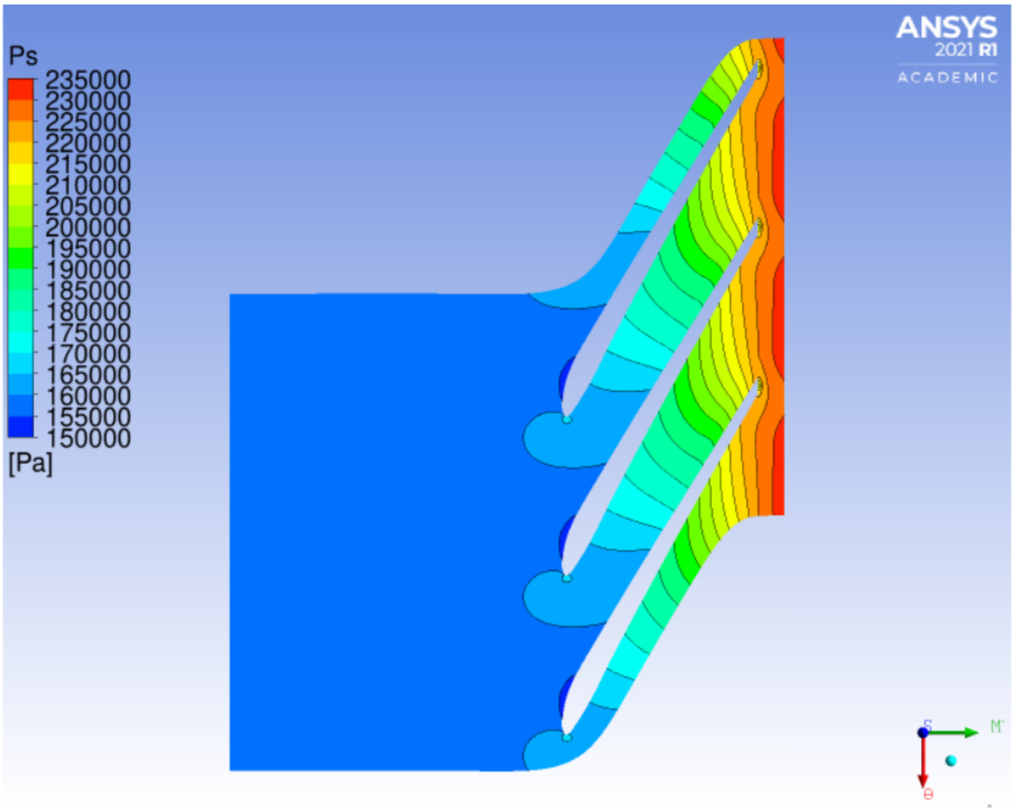

Figure 4.14: Static pressure contour, blade to blade view

Figure 4.14 shows the static pressure for the blade-to-blade view of case B. The pressure gradient gradually increases from the $1.5bar$ to around $2.35bar$ near the blade trailing edge. The highest pressure ($2.35bar$) happens near the positive meridional direction.

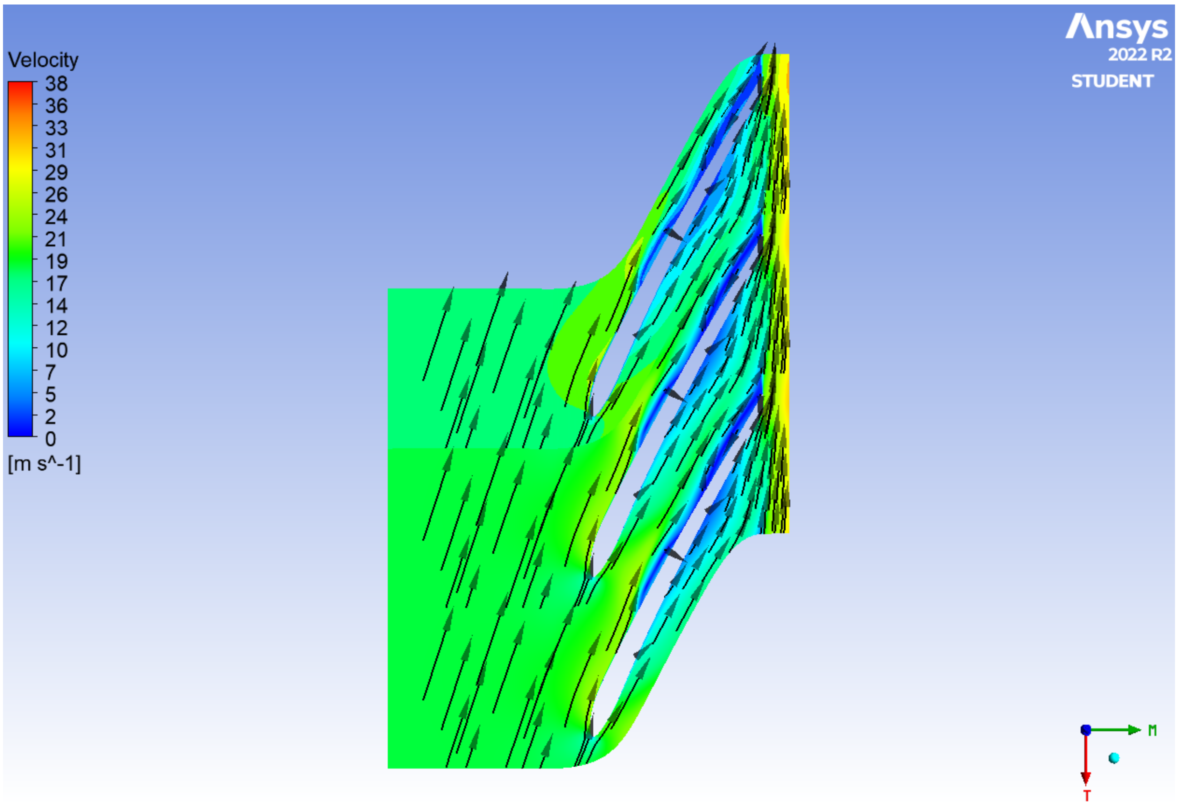

Figure 4.15: Velocity contour, blade to blade view

Figure 4.6 shows the velocity distribution for the blade-to-blade view of case B. Lowest velocity value occurs under the blade chamber (high-pressure zone). The velocity vectors show much less separation here, where there are more inclined vectors to the blades.

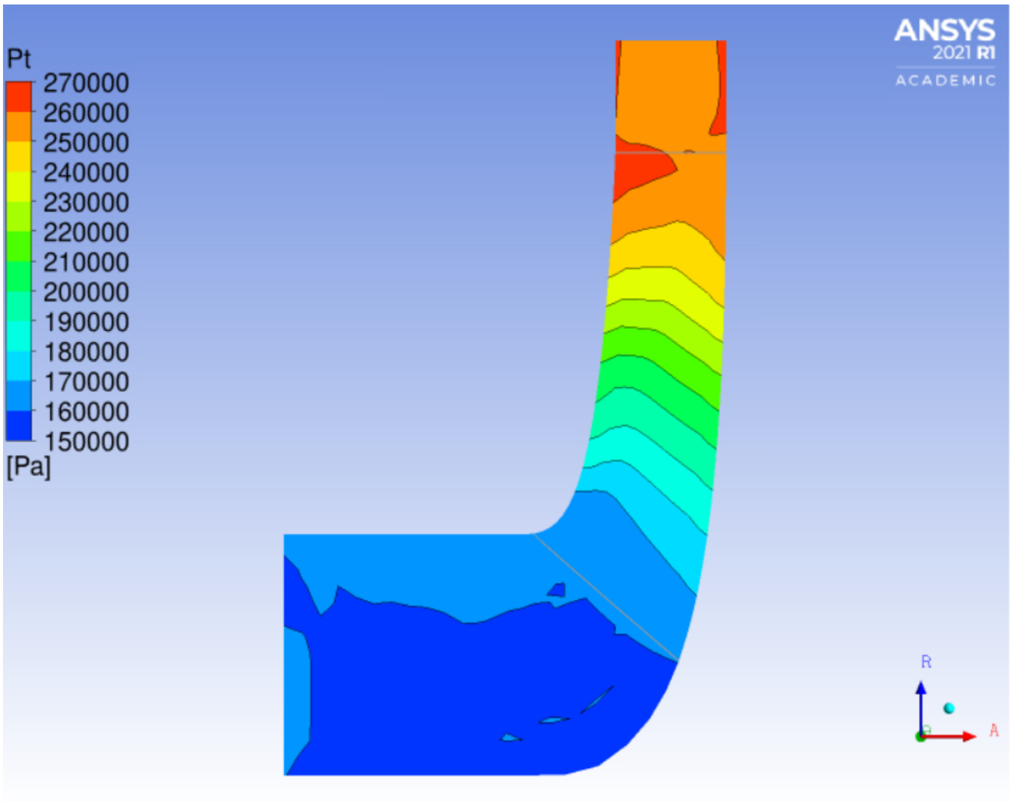

Figure 4.16: Mass averaged total pressure contour, meridional surface view

Figure 4.16 shows the total pressure distribution across the meridional cross-section. The total pressure inlet starts from $1.5bar$ in the eye to $2.6bar$ in the volute region. This pressure increases from the eye gradually to the volute. There is a high-pressure spot of $2.7bar$ near the volute exit; however, it is not located in the far radial direction.

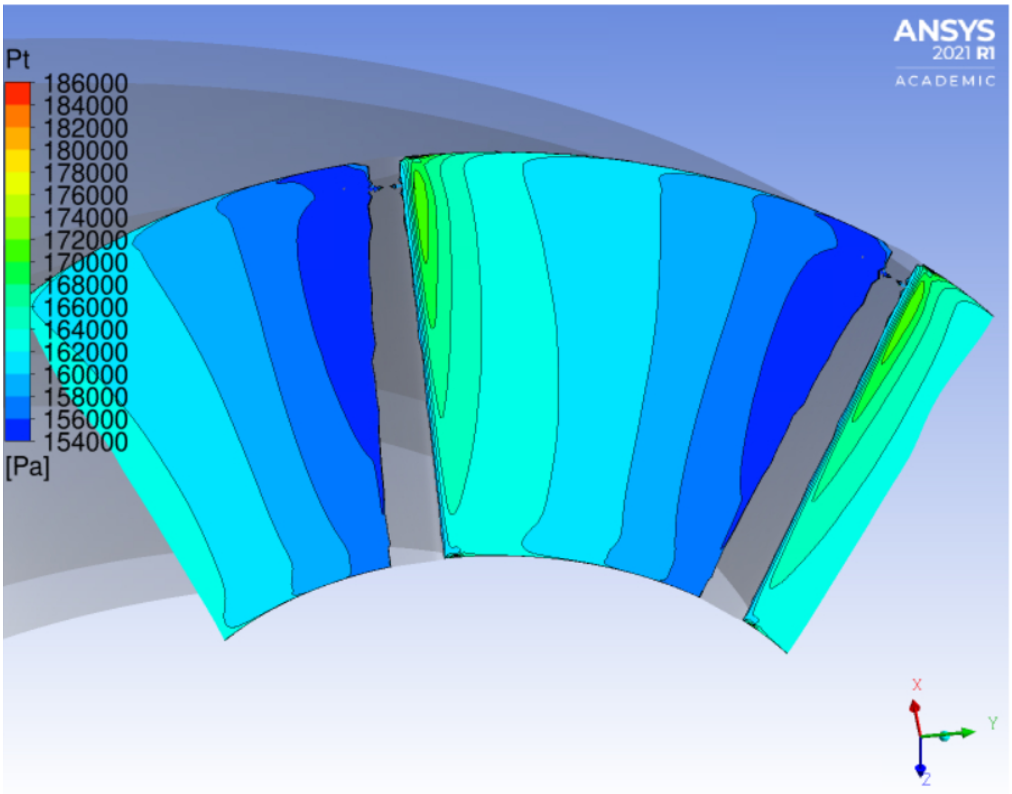

Figure 4.17: Total pressure contour, blade LE

Figure 4.17 shows the total pressure distribution across the blades leading edge cross-section. There is a gradual pressure increase from the pressure side to the suction side of the blades. The bigger value is near the shroud surface of the pressure side, where the flow can reach the $1.86bar$ locally at some points.

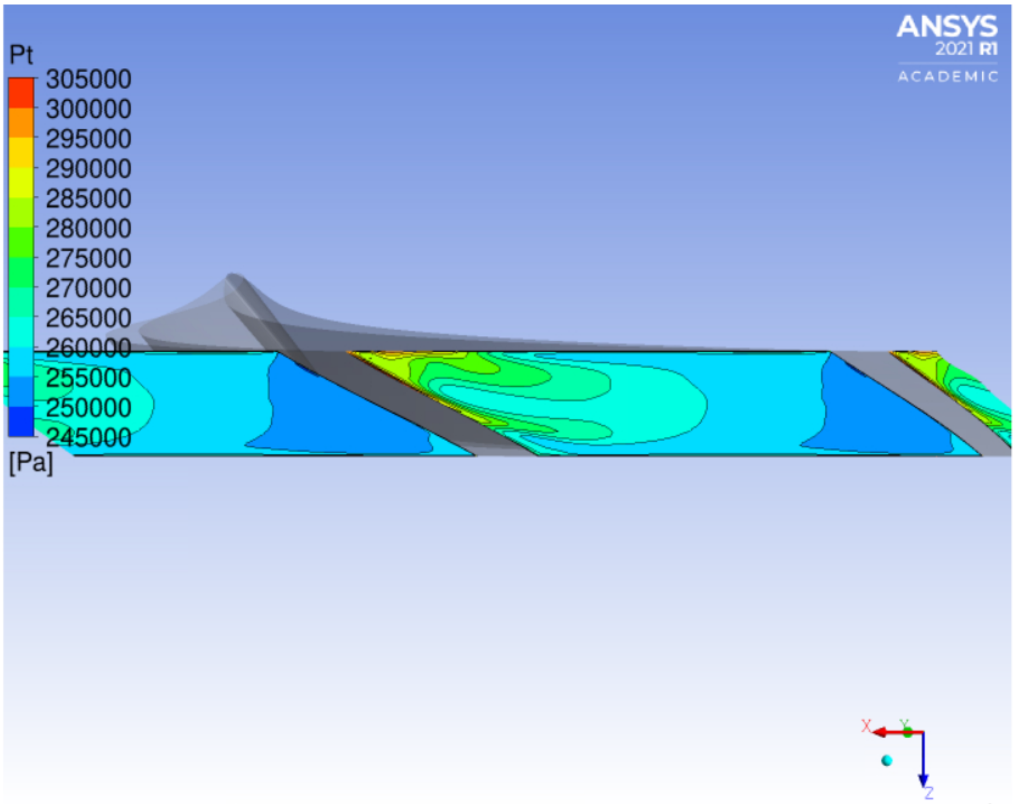

Figure 4.18: Total pressure contour, blade TE

Figure 4.18 shows the total pressure distribution across the blades trailing edge cross-section. There is a lower pressure gradient on the suction side which is thin because of the sectional view, and a higher pressure gradient on the pressure side to an extent of $2.9bar$. This higher pressure can reach a value of $3.1bar$ locally at some point because of the flow around the pressure side in the shroud surface. The pressure outlet of $2.55bar$ is almost visible in the whole outlet section.

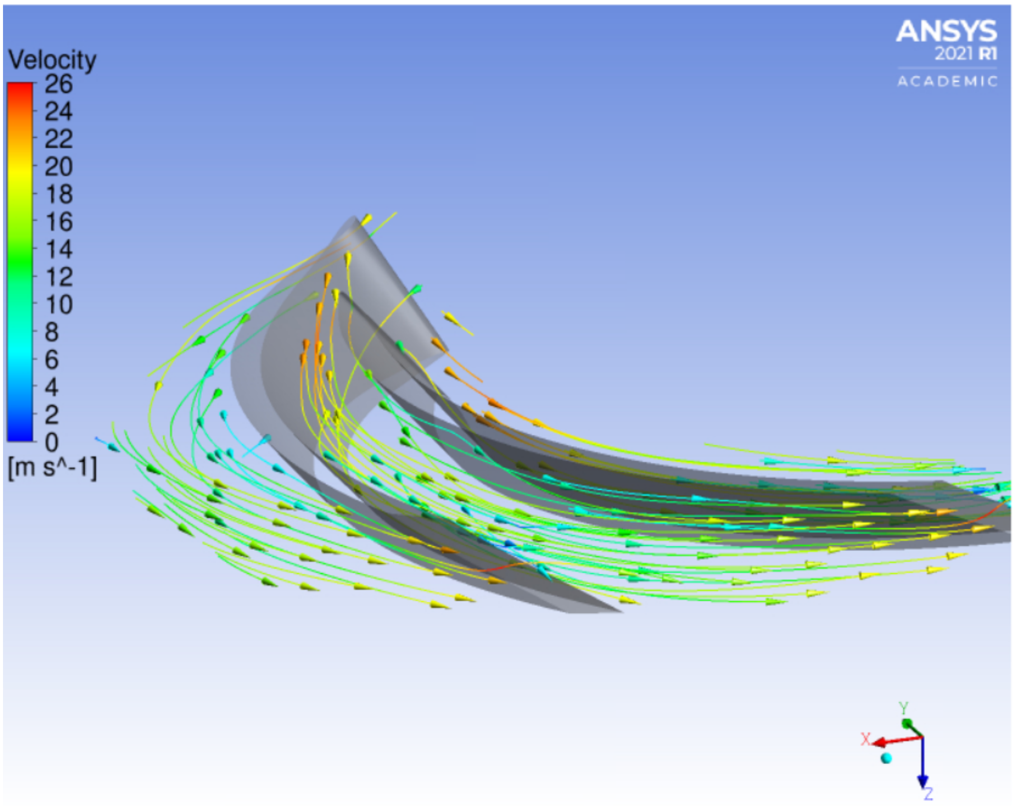

Figure 4.19: Velocity vectors TE view

Figure 4.19 shows the velocity vectors in the trailing edge sectional view. The velocity vectors in design "B" are not inclined to the blades; therefore, it causes less flow separation compared to the case "A". Less separation is mainly because of the thicker blades that lead to better control over flow passing through the pump.

4.4 Comparison Between Design "A" and "B"

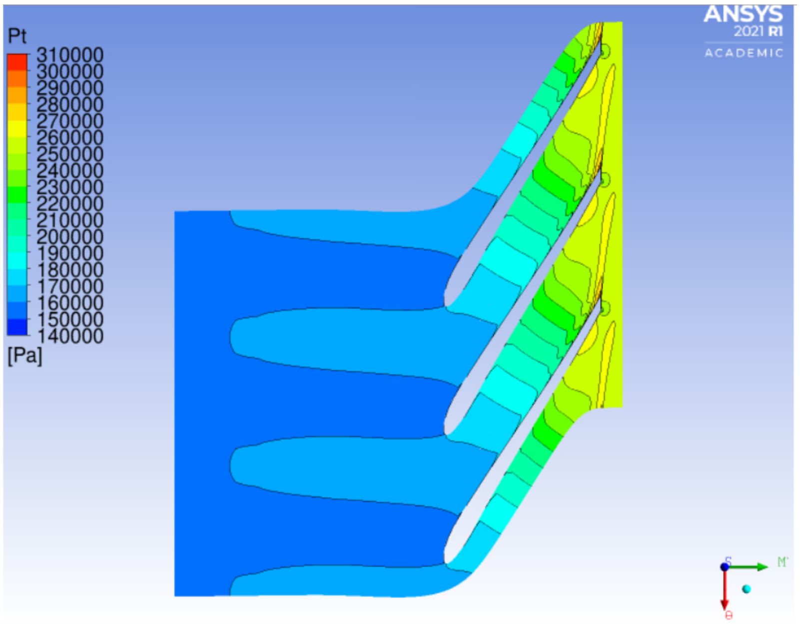

Figure 4.20: Total pressure contour, blade to blade view design A

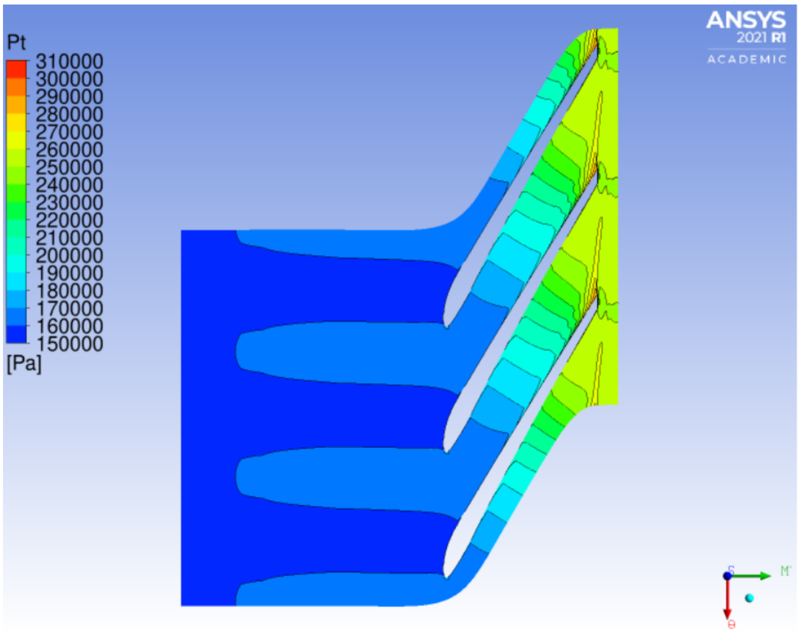

Figure 4.21: Total pressure contour, blade to blade view design B

Higher pressure in the negative meridional direction is observed for the case "B" in comparison to the "A". Both contours show a gradual total pressure increase from $1.5bar$ to $2.6bar$. Besides, high-pressure gradients near the trailing edge occur locally in both cases.

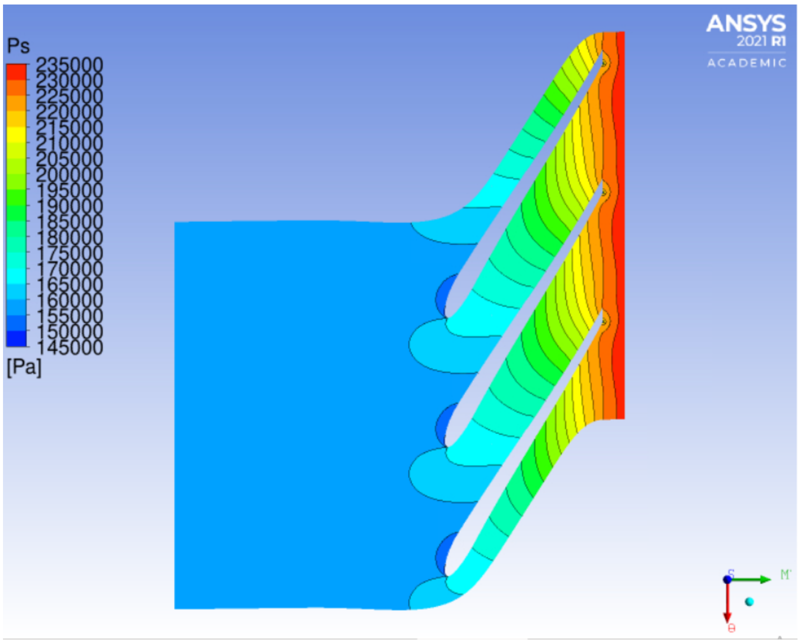

Figure 4.22: Static pressure contour, blade to blade view A

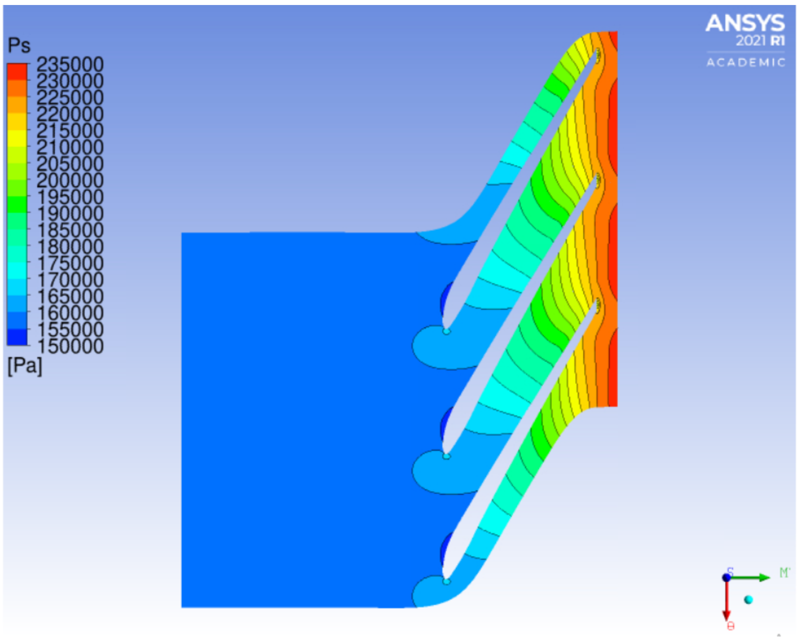

Figure 4.23: Static pressure contour, blade to blade view B

Both contours look the same because the static pressure for both cases is almost similar. A gradual increase from $1.5bar$ to $2.3bar$ near the trailing edges.

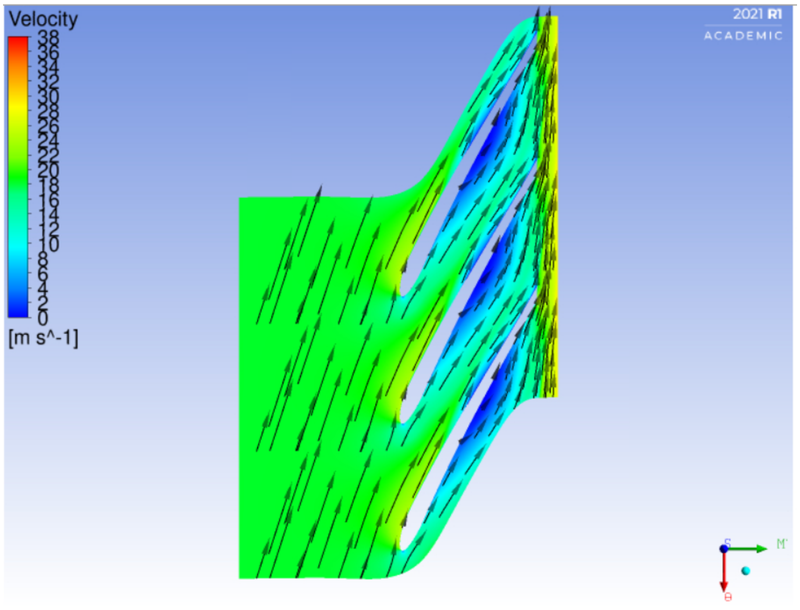

Figure 4.24: Velocity contour, blade to blade view design A

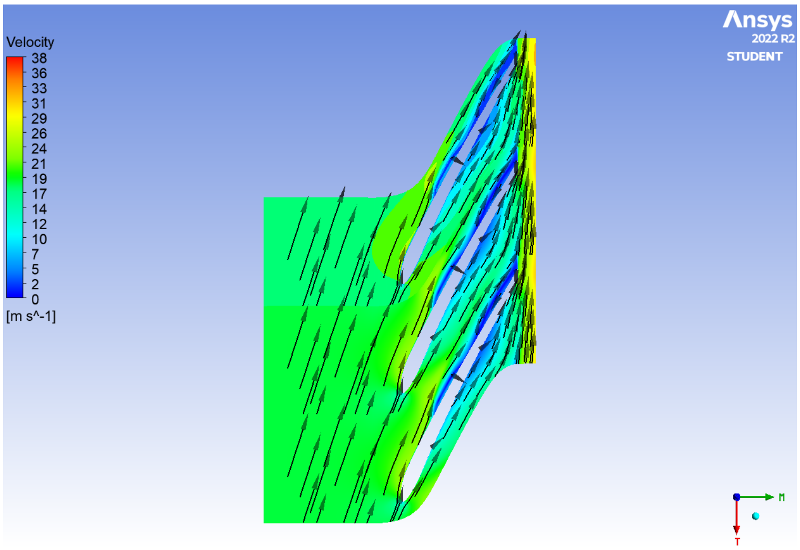

Figure 4.25: Velocity contour, blade to blade view B

The flow in case "*A*" shows more separation in velocity vectors, where the flow does not follow the blade perfectly, but in case "*B*", the flow is more inclined to the vanes. This is due to more control over the flow in case "*B*" compared to the first one. The velocity in case "*A*" takes a higher value because of the flow separation, which leads to an increase of momentum transport between the fluid layers.

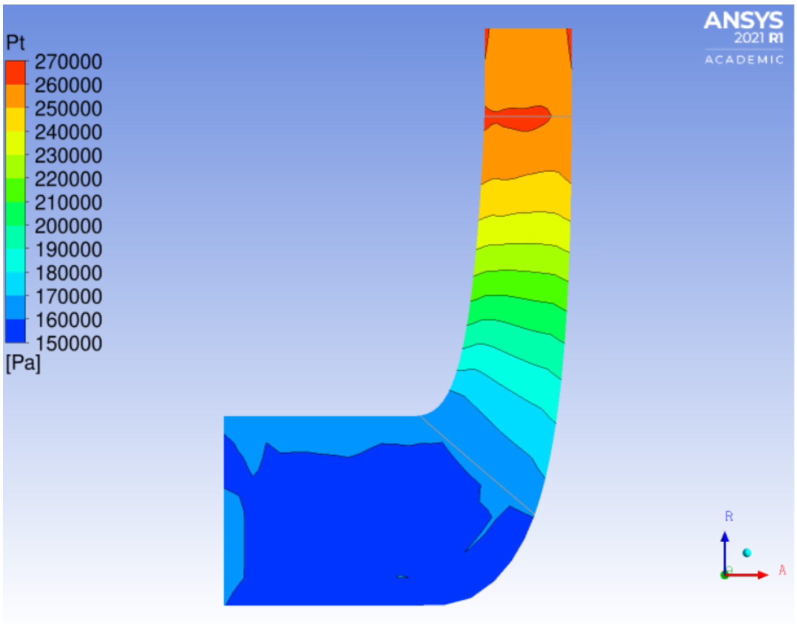

Figure 4.26: Mass averaged total pressure contour, meridional surface view A

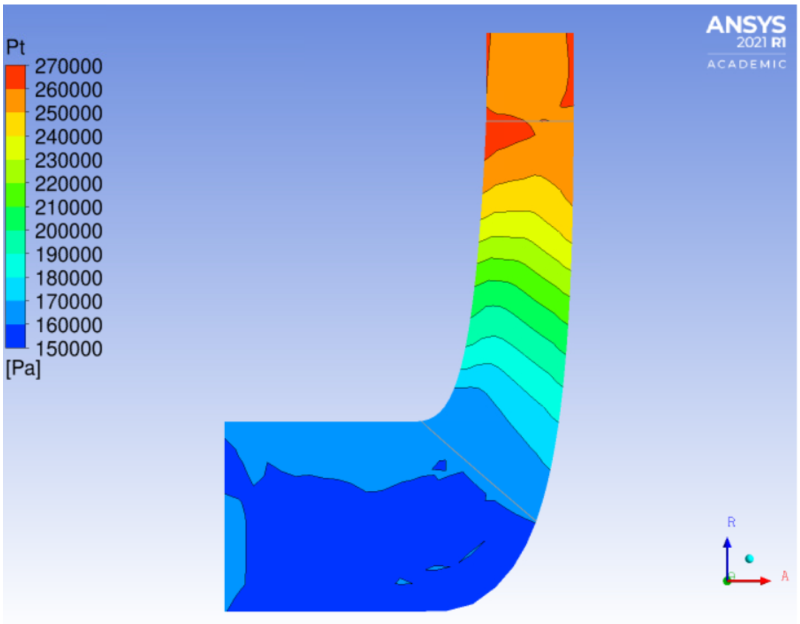

Figure 4.27: Mass averaged total pressure contour, meridional surface view B

Both contours reflect the same information because the operating condition is somehow similar in both cases. It indicates a pressure rise of 1.5*bar* in the eye intake to 2.6*bar* in the outlet.

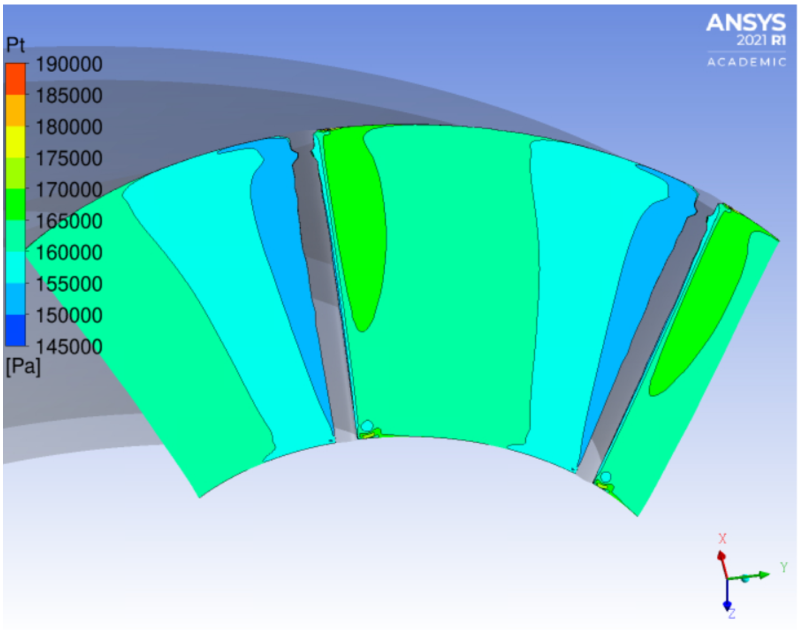

Figure 4.28: Total pressure contour, blade LE design A

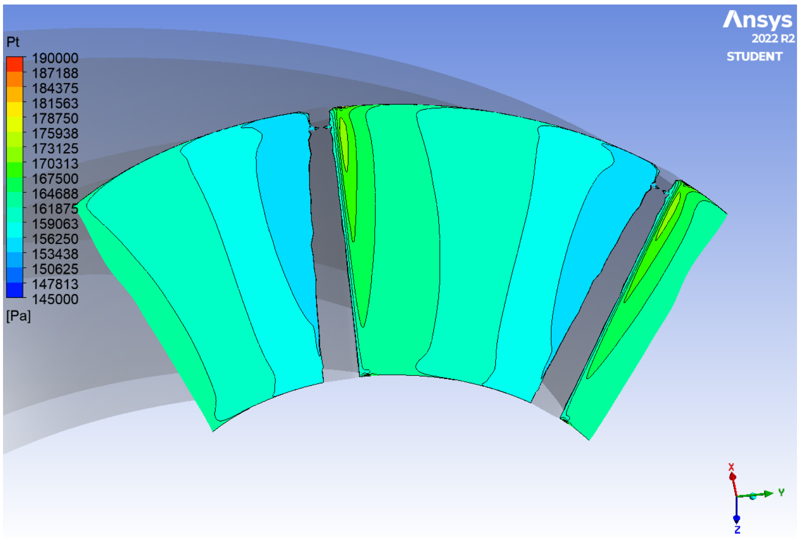

Figure 4.29: Total pressure contour, blade LE design B

In the leading edge cross-section, the pressure gradient change is more gradual in design "*B*" in comparison to the design "*A*". However, case "*B*" reflects a stronger gradient near the shroud surface of the pressure side because the shroud's path is more narrow in comparison to the hub surface path.

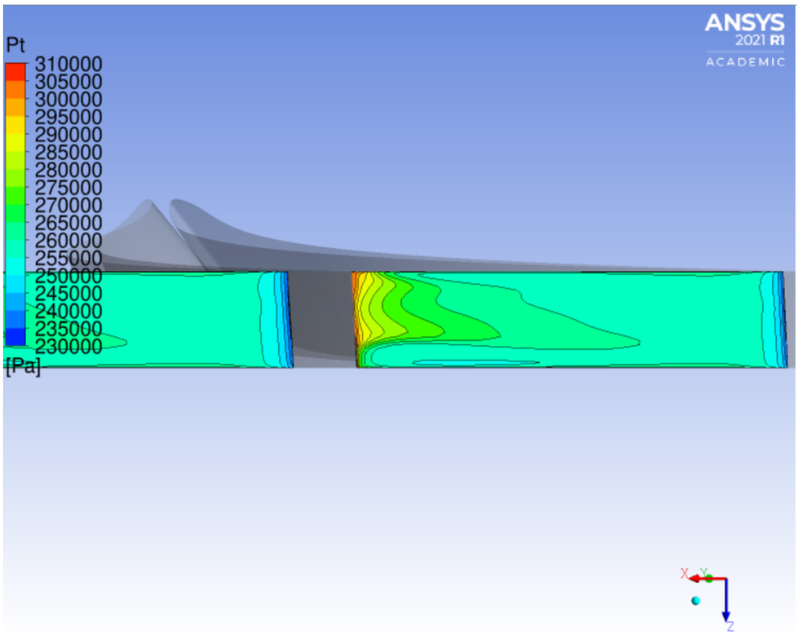

Figure 4.30: Total pressure contour, blade TE design A

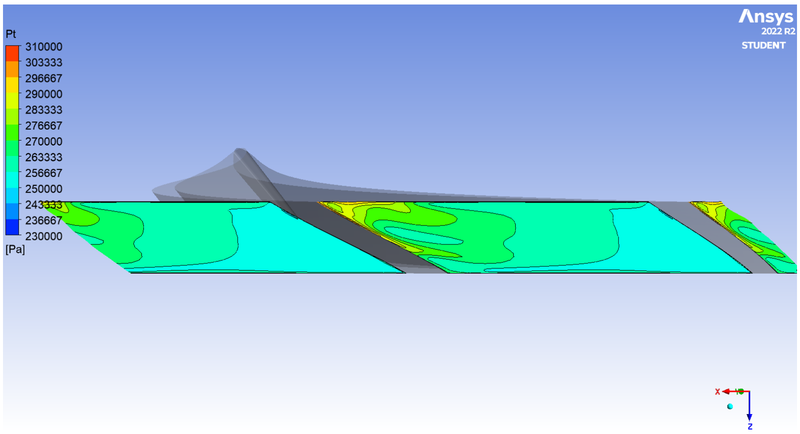

Figure 4.31: Total pressure contour, blade TE design B

In case "*A*" the blade position on the hub surface is somehow vertical in comparison to the inclined blades of case "*B*". This has made higher pressure on the trailing edge ($2.4bar$ in comparison to the $2.3bar$). Both cases show a strong pressure gradient near the pressure side shroud surface and a lower pressure gradient on the suction side.

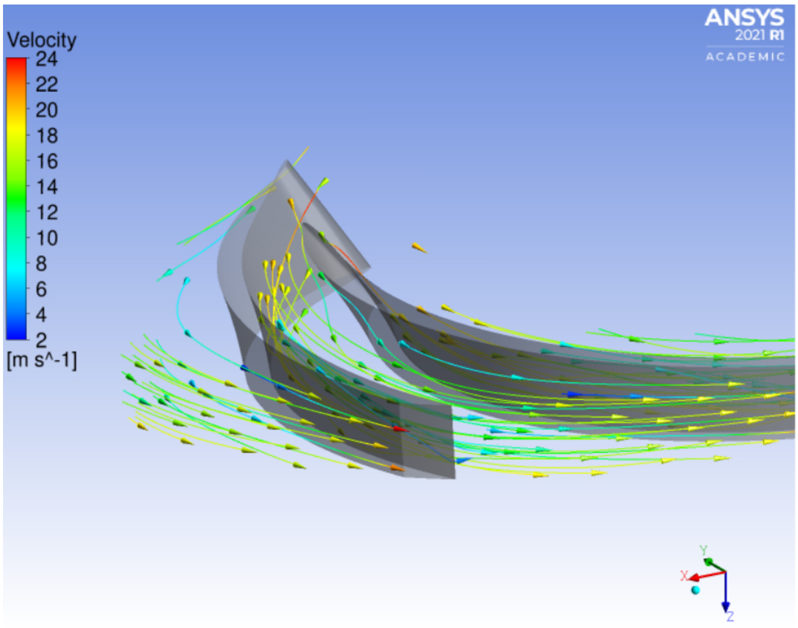

Figure 4.32: Velocity vectors design A

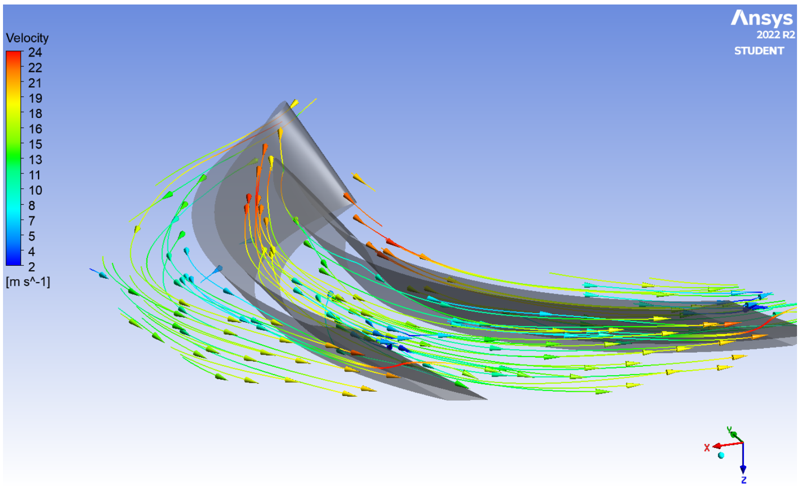

Figure 4.33: Velocity vectors design B

The flow separation in the case "A" can be seen particularly near the leading edge shroud surface, where the vectors do not follow the blades' geometry. This can be observed in the suction side leading edge too, where the velocity vectors in case "B" are more inclined to the blade's curvature.

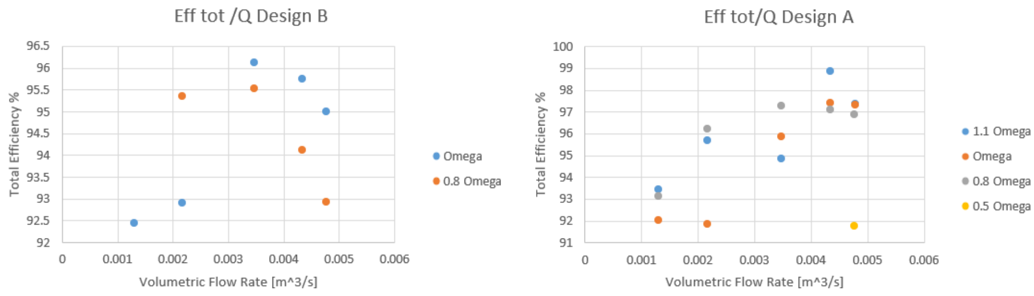

Figure 4.34: Total efficiency by volumetric flow rate comparison
Design ”B” shows higher total efficiency generally because this case has less flow separation due to the modified geometry, where we have increased the blade thickness, and the blades are more inclined to the hub surface with a non-vertical root-to-hub attachment.

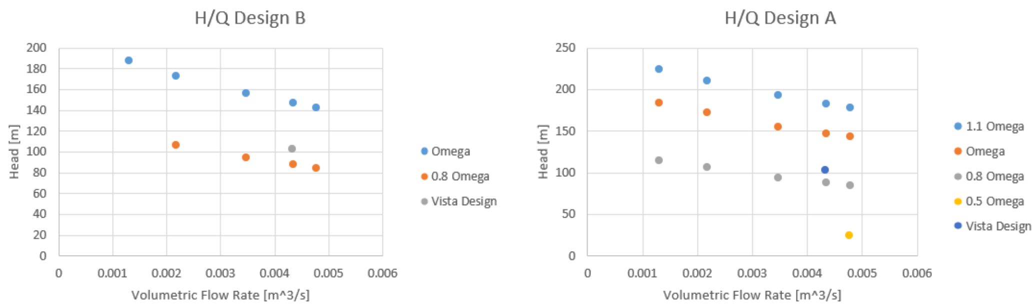

Figure 4.35: Head rise per stage by volumetric flow rate comparison
Both cases follow almost the same behavior for the hear rise per stage by volumetric flow rate. This is due to the similar Vista input for both cases. The head rise per stage and volumetric flow rate are very similar in both design and existing off-design points for both cases.

4.5 Off-Design Simulations

4.5.1 $30\%\dot{m}_{Design}$, $\Omega = \Omega_{Design}$

Parameter	Value	Unit
mass flow	0.089	kg/s
volumetric flow	0.00130	m^3/s
rotational speed	12312	RPM
head	187.76	m
shaft power	177.08	W
total efficiency	92.44	$\%$
static efficiency	60.69	$\%$
pressure ratio	1.51	-

Table 4.3: Booster Pump General Characteristics for Design "B" at $30\%\dot{m}_{Design}$, $\Omega = \Omega_{Design}$

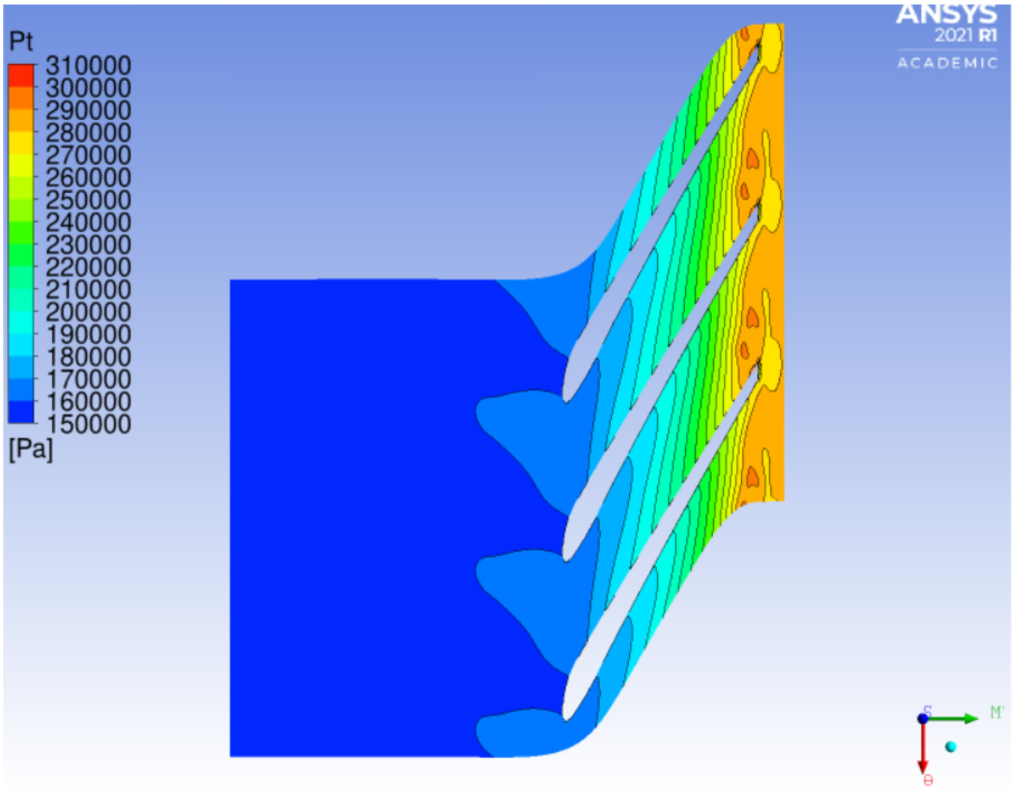

Figure 4.36: Total pressure contour, blade to blade view

Figure 4.36 shows the total pressure for the blade-to-blade view of the "B" off-design case with $30\%\dot{m}_{Design}$, $\Omega = \Omega_{Design}$. The pressure gradient gradually increases from the $1.5bar$ to $2.9bar$ near the blade trailing edge. The highest pressure ($3.1bar$) occurs near the blade trailing edge . The pressure gradient in the meridional direction has a higher value in comparison to the design point.

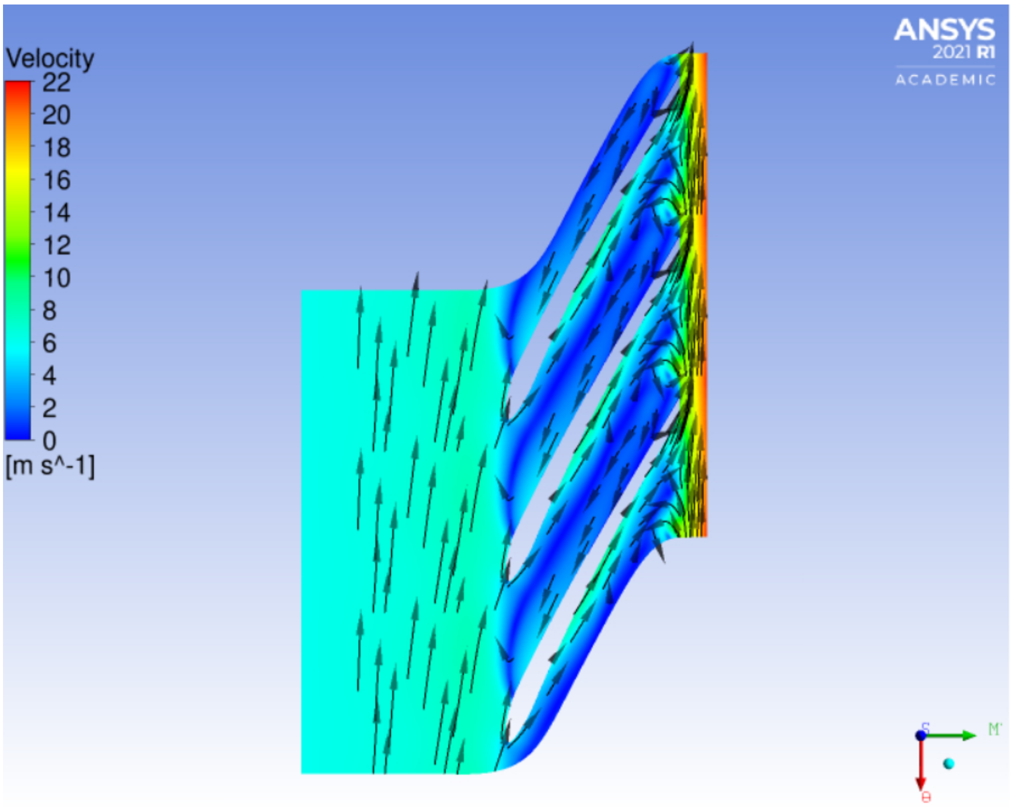

Figure 4.37: Velocity contour, blade to blade view
Figure 4.37shows the velocity distribution for the blade-to-blade view of case "B" off-design case with $30\%\dot{m}_{Design}$, $\Omega = \Omega_{Design}$. The lowest velocity value occurs under the blade chamber (high-pressure zone). The flow has more separation here because the mass flow is almost one-third of the design point, and it makes the velocities decrease drastically.

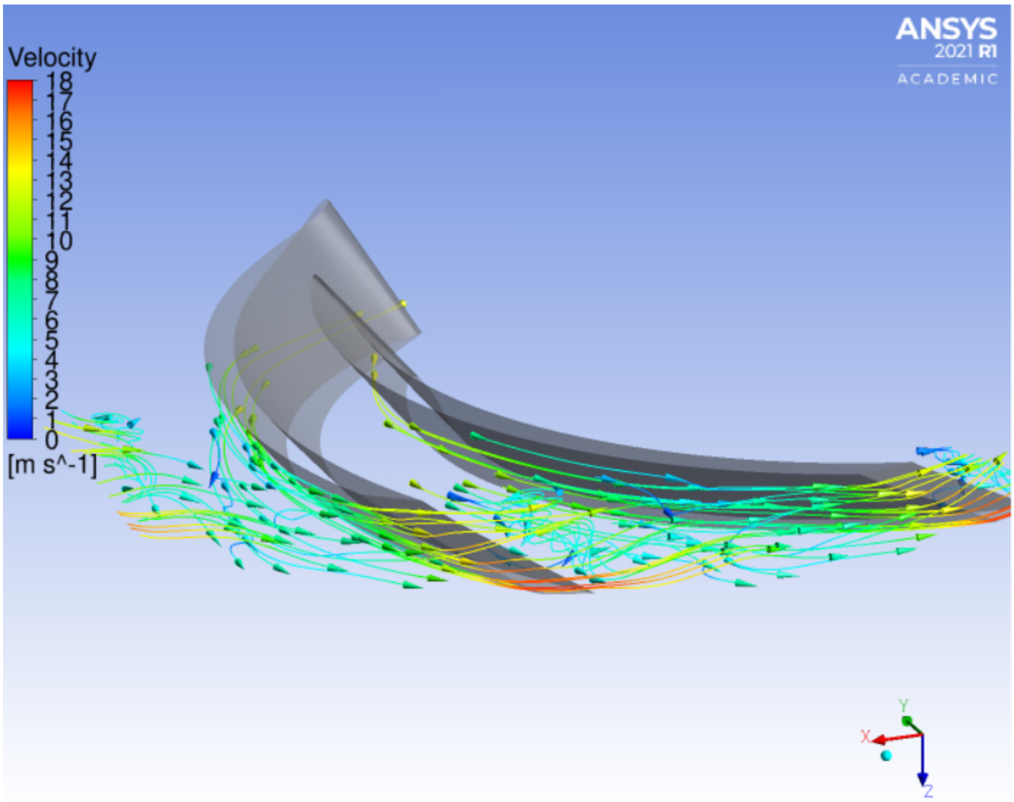

Figure 4.38: Velocity vectors TE view

Figure 4.37 shows the velocity vectors in the trailing edge sectional view of the "B" off-design case with $30\%\dot{m}_{Design}$, $\Omega = \Omega_{Design}$. There is a sever flow separation on the suction side of the blade. The velocity vectors have high separation near the trailing edge which is illustrated. The flow follows the pressure side curve alongside the blade more in comparison to the suction side.

4.5.2 $50\%\dot{m}_{Design}$, $\Omega = \Omega_{Design}$

Parameter	Value	Unit
mass flow	0.149	kg/s
volumetric flow	0.00217	m^3/s
rotational speed	12312	RPM
head	173.44	m
shaft power	272.75	W
total efficiency	92.91	%
static efficiency	63.95	%
pressure ratio	1.50	-

Table 4.4: Booster Pump General Characteristics for Design "B" at $50\%\dot{m}_{Design}$, $\Omega = \Omega_{Design}$

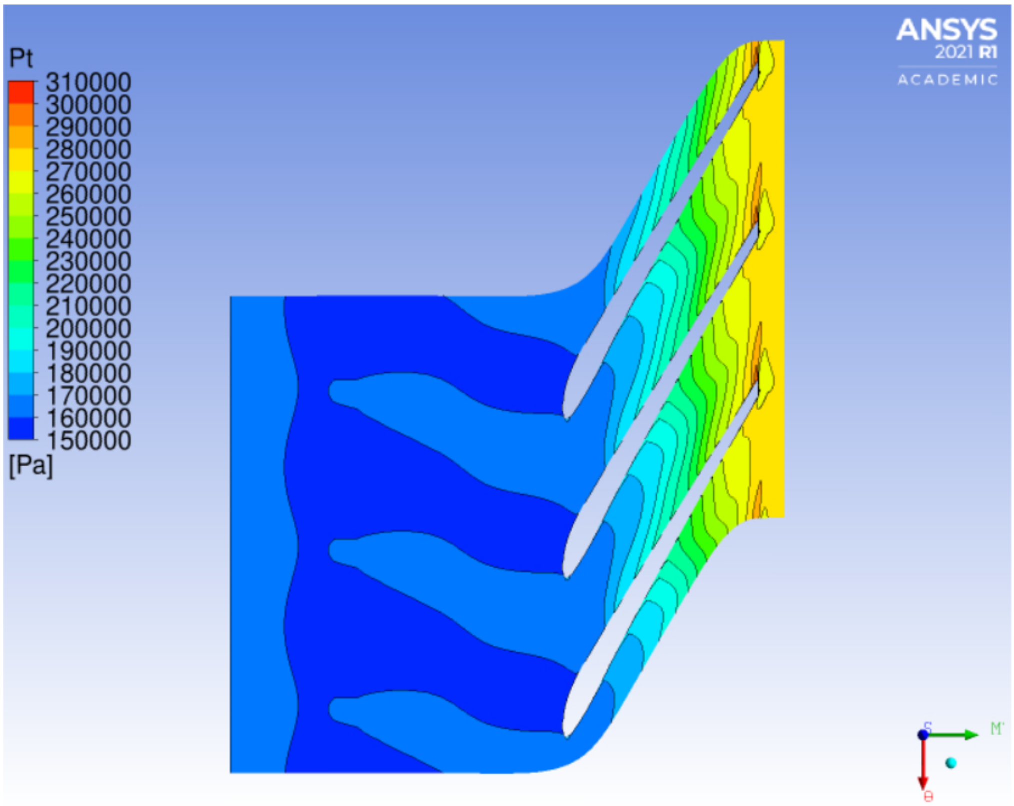

Figure 4.39: Total pressure contour, blade to blade view

Figure 4.39 shows the total pressure for the blade-to-blade view of the "B" off-design case with $50\%\dot{m}_{Design}$, $\Omega = \Omega_{Design}$. The pressure gradient gradually increases from the $1.5bar$ to $2.8bar$ near the blade trailing edge with the maximum value of $3.1bar$. The pressure gradient in the meridional direction has a higher value in comparison to the design point. Besides, in the flow layers with separated boundaries, small pressure differences are observed in the negative direction of the meridional axis.

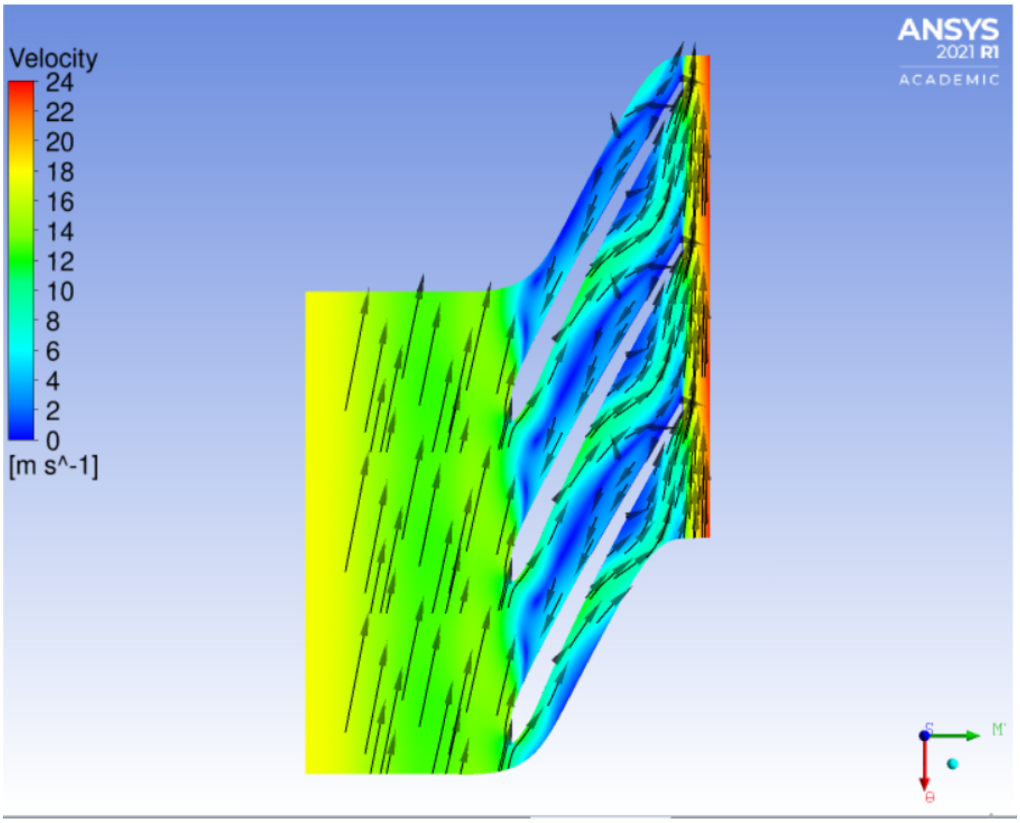

Figure 4.40: Velocity contour, blade to blade view

Figure 4.40 shows the velocity distribution for the blade-to-blade view of ”B” off-design case with $50\%\dot{m}_{Design}$, $\Omega = \Omega_{Design}$. The lowest velocity value occurs under the blade chamber (high-pressure zone). The flow separation occurs here because the mass flow is lower than the design point; however, the separation is less compared to the $30\%\dot{m}_{Design}$ point.

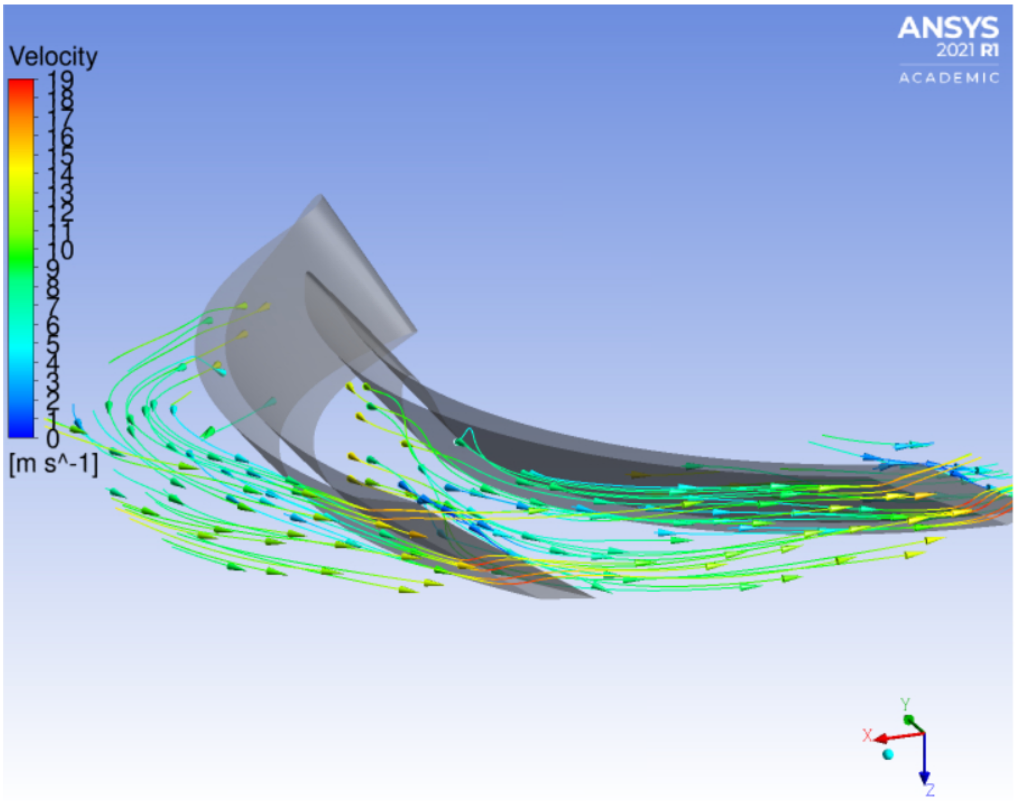

Figure 4.41: Velocity vectors TE view

Figure 4.41 shows the velocity vectors in the trailing edge sectional view of the "B" off-design case with $50\%\dot{m}_{Design}$, $\Omega = \Omega_{Design}$. The velocity vector separation occurs near the blade's leading edge suction side.

4.5.3 $80\%\dot{m}_{Design}$, $\Omega = \Omega_{Design}$

Parameter	Value	Unit
mass flow	0.238	kg/s
volumetric flow	0.00347	m^3/s
rotational speed	12312	RPM
head	156.45	m
shaft power	380.48	W
total efficiency	96.13	$\%$
static efficiency	68.995	$\%$
pressure ratio	1.47	-

Table 4.5: Booster Pump General Characteristics for Design "B" at $80\%\dot{m}_{Design}$, Ω_{Design}

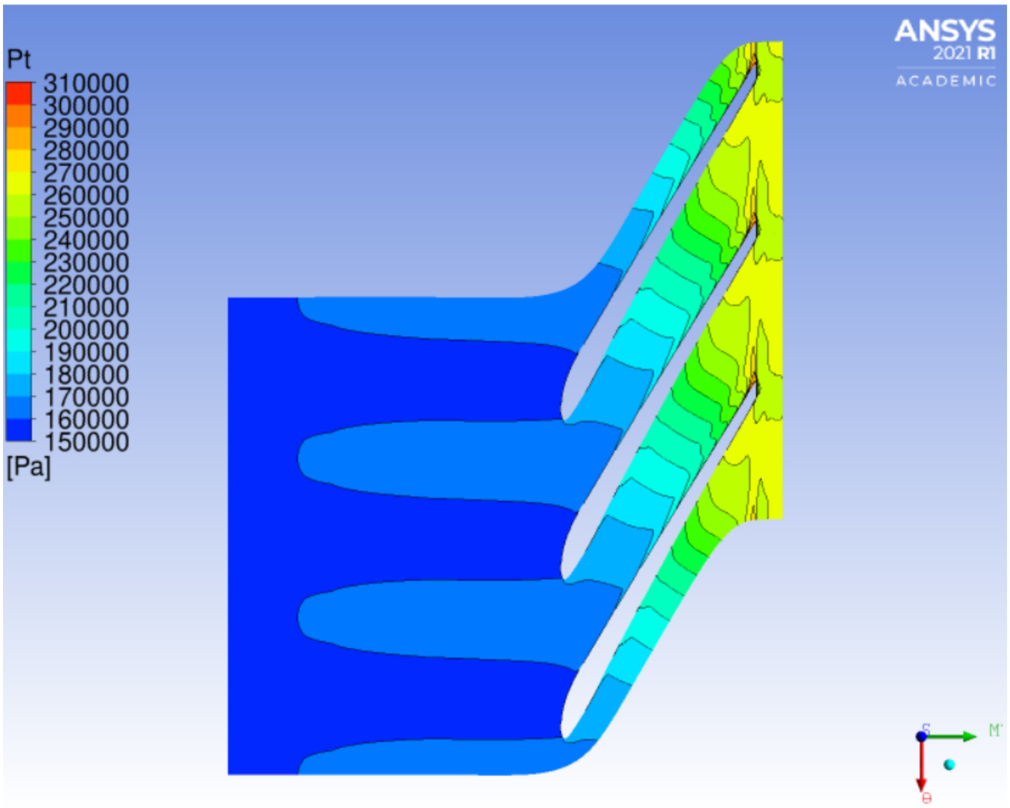

Figure 4.42: Total pressure contour, blade to blade view

Figure 4.42 shows the total pressure for the blade-to-blade view of the "B" off-design case with $80\%\dot{m}_{Design}$, $\Omega = \Omega_{Design}$. The pressure gradient gradually increases from the $1.5bar$ to $2.7bar$ near the blade trailing edge with the highest pressure ($3.1bar$) happens there. The pressure gradient in the meridional direction has a higher value in comparison to the design point. Besides, in the flow layers with separated boundaries, small pressure differences are observed in the negative direction of the meridional axis.

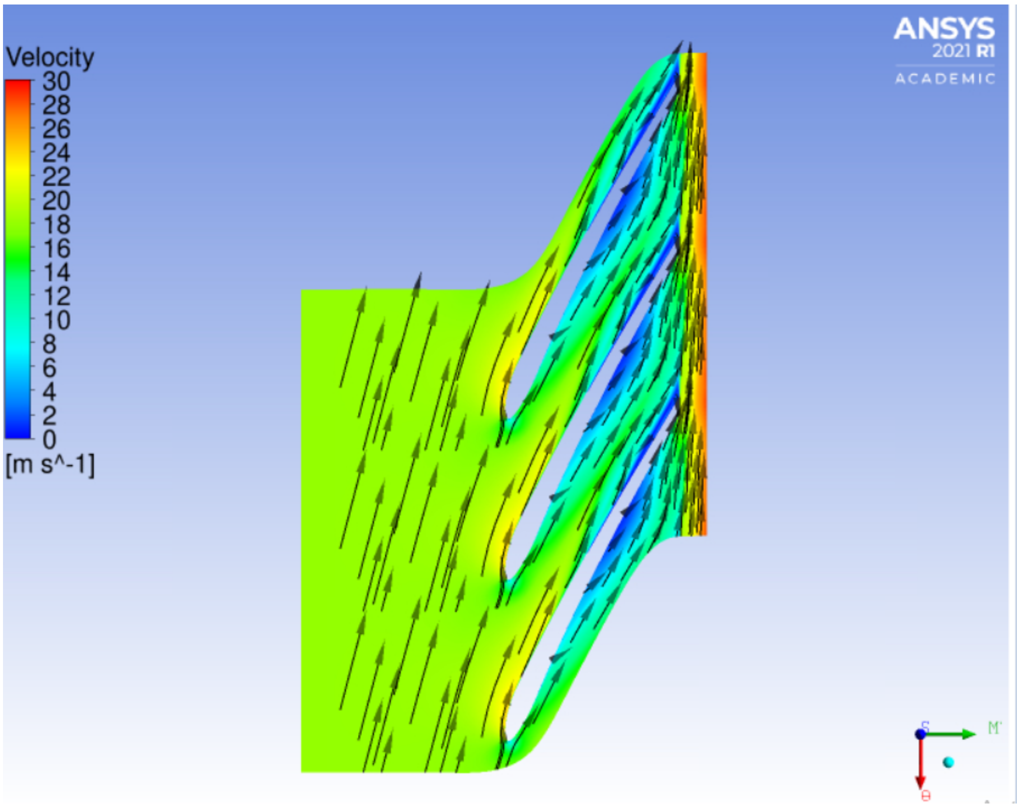

Figure 4.43: Velocity contour, blade to blade view

Figure 4.43 shows the velocity distribution for the blade-to-blade view of "B" off-design case with $80\%\dot{m}_{Design}$, $\Omega = \Omega_{Design}$. The lowest velocity value occurs under the blade chamber (high-pressure zone). The flow separation occurs here because the mass flow is lower than the design point; however, the separation is less compared to the other off-design cases with the lower mass flow.

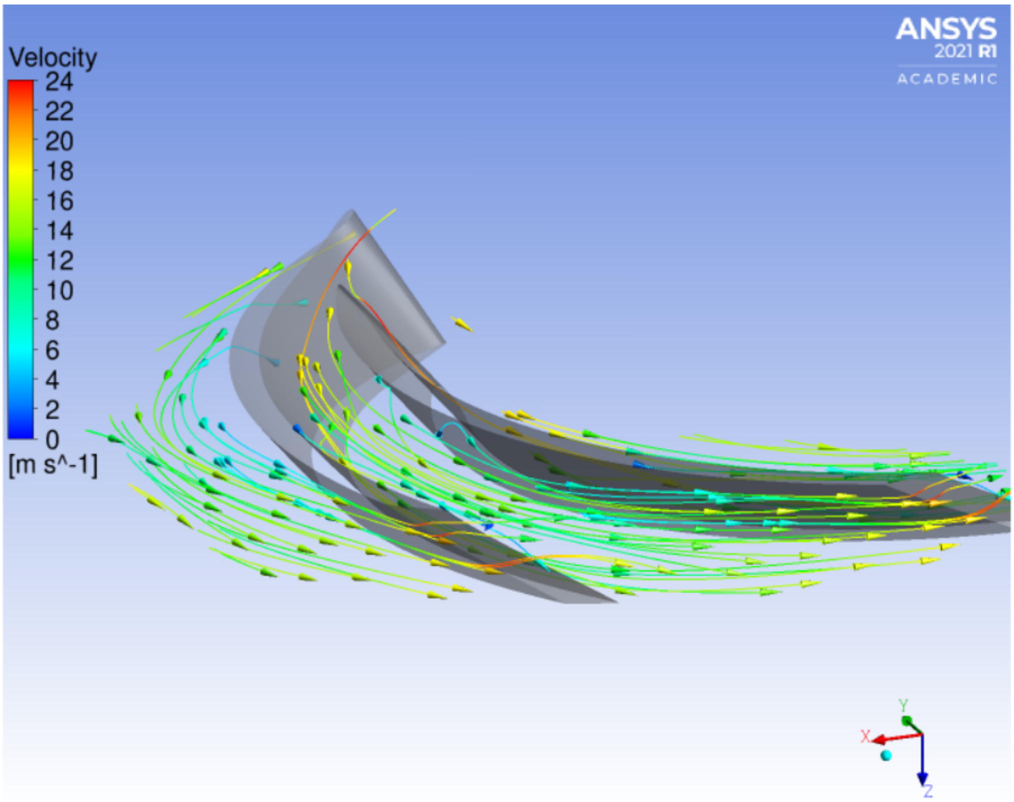

Figure 4.44: Velocity vectors TE view

Figure 4.44 shows the velocity vectors in the trailing edge sectional view of the "B" off-design case with $80\%\dot{m}_{Design}$, $\Omega = \Omega_{Design}$. The velocity vector separation occurs near the blade's leading edge and its trailing edge; however, the flow separation is less, and the flow is more inclined to the blade in comparison to the other off-design cases.

4.5.4 $110\%\dot{m}_{Design}$, $\Omega = \Omega_{Design}$

Parameter	Value	Unit
mass flow	0.328	kg/s
volumetric flow	0.00477	m^3/s
rotational speed	12312	RPM
head	142.93	m
shaft power	483.53	W
total efficiency	95.00	%
static efficiency	69.55	%
pressure ratio	1.45	-

Table 4.6: Booster Pump General Characteristics for Design "B" at $110\%\dot{m}_{Design}$, Ω_{Design}

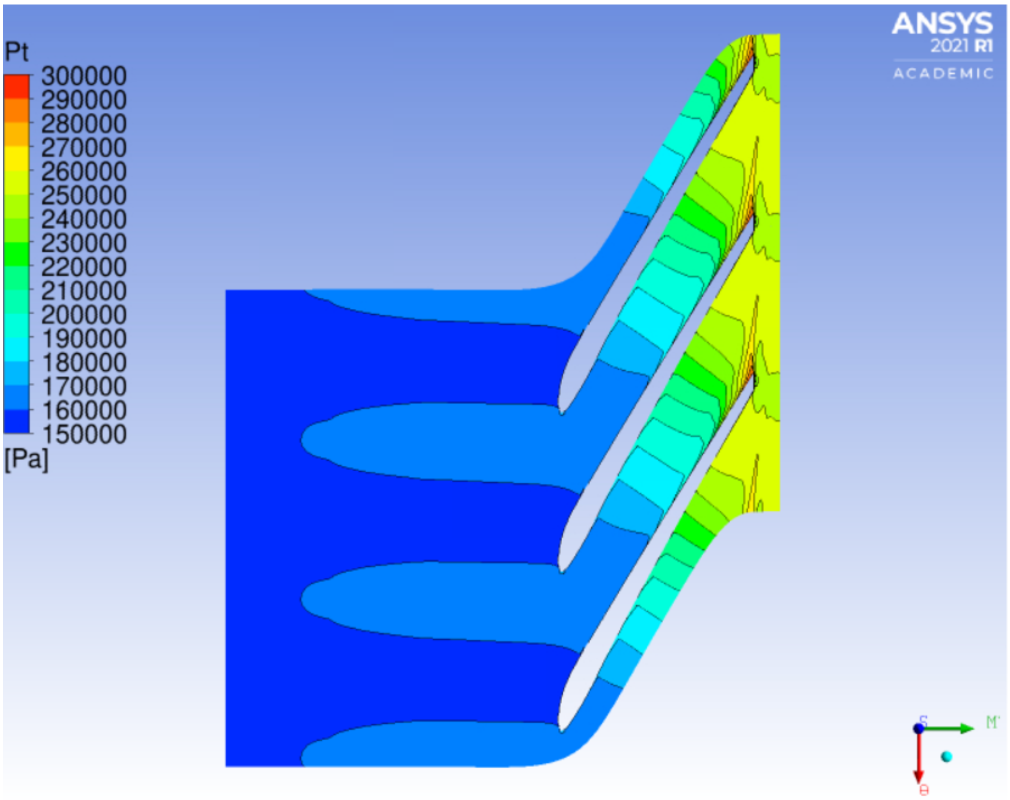

Figure 4.45: Total pressure contour, blade to blade view

Figure 4.45 shows the total pressure for the blade-to-blade view of the "B" off-design case with $110\% \dot{m}_{Design}$, $\Omega = \Omega_{Design}$. The pressure gradient gradually increases from the $1.5 bar$ to $2.6 bar$ near the blade trailing edge, where the highest pressure ($3.0 bar$) occurs. Local high-pressure gradients close to the blade's trailing edge are observed. Besides, in the flow layers with separated boundaries and small pressure differences exist in the negative direction of the meridional axis.

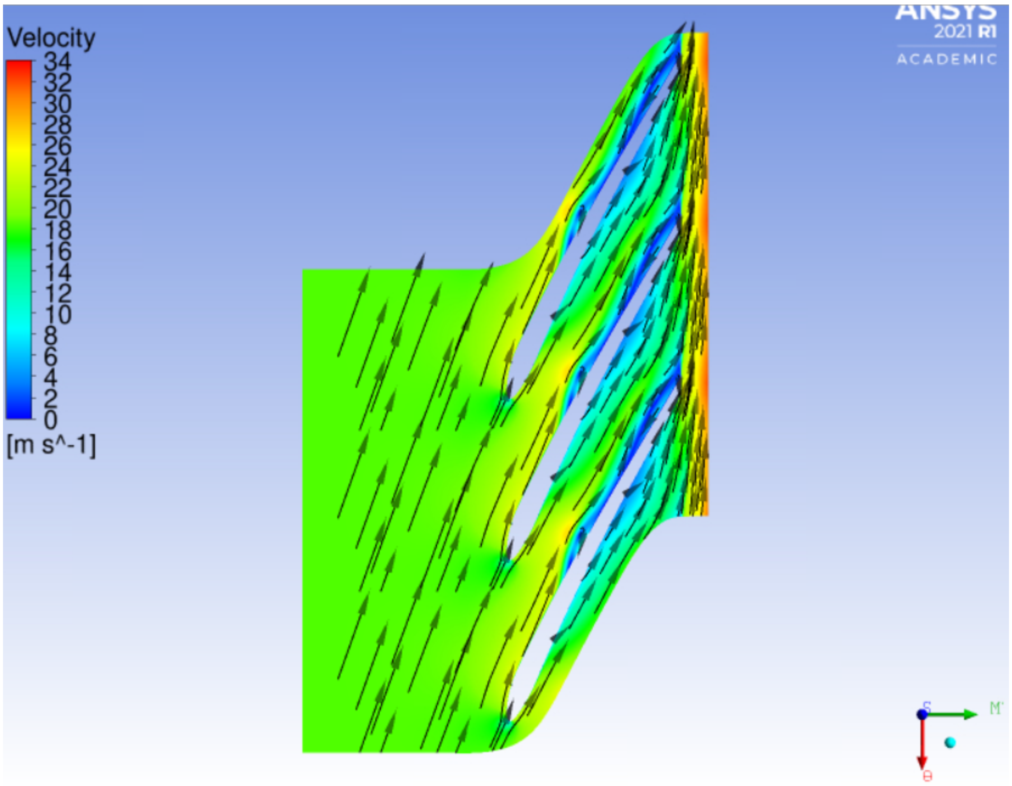

Figure 4.46: Velocity contour, blade to blade view
Figure 4.46 shows the velocity distribution for the blade-to-blade view of "B" off-design case with $110\%\dot{m}_{Design}$, $\Omega = \Omega_{Design}$. The lowest velocity value occurs under the blade chamber (pressure side).

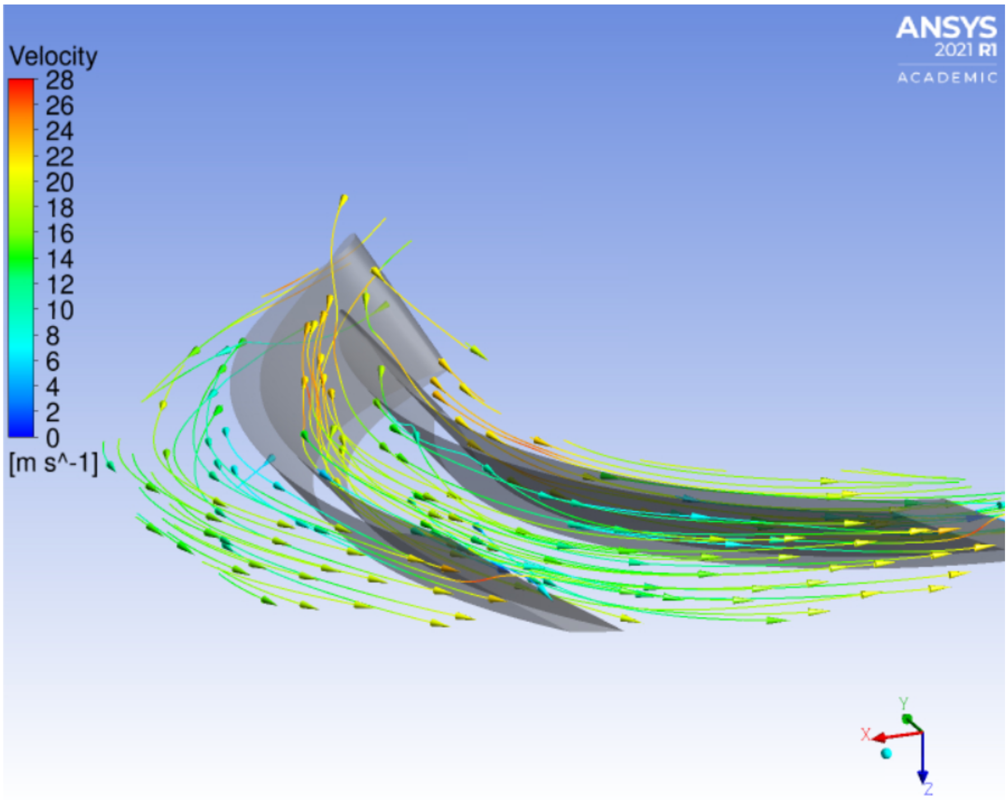

Figure 4.47: Velocity vectors TE view

Figure 4.47 shows the velocity vectors in the trailing edge sectional view of the "B" off-design case with $110\%\dot{m}_{Design}$, $\Omega = \Omega_{Design}$. The velocity vector separation occurs near the blade's leading edge; however, the flow separation is less, and the flow is more inclined to the blade in the other regions.

4.5.5 $50\%\dot{m}_{Design}$, $80\%\Omega_{Design}$

Parameter	Value	Unit
mass flow	0.149	kg/s
volumetric flow	0.00217	m^3/s
rotational speed	9849.6	RPM
head	106.37	m
shaft power	163	W
total efficiency	95.35	%
static efficiency	66.86	%
pressure ratio	1.31	-

Table 4.7: Booster Pump General Characteristics for Design "B" at $50\%\dot{m}_{Design}$, $80\%\Omega_{Design}$

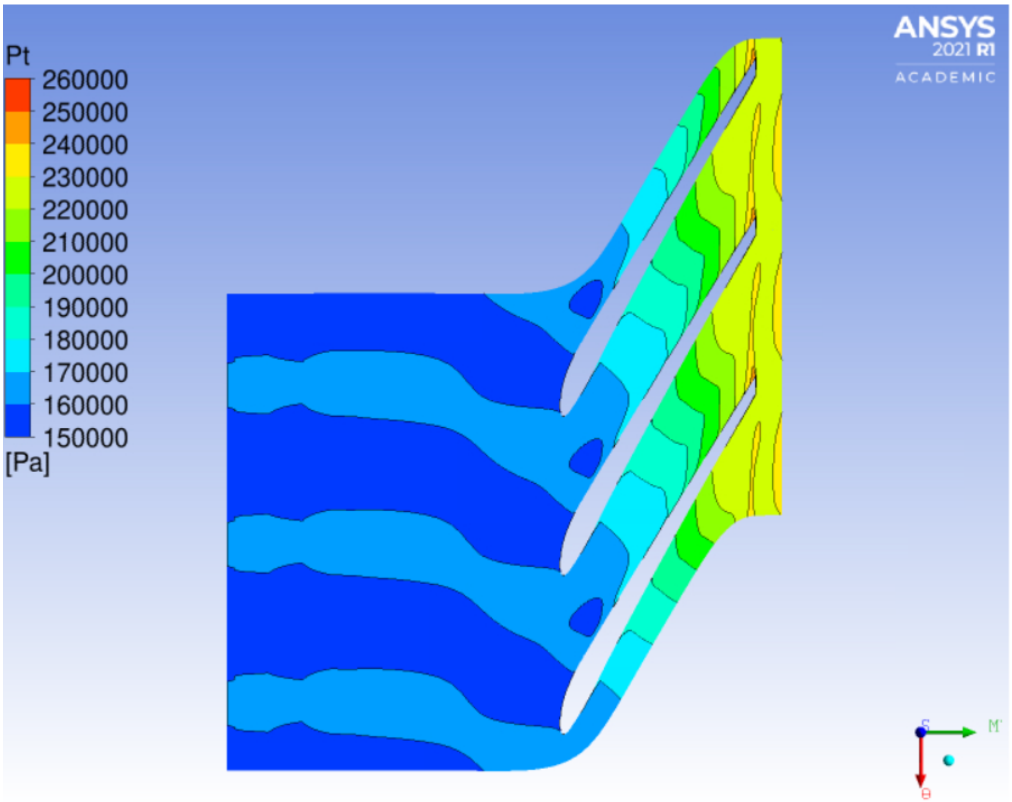

Figure 4.48: Total pressure contour, blade to blade view

Figure 4.48 shows the total pressure for the blade-to-blade view of the "B" off-design case with $50\%\dot{m}_{Design}$, $80\%\Omega_{Design}$. The pressure gradient gradually increases from the $1.5bar$ and $1.6bar$ to $2.3bar$ near the blade trailing edge. The pressure contour here looks more separated in all regions, and the sharp gradients to a maximum value of $2.6bar$ at the trailing edge can be observed in some small local points on trailing edges.

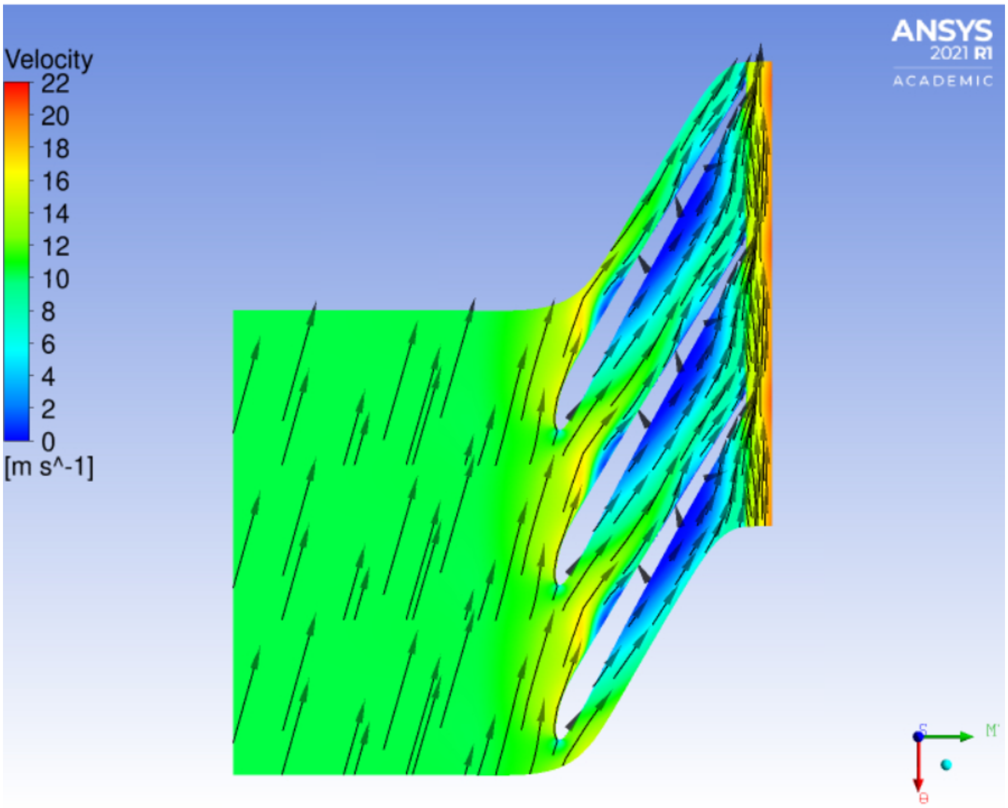

Figure 4.49: Velocity contour, blade to blade view

Figure 4.49 shows the velocity distribution for the blade-to-blade view of the "B" off-design case with $50\%\dot{m}_{Design}$, $80\%\Omega_{Design}$. The lowest velocity value occurs under the blade chamber (high-pressure zone). The flow separation occurs here because the mass flow is half the design point, and the rotational speed is high to deliver this low mass flow.

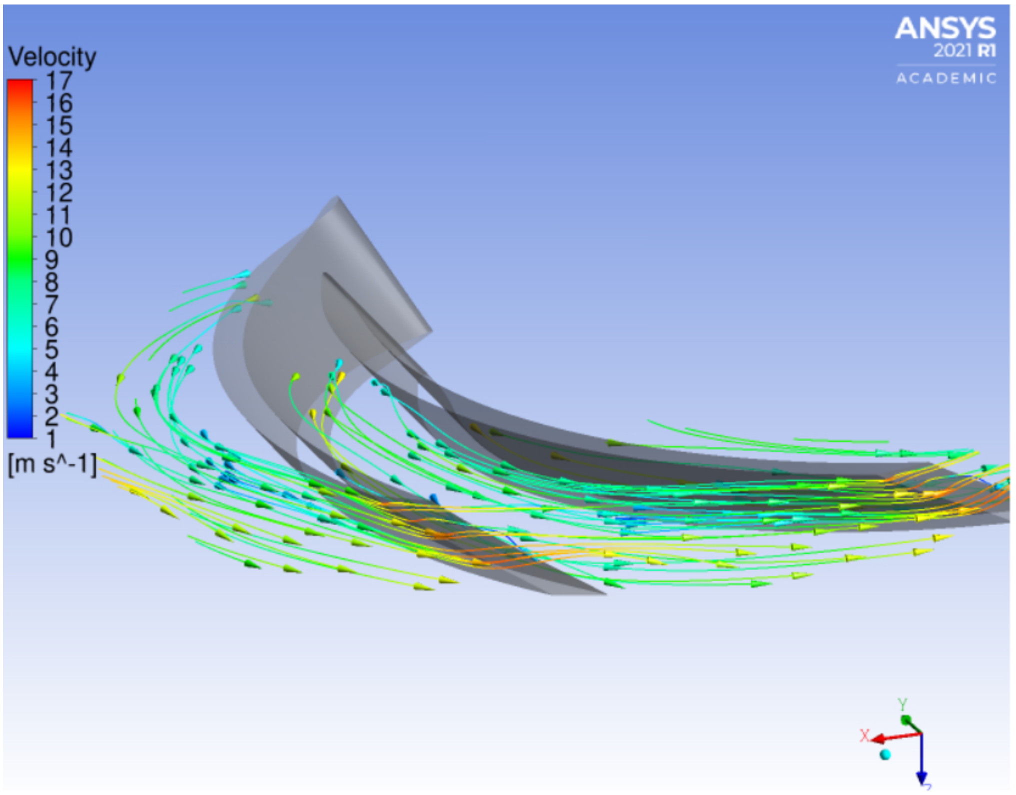

Figure 4.50: Velocity vectors TE view

Figure 4.50 shows the velocity vectors in the trailing edge sectional view of the ”B” off-design case with $50\%\dot{m}_{Design}$, $80\%\Omega_{Design}$. The velocity vector separation occurs near the blade's trailing edge. On the suction side of the blade, some separation can be observed too, where the flow has made a larger curvature radius compared to the blade chamber line.

4.5.6 $80\%\dot{m}_{Design}$, $80\%\Omega_{Design}$

Parameter	Value	Unit
mass flow	0.238	kg/s
volumetric flow	0.00347	m^3/s
rotational speed	9849.6	RPM
head	94.47	m
shaft power	231.2	W
total efficiency	95.53	%
static efficiency	69.36	%
pressure ratio	1.29	-

Table 4.8: Booster Pump General Characteristics for Design "B" at $80\%\dot{m}_{Design}$, $80\%\Omega_{Design}$

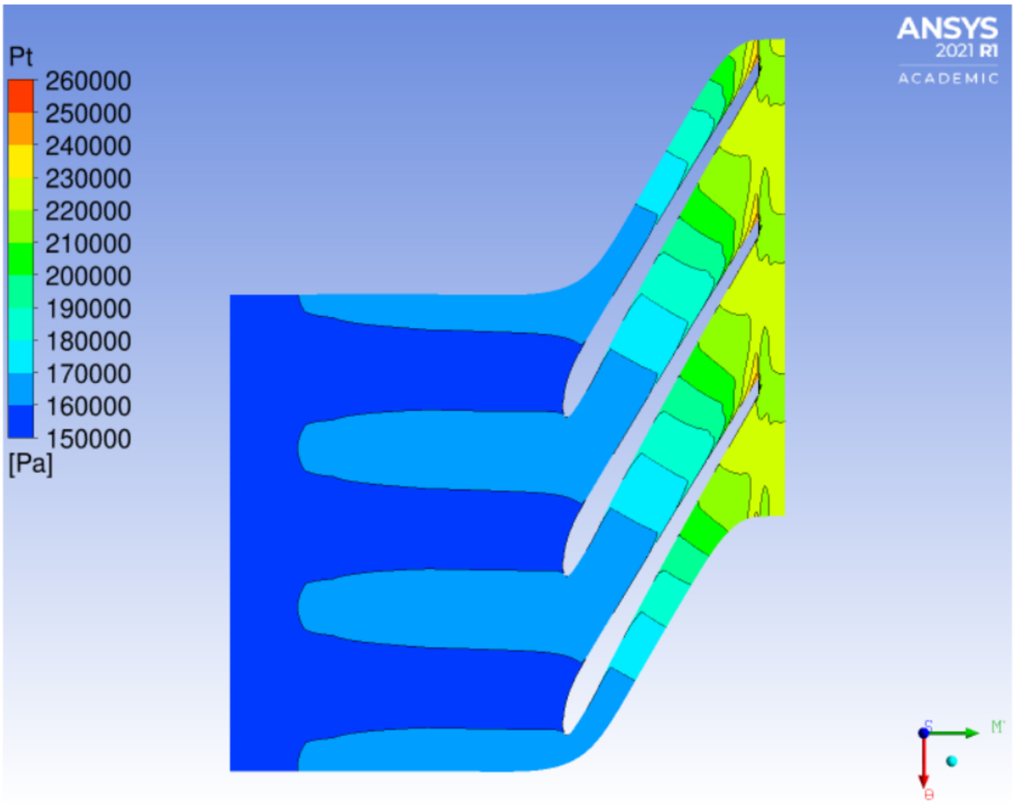

Figure 4.51: Total pressure contour, blade to blade view

Figure 4.51 shows the total pressure for the blade-to-blade view of the "B" off-design case with $80\%\dot{m}_{Design}$, $80\%\Omega_{Design}$. The pressure gradient gradually increases from the $1.5bar$ and $1.6bar$ to $2.3bar$ near the blade trailing edge. The pressure contour here looks more separated in all regions, and the sharp gradients to $2.6bar$ at the trailing edge can be observed in some small local points.

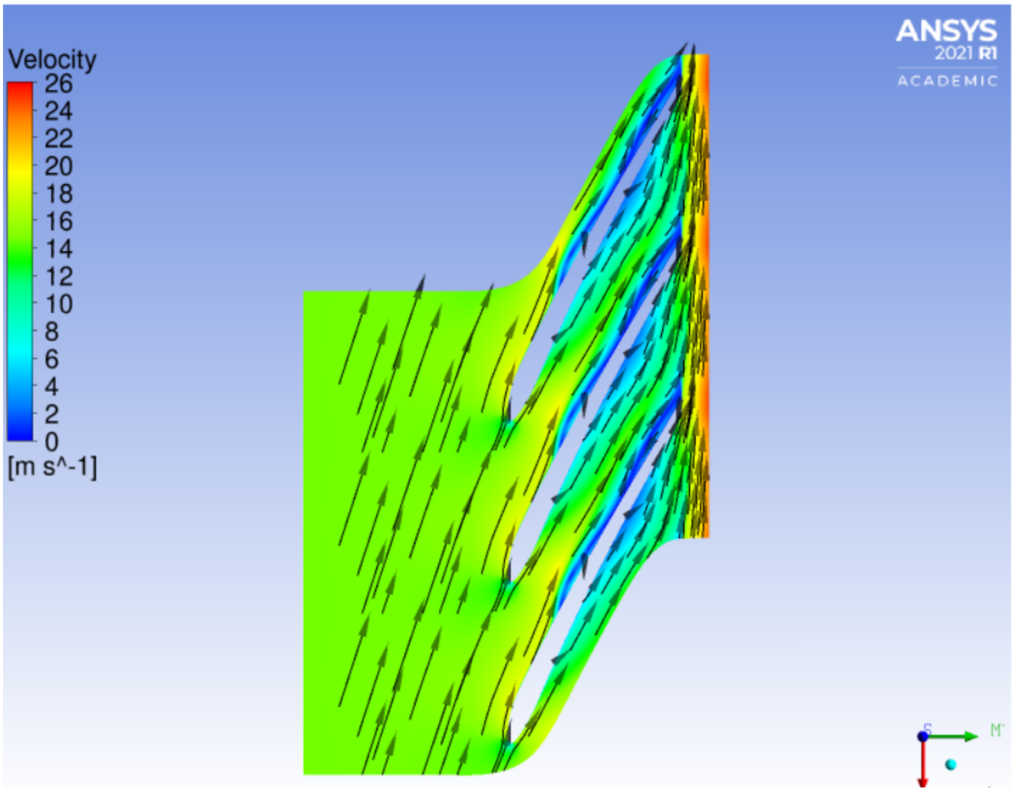

Figure 4.52: Velocity contour, blade to blade view

Figure 4.52 shows the velocity distribution for the blade-to-blade view of the "B" off-design case with $80\%\dot{m}_{Design}$, $80\%\Omega_{Design}$. The lowest velocity value occurs under the blade chamber (high-pressure zone). The flow separation can be observed in some regions near the blades; however, the flow separation here is not as severe as in off-design cases with lower mass flows or rotational speeds.

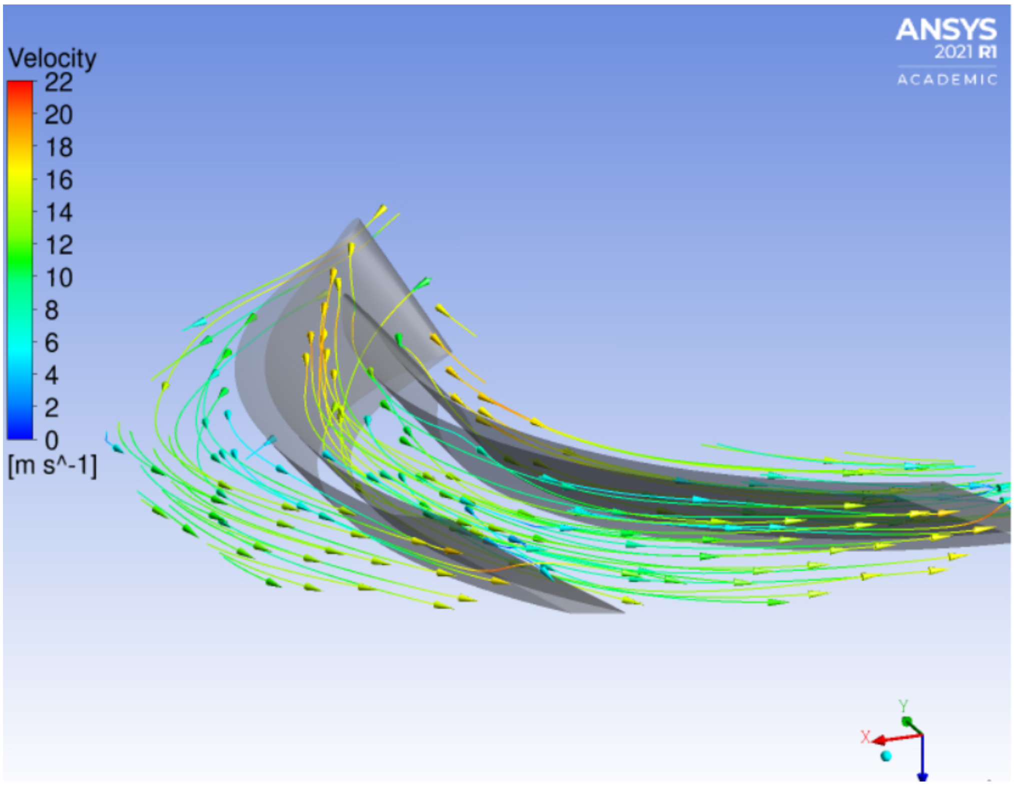

Figure 4.53: Velocity vectors TE

Figure 4.53 shows the velocity vectors in the trailing edge sectional view of the "B" off-design case with $80\%\dot{m}_{Design}$, $80\%\Omega_{Design}$. The velocity vector separation occurs near the blade's leading edge. The separation of the velocity vectors is not considerable in this contour.

4.5.7 $\dot{m} = \dot{m}_{Design}$, $80\%\Omega_{Design}$

Parameter	Value	Unit
mass flow	0.298	kg/s
volumetric flow	0.00433	m^3/s
rotational speed	9849.6	RPM
head	88.11	m
shaft power	273.57	W
total efficiency	94.12	%
static efficiency	69.28	%
pressure ratio	1.28	-

Table 4.9: Booster Pump General Characteristics for Design "B" at $\dot{m} = \dot{m}_{Design}$, $80\%\Omega_{Design}$

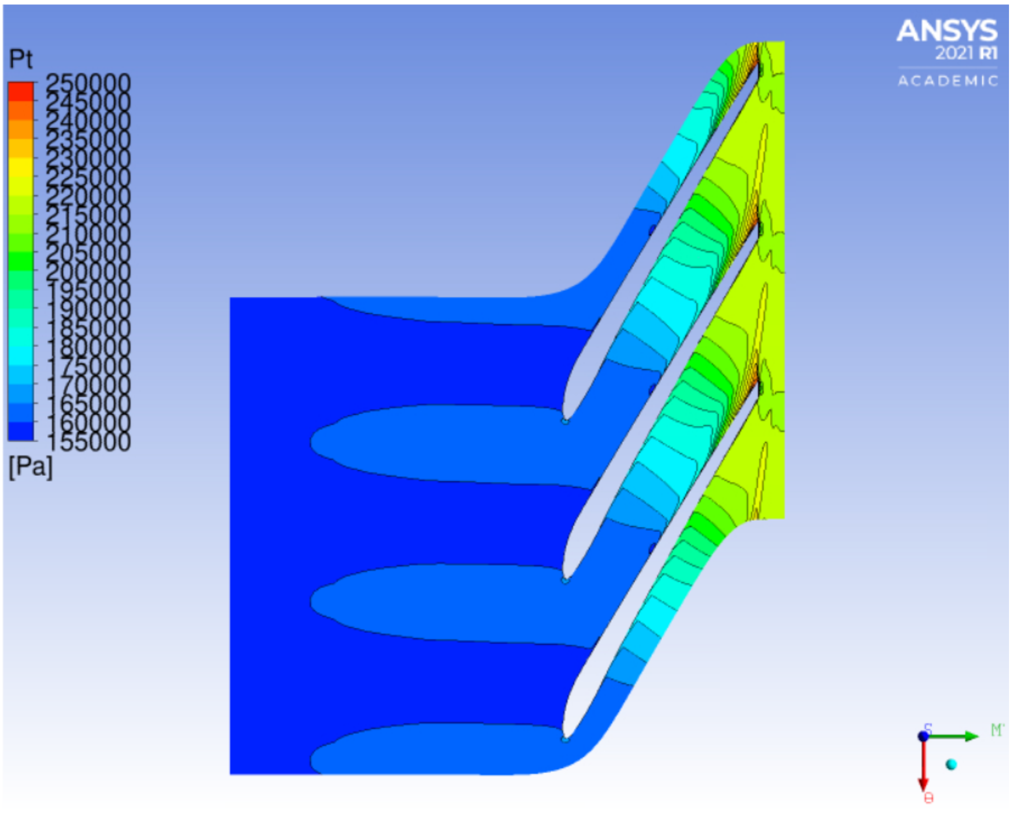

Figure 4.54: Total pressure contour, blade to blade view

Figure 4.54 shows the total pressure for the blade-to-blade view of the "*B*" off-design case with $\dot{m} = \dot{m}_{Design}$, $80\%\Omega_{Design}$. The pressure gradient gradually increases from the $1.6bar$ and $1.7bar$ to $2.2bar$ near the blade trailing edge. The pressure gradient is more gradual in this case since the mass flow is equal to the design point mass flow. Some sharp gradients can be observed near the trailing edges locally.

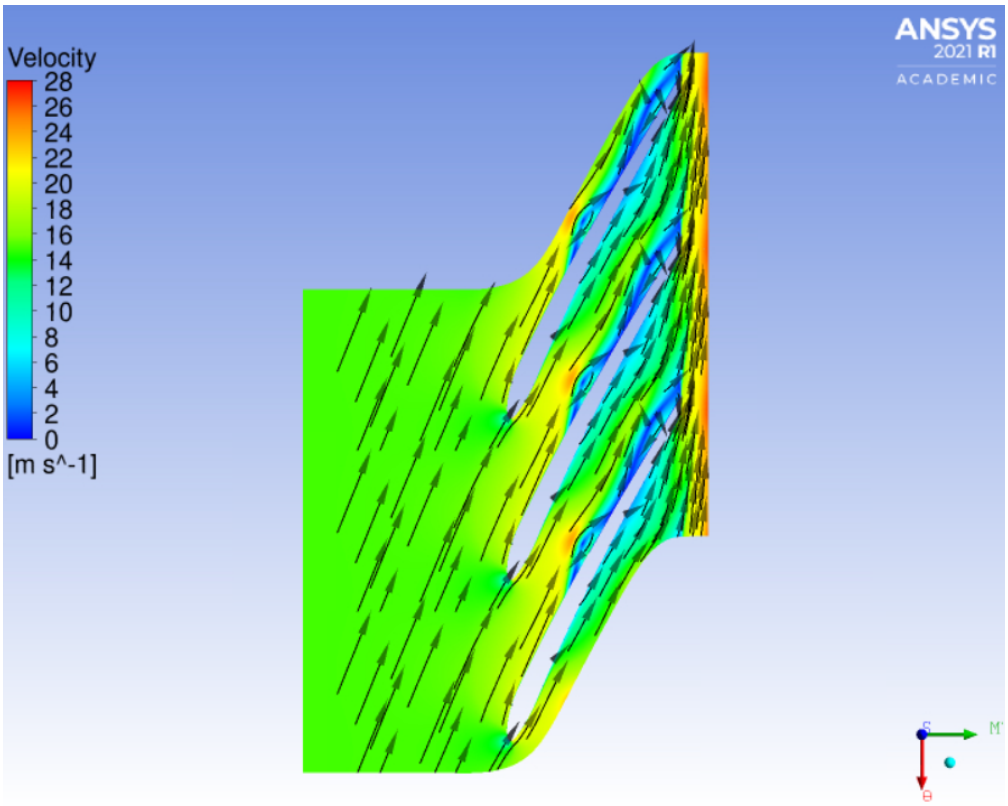

Figure 4.55: Velocity contour, blade to blade view

Figure 4.55 shows the velocity distribution for the blade-to-blade view of the "B" off-design case with $\dot{m} = \dot{m}_{Design}$, $80\%\Omega_{Design}$. The lowest velocity value occurs under the blade chamber (high-pressure zone). The flow separation can be observed in some regions near the blades; however, the flow separation here is not as severe as in off-design cases with lower mass flows or rotational speeds because the mass flow is equal to the design point suggestion.

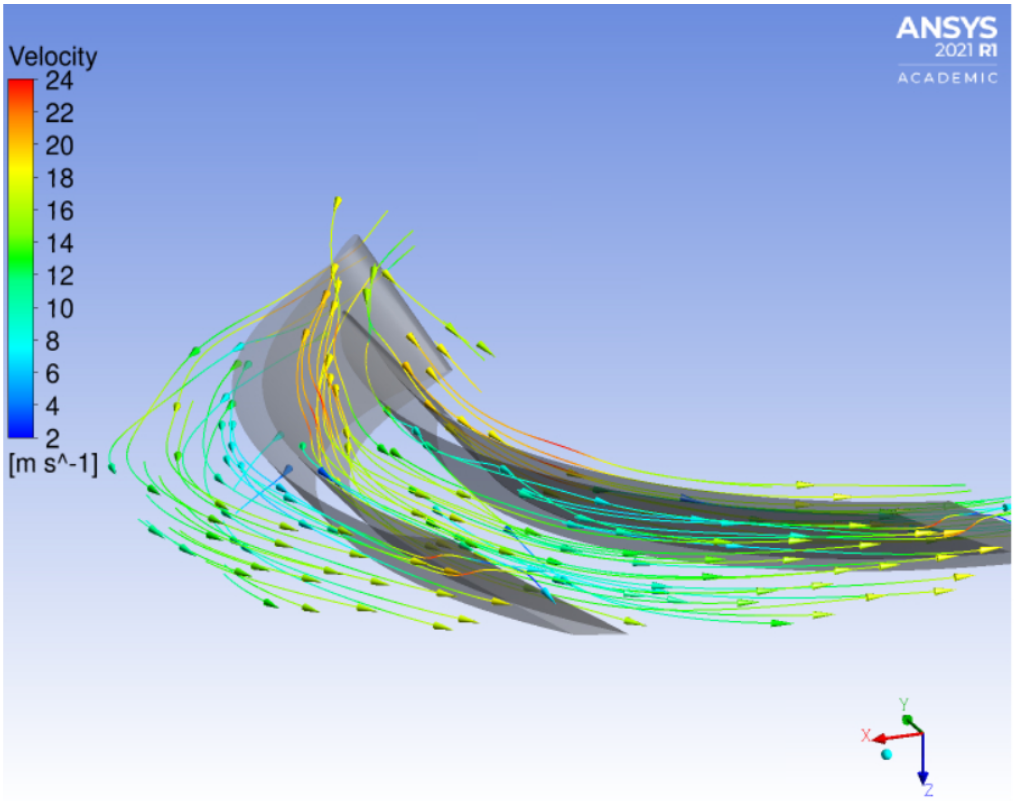

Figure 4.56: Velocity vectors TE view

Figure 4.56 shows the velocity vectors in the trailing edge sectional view of the "B" off-design case with $\dot{m} = \dot{m}_{Design}$, $80\%\Omega_{Design}$. The velocity vector separation occurs near the blade's leading edge. This separation is more visible in the pressure side.

4.5.8 $110\%\dot{m}_{Design}$, $80\%\Omega_{Design}$

Parameter	Value	Unit
mass flow	0.328	kg/s
volumetric flow	0.00477	m^3/s
rotational speed	9849.6	RPM
head	84.55	m
shaft power	292.46	W
total efficiency	92.93	$\%$
static efficiency	68.56	$\%$
pressure ratio	1.27	-

Table 4.10: Booster Pump General Characteristics for Design "B" at $110\%\dot{m}_{Design}$, $80\%\Omega_{Design}$

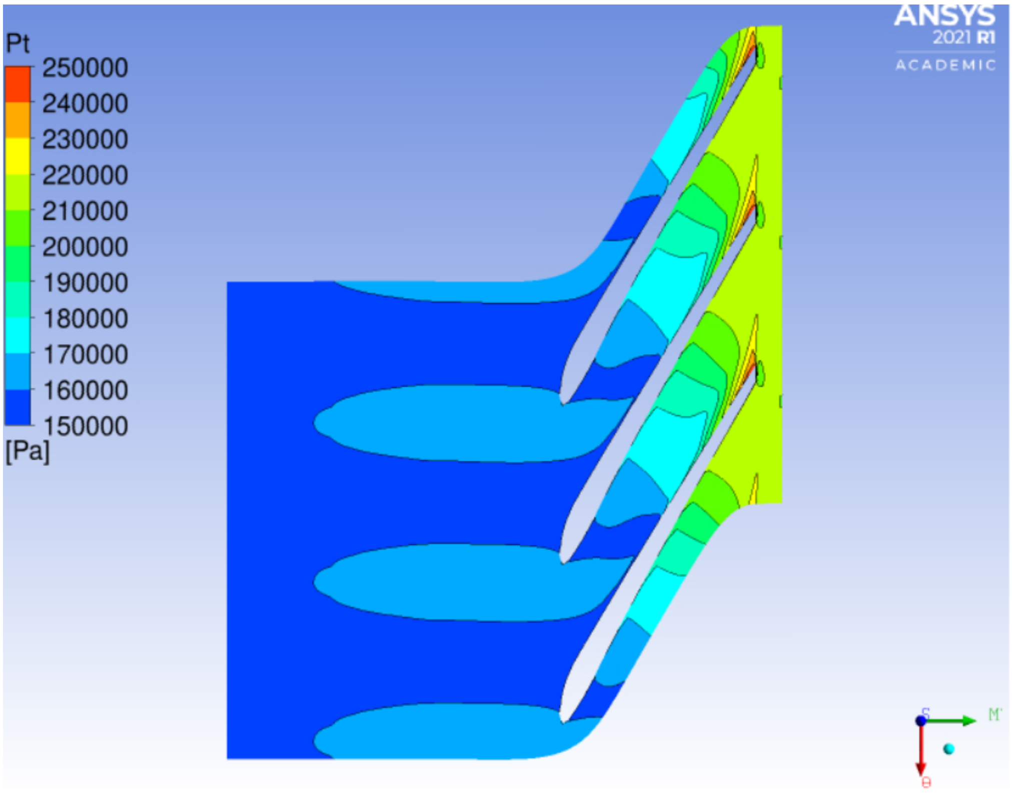

Figure 4.57: Total pressure contour, blade to blade view

Figure 4.57 shows the total pressure for the blade-to-blade view of the "B" off-design case with $\dot{m} = \dot{m}_{Design}$, $110\%\Omega_{Design}$. The pressure gradient gradually increases from the $1.5bar$ and $1.6bar$ to $2.2bar$ near the blade trailing edge. The pressure gradient is more gradual in this case since the mass flow is equal to the design point mass flow. Some sharp gradients can be observed near the trailing edges locally. Because rotational speed is higher than the design point, then it affects the flow pressure to be higher in comparison to the design point's rotational speed performance.

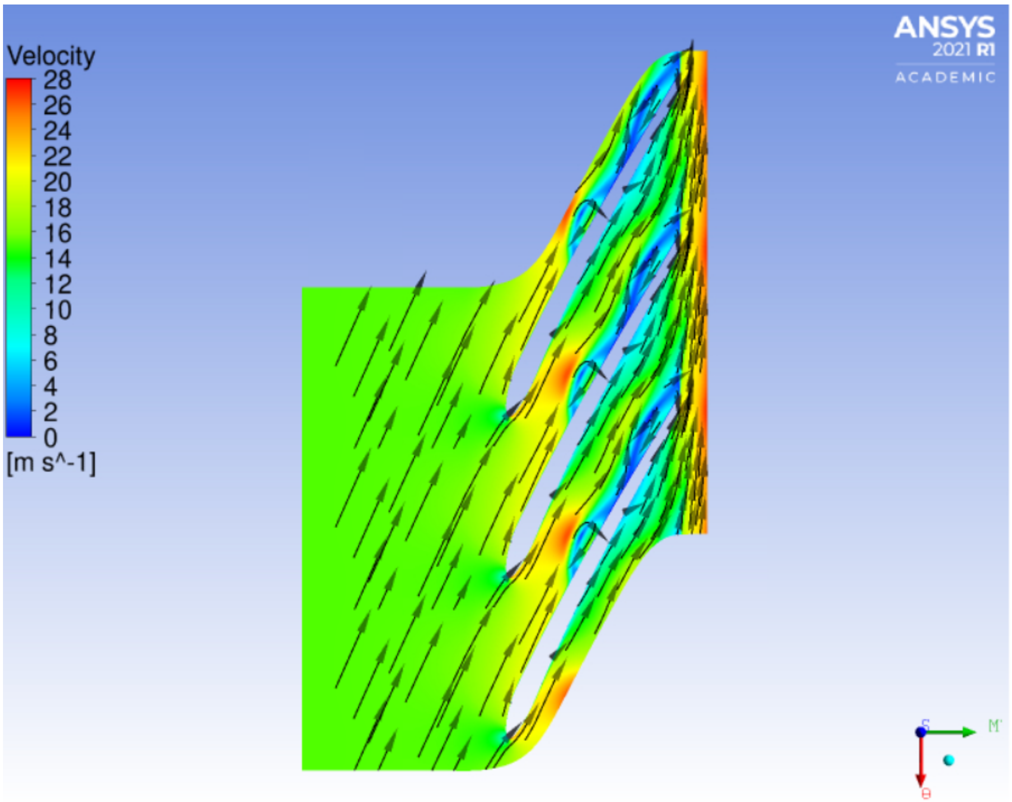

Figure 4.58: Velocity contour, blade to blade view

Figure 4.58 shows the velocity distribution for the blade-to-blade view of the "B" off-design case with $\dot{m} = \dot{m}_{Design}$, $110\%\Omega_{Design}$. The lowest velocity value occurs under the blade chamber (high-pressure zone). The flow separation can be seen on the suction side of the blades as the velocity vector circulation are visible.

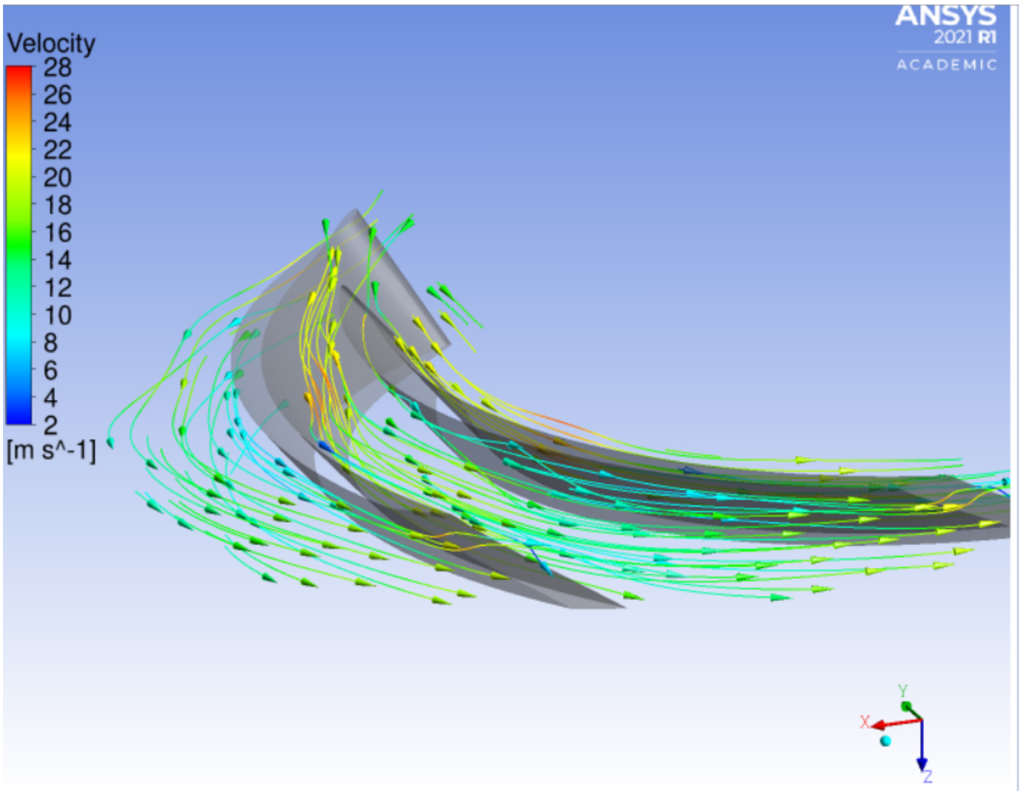

Figure 4.59: Velocity vectors TE view

Figure 4.59 shows the velocity vectors in the trailing edge sectional view of the "B" off-design case with $\dot{m} = \dot{m}_{Design}$, $110\%\Omega_{Design}$. The velocity vector separation occurs near the blade's leading, where the velocity vectors have larger values because of the total pressure increase as the result of the rotational speed increase.

5

Conclusion and Future work

5.1 Conclusion

This study proposes the general fuel system configuration for the liquid hydrogen fuel system based on the A321 twin-engine short-medium range civil aircraft. This fuel system includes a piping network and hydraulic components to deliver fuel efficiency to the aircraft combustion chambers. The liquid hydrogen is kept in cryogenic condition ($22K, 1.6bar$) and must be delivered at the pressure of $40.6bar$ during the maximum take-off stage. The proposed piping network does not have much heat transfer in the case of vacuum-jacket pipelines. Several valves are suggested to be implemented in the system, including shut-off, cross-feed, non-return, relief, and regulator valves, plus fittings like 90^o elbow and tee. It is required that airplanes carry at least three cross-feed valves to be able to operate in case of an emergency incident, which makes it necessary to deliver the fuel from the left/right rear tanks to the opposite side engine. The twin-engine airplane needs at least six booster pumps according to the regulations to meet the safety requirements. The second part of the project considers booster pump performance. Booster pumps are responsible for delivering the fuel from the tanks to the fuel lines. The centrifugal configuration is the recommended type of turbomachine for this duty. The proposed booster pump has seven vanes, three stages, and a $104m$ head rise per stage. The design point for the booster pump is the mass flow of $0.298kg/s$ and rotational speed of $12312RPM$ based on the non-dimensional numbers equations. The new modified design case of "A" is named "B", which has thicker blades that are more inclined to the hub surface. This new blade geometry helps to reduce the flow separation drastically while improving efficiency. Several off-design simulation points are made for both cases.

5.2 Future Work

The liquid hydrogen fuel system is a new approach toward sustainability in the aviation sector, so it is likely to find the future topic in this field interesting for later studies. There are some suggestions:

1. CFD simulation of the booster pump including cavitation model
2. Taking the mechanical losses and frictions into account for the pump's performance to reflect the shaft power value close to the reality
3. More modifications on blade geometry to achieve the minimum flow separation
4. CFD simulation set up for valves and other hydraulic components

Bibliography

[1] G Daniel Brewer. *Hydrogen aircraft technology.* Routledge, 2017.

[2] Yi Tu, Xuanren Chen, Liang Yin, Qiuyun Zheng, and Yu Zeng. Numerical study on pipeline pressure surge of the large aircraft fuel system. *Shock and Vibration*, 2022, 2022.

[3] DirectMaterial. Elbow fittings. URL `https://www.directmaterial.com/fittings-what-is-an-elbow`.

[4] Airbus. Tee fitting, . URL `http://www.thepipefittings.com/pipe-tee.html`.

[5] Sydney Lawrence Dixon and Cesare Hall. *Fluid mechanics and thermodynamics of turbomachinery.* Butterworth-Heinemann, 7th edition, 2013.

[6] Jae-Hoon Lee, Si-Pom Kim, and Geun-Ho Lee. Numerical analysis and experimental verification based on design parameter variation of vacuum-insulated pipe for cryogenics. In *International Symposium on Mechanical Engineering and Material Science (ismems-16)*, pages 488–493. Atlantis Press, 2016.

[7] Frank M White. *Fluid mechanics.* Tata McGraw-Hill Education, 7th edition, 2009.

[8] ANSYSÕ Turbogrid. Release 14.5, components system, ansys turbogrid user's guide. ansys.

[9] Airbus. A321eno features, . URL `https://aircraft.airbus.com/en/aircraft/a320-the-most-successful-aircraft-family-ever/a321neo`.

[10] worldbank. pssnger. URL `https://data.worldbank.org/indicator/IS.AIR.PSGR`.

[11] statistics. fuelglobe. URL `https://www.statista.com/statistics/655057/fuel-consumption-of-airlines-worldwide/#:~:text=The%20global%20fuel%20consumption%20by,57%20billion%20gallons%20in%202021`.

[12] unorg. warming. URL `https://www.un.org/en/un75/climate-crisis-race-we-can-win`.

[13] eea. euemission. URL `https://www.eea.europa.eu/policy-documents/ec-2020-2050-long-term-strategy#:~:text=The%20EU%20aims%20to%20be,action%20under%20the%20Paris%20Agreement%20`.

[14] A Contreras, S Yiğit, K Özay, and TN Veziroğlu. Hydrogen as aviation fuel: a comparison with hydrocarbon fuels. *International Journal of Hydrogen Energy*, 22(10-11):1053–1060, 1997.

[15] FederalRegulations1. Fed regulations 1. URL https://www.ecfr.gov/current/title-14/chapter-I/subchapter-C/part-25.

[16] Chevron. aviation fuels technical review. URL https://www.cgabusinessdesk.com/document/aviation_tech_review.pdf.

[17] Hans W Pohl and Valentin V Malychev. Hydrogen in future civil aviation. *International journal of hydrogen energy*, 22(10-11):1061–1069, 1997.

[18] Grudnfos. non return valve. URL https://www.grundfos.com/solutions/learn/research-and-insights/non-return-valve.

[19] Wermac. Relief valve. URL https://www.wermac.org/valves/valves_pressure_relief.html.

[20] MPC. Regulator valve. URL https://www.mpofcinci.com/blog/hydraulic-flow-control-valves/.

[21] Norgren. shutoff valve1. URL https://www.norgren.com/uk/en/expertise/industrial-automation/what-is-a-shut-off-valve.

[22] GMS instrument. shutoff valve. URL https://gms-instruments.com/blog/what-is-a-shut-off-valve/#:~:text=Shut%20off%20valves%20are%20designed,off%20valve%20has%20many%20names.

[23] digilander. Crossfedd valve. URL https://digilander.libero.it/andreatheone/enginefuelfeed.htm.

[24] FederalRegulations2. Fed regulations 2. URL https://www.ecfr.gov/current/title-14/chapter-I/subchapter-C/part-23.

[25] Claus Borgnakke and Richard Edwin Sonntag. *Fundamentals of thermodynamics*. John Wiley & Sons, 2022.

[26] Yunus A Cengel, Michael A Boles, and Mehmet Kanoğlu. *Thermodynamics: an engineering approach*, volume 5. McGraw-hill New York, 2011.

[27] Johann Friedrich Gülich. *Centrifugal pumps*, volume 2. Springer, 2008.

[28] Mohinder L Nayyar. *Piping handbook*. McGraw-Hill Education, 2000.

[29] Fractory. aviation fuels technical review. URL https://fractory.com/stainless-steel-finishes-en-astm/#:~:text=The%20surface%20finish%20has%20a,from%200.4%20to%201.0%20micrometers.

[30] Roy Langton, Chuck Clark, Martin Hewitt, and Lonnie Richards. *Aircraft fuel systems*. John Wiley & Sons, 2009.

[31] vacuum. vacuum. URL https://cryoworks.net/vacuum-insulated-pipe-vip/.

[32] VJACME. Vjacme. URL https://www.acmecryo.com/wp-content/uploads/2021/04/ACM-Vacuum-Jacketed-Pipe-Brochure.pdf.

[33] Jun Li, Lingfeng Tang, and Yaoyao Zhang. The influence of blade angle on the performance of plastic centrifugal pump. *Advances in Materials Science and Engineering*, 2020, 2020.

[34] K Alawadhi, B Alzuwayer, TA Mohammad, and MH Buhemdi. Design and optimization of a centrifugal pump for slurry transport using the response surface method. machines 2021, 9, 60, 2021.

[35] VA Gundale and GR Joshi. A simplified 3d model approach in constructing the plain vane profile of a radial type submersible pump impeller. *Research Journal of Engineering Sciences*, 2(7):33–37, 2013.

[36] I Ariga and M Umezawa. The effect of impeller exit rake angle on the internal flow of centrifugal compressor impeller. In *13th Australasian Fluid Mechanics Conference, Monash University, Melbourne Australia*, pages 13–18, 1998.

[37] Krishna Kumar Yadav, Karun Mendiratta, and VK Gahlot. Optimization of the design of radial flow pump impeller though cfd analysis. *International Journal of Research in Engineering and Technology*, 5(11):157–161, 2016.

[38] E Korkmaz, Mustafa Gölcü, and C Kurbanoğlu. Effects of blade discharge angle, blade number and splitter blade length on deep well pump performance. 2017.

[39] Hermann Schlichting and Joseph Kestin. *Boundary layer theory*, volume 121. Springer, 1961.

[40] Siemens. Simense. URL https://volupe.se/.

[41] ANSYS CFX-Solver. Theory guide. *Release ll*, 2006.
url

DEPARTMENT OF SOME SUBJECT OR TECHNOLOGY
CHALMERS UNIVERSITY OF TECHNOLOGY
Gothenburg, Sweden
www.chalmers.se

CHALMERS
UNIVERSITY OF TECHNOLOGY